Highway Safety Research Institute
Institute of Science and Technology
The University of Michigan
Ann Arbor, Michigan 48105

TIRE PERFORMANCE CHARACTERISTICS AFFECTING VEHICLE RESPONSE TO STEERING AND BRAKING CONTROL INPUTS

Howard Dugoff
Paul S. Fancher
Leonard Segel

August 1969

Final Report for Period May 1968 - August 1969

Prepared for

Tire System Section
Office of Vehicle Systems Research
NATIONAL BUREAU OF STANDARDS
Washington, D. C. 20234

CST - 460

This report was prepared in fulfillment of the National Bureau of Standards Contract CST-460 (funded by the National Highway Safety Bureau through the NBS, Contract FH-11-6090). The opinions, findings, and conclusions expressed in this publication are those of the authors and not necessarily those of the National Bureau of Standards nor the National Highway Safety Bureau.

ABSTRACT

A theoretical study of the influence of tire-mechanics characteristics on the behavior of an automobile undergoing maneuvers requiring the tires to produce combined longitudinal and lateral forces was performed. A simulation model specifically designed to study vehicle response under skidding and near-skidding conditions was developed and mechanized on an analog computer. The model included a representation of wheel rotational degrees of freedom, and relationships expressing the longitudinal and lateral tire shear force components as analytical functions of tire normal load, sideslip and inclination angles, and longitudinal slip. The tire shear force relationships, derived by extrapolating from the existing theory of the traction mechanics for a freely rolling tire, were shown to agree qualitatively with available experimental data. The simulation was applied to examine the influence on vehicle responses to various open-loop steering and brake-control inputs of variations in the values of three parameters: lateral tire stiffness, longitudinal tire stiffness, and the coefficient of friction at the tire-road interface.

CONTENTS

1. INTRODUCTION

The broad purpose of the study reported herein was to investigate the influence of mechanical characteristics of pneumatic tires on the behavior of an automobile undergoing maneuvers requiring the tires to produce combined longitudinal and lateral forces. To this end the study was directed toward accomplishing the following specific tasks:

1. Compile and synthesize existing theoretical and experimental information on the mechanics of pneumatic tires to develop a mathematical representation describing the dependence of tire-traction components on (1) the kinematic variables associated with the tire's rolling/sliding motion and (2) the mechanical properties of the tire.
2. Incorporate the tire mechanics representation in an analog-computer simulation of the dynamics of a motor vehicle formulated specifically for the purpose of this investigation.
3. Using this simulation, perform a parametric study to examine the extent to which a vehicle's responses to various specified combinations of brake, throttle, and steering control inputs are affected by realistic variations in the values of principal tire-mechanical characteristics.

In accordance with the study objective, the analysis emphasized the characterization of the traction mechanics of the pneumatic tire, rather than the exact representation of the mechanics of the automobile. Only those factors reckoned on the basis of past research experience to exert a "first-order" influence on the directional behavior of a motor vehicle operated at, or near, the friction limit were included in the mathematical representation of the automobile.

In general, the shear force generated at the tire-road interface is a function of a multiplicity of variables describing (1) the geometric and material properties of the road surface, (2) the state of interface contamination, (3) the mechanical properties of the tire, and (4) the kinematics of the tire's rolling/sliding motion. In the study reported herein, the effects of road variables and interface contamination were not considered. Tire-road friction was described in terms of a friction coefficient μ whose dependence upon road and interface contamination properties was left unspecified and unexplored.

Another important constraint on the scope of the study was that differences in properties among the four tires mounted on a vehicle at any one time were not considered. That is, simulation conditions were restricted to cases where the properties of all four tires were identical.

Section 2 of this report is concerned with the mathematical modeling of tire-traction mechanics. The representation developed here is discussed in light of previous related research and the current study objectives. Tire characteristics curves generated on the basis of the model are compared with available experimental data. Section 3 discusses the vehicle mechanics model, its mechanization on the analog computer, and the format and scope of the parametric study in which it was applied. Significant simulation results are presented and discussed in Section 4, and the principal conclusions and recommendations deriving from the study are summarized in Section 5. The derivation of the tire mechanics representation, detailed description of the simulation model, and a discussion of some simulation results of secondary interest are included in Appendices to the report.

2. MATHEMATICAL REPRESENTATION OF TIRE TRACTION MECHANICS

2.1. DEFINITIONS AND INTRODUCTORY REMARKS

Let us consider a tire moving parallel to the ground at a velocity V, with a slip angle α, and an inclination angle γ, as shown schematically in Figure 1. Let F_z represent the normal load exerted on the tire by the road (see Figure 1), and let s represent the longitudinal slip ratio, defined by

$$s = 1 - \frac{\Omega R_e}{u_w} \quad . \tag{1}$$

Ω is the wheel spin velocity (see Figure 1); u_w is the component of the tire velocity (V) along the longitudinal (x') axis (see Figure 1); and R_e is the effective rolling radius of the tire, defined as

$$R_e = \frac{u_w}{\Omega_o} \quad , \tag{2}$$

where Ω_o is the angular velocity of a tire <u>rolling freely</u> with all other kinematics equivalent.

In light of the study objectives and constraints outlined in the Introduction, let us symbolically define a set of "tire-traction performance relationships" of the form

$$F_{xw} = f_1(F_z, \alpha, s, \gamma, V, \mu_o, t_1, \ldots, t_n), \tag{3}$$

$$F_{yw} = f_2(F_z, \alpha, s, \gamma, V, \mu_o, t_1, \ldots, t_n), \tag{4}$$

$$M_z = f_3(F_z, \alpha, s, \gamma, V, \mu_o, t_1, \ldots, t_n). \tag{5}$$

F_{xw}, F_{yw}, and M_z are, respectively, the longitudinal tire force, the lateral tire force, and the tire aligning torque, all defined as indicated in Figure 1; μ_o is a nominally defined friction

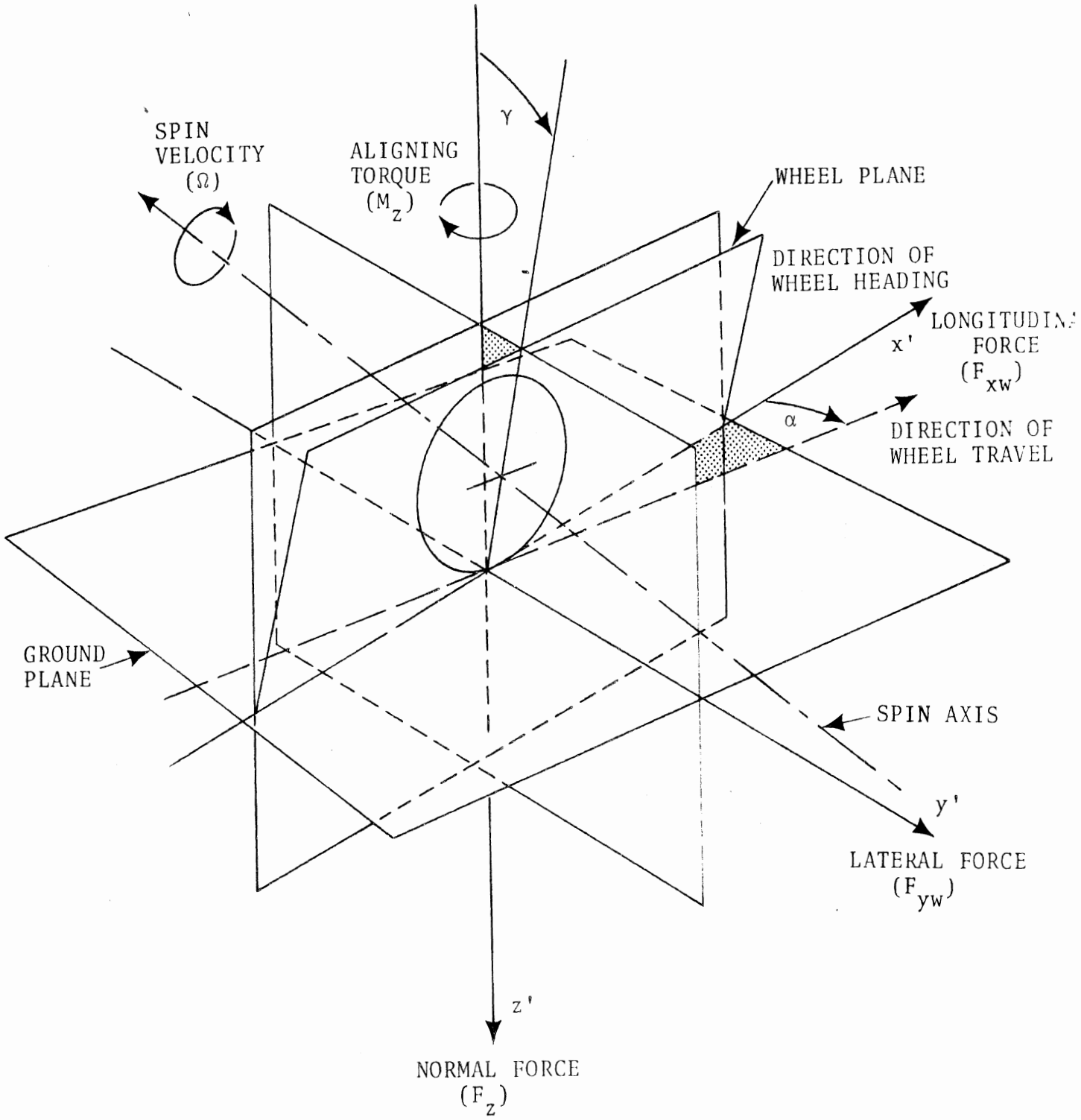

FIGURE 1. TIRE AXIS SYSTEM AND KINEMATIC VARIABLES

coefficient, a property of tire characteristics and the ambient roadway surface conditions; and $t_1,\ldots,t_n$ are variables describing all other tire properties significantly influencing traction mechanics*.

In analytical terms, the first requisite for the achievement of the study objective was the determination of functional forms for each of the f_i's of equations 3, 4, and 5. It was recognized from the outset that the existing state of theoretical and empirical knowledge of pneumatic tire mechanics by no means constituted a wholly adequate foundation for research to this end. Accordingly the tire modeling activity was viewed as exploratory. It was intended to provide a mathematical representation which would agree at least qualitatively with the very limited available data and could serve as the basis for parametric studies designed to identify priorities for subsequent experimental and/or theoretical work on tire mechanics.

In terms of gross effect on the directional response of an automotive vehicle, tire aligning torques clearly are of a lesser order of importance than either lateral or longitudinal forces. Principally they affect the steering system's degree of freedom through variations in the yawing moments exerted about the steering kingpins [1].** Accordingly, and in light of the virtual nonexistence of experimental data on tire aligning torques under conditions of combined lateral and longitudinal slip, it was decided to approximate the actual dependence of aligning torque on the kinematic variables of influence by setting

---

* Note that "tire dynamics" effects (i.e., dependence of tire forces and moments on the time derivatives of the kinematic variables) have been neglected. This may or may not be a justifiable assumption -- virtually no data exist to evaluate it -- but it is certainly a conventional one.

** The numbers in brackets refer to the list of references appended to the paper.

$$M_z = - x_p F_{yw} \qquad (6)$$

where x_p, the "pneumatic trail," is assumed invariant with respect to changes in the values of all kinematic variables. Although more or less conventional this assumption is known to be in considerable error when appreciable sliding takes place in the tire contact patch [2]. Its adoption for the purposes of the present study is regarded as justified for purely practical reasons. The development of a more accurate tire aligning torque model certainly appears to be a suitable objective for future research.

2.2. BACKGROUND

In discussing the traction mechanics of the pneumatic tire as represented by equations 3, 4, and 5, it is profitable to distinguish among three different performance domains:

1. Free rolling ($s = 0$),
2. Straight running ($\alpha = 0$),
3. Combined side and longitudinal slip

Strictly speaking, the performance of a tire in use on a moving vehicle generally falls in domain 3. From a practical standpoint, however, the analysis of vehicle dynamics in rather broadly defined classes of motions may be adequately performed by assuming tire performance to be restricted to one of the first two, simpler domains. Accordingly, the great bulk of previous experimental and theoretical research on the mechanics of pneumatic tires has been devoted to the study of these less complicated performance regimes.

Motivated by the demands of the vehicle stability and control analyst, previous investigators have compiled a relatively extensive body of tire mechanics data for the case of the freely rolling tire. Systematic measurements [e.g., 3-8] have been made of both lateral forces (F_{yw}) and aligning torques (M_z) as functions of vertical load (F_z), sideslip angle (α), inclination angle (γ), and to a much lesser extent, velocity (V) . In addition,

Fiala [9] has developed a mathematical model expressing F_{yw} as a function of F_z, α, and γ, which has been shown to compare favorably with experimental data over wide ranges of test conditions [8-10].

Under conditions of zero sideslip and inclination angle, the tire generates contact forces only in the longitudinal direction. A substantial quantity of experimental data have been obtained under these conditions, relating the longitudinal force F_{xw} to V, F_z, and, primarily, s [e.g., 11-14]. Unlike the case of the freely rolling tire, however, no accepted analytical model expressing the functional relationship among the variables of influence is known to exist.

For the case of the tire rolling with combined side and longitudinal slip, available experimental data are extremely limited [5, 7, 8, 15-17]. By far the most valuable source is the measurements obtained by Holmes and Stone [17] using the Road Research Laboratory (Ministry of Transport, U.K.) controlled-slip tire test vehicle [18]. Previous analysts of the mechanics of vehicles in combined steering/braking maneuvers [e.g., 19-21] have employed a "friction circle" concept to account for the simultaneous effects of side and longitudinal tire slip. This concept appears to be valid in a qualitative sense; it states that the total shear force vector cannot exceed the normal force times a prevailing friction coefficient. However, recent experimental data [15-17] indicate that tire force predictions based on friction circle theories may be in considerable error. Moreover, the previous analyses have involved the assumption that the longitudinal traction component is a quantity imposed a priori, to be accounted for insofar as it may affect the lateral traction component, but invariant with respect to the generalized trajectory of motion. As has been noted previously [22], this practice is analogous to the situation prevailing with respect to the prediction of tire cornering forces prior to the introduction of the slip angle concept. The modern analyses of vehicle directional dynamics

(in the absence of significant longitudinal traction) [e.g., 23] have revealed that the essence of dynamic performance is the interdependence of the applied forces and moments and the kinematic variables of motion. It therefore appears clear that the accurate prediction of vehicle motions involving combined steering and braking requires the representation of tire force and moment components as explicit functions of both side and longitudinal slip.

2.3. ON THE DERIVATION OF THE TIRE MECHANICS MODEL

In view of the large number of independent variables involved, a strictly empirical determination of tire traction relationships of the form of equations 3 through 5 would require a tremendous data base, certainly far in excess of the comparatively meager results cited in the preceeding section. On the other hand, the theoretical model developed by Fiala [9] for the case of the freely rolling tire does provide a starting point for the formulation of a more general set of relationships, applicable to the case of a tire rolling with both side and longitudinal slip.

The derivation of a set of tire traction relationships based on extrapolations of Fiala's arguments is presented in Appendix A. The derived relationships represent both an extension and a simplification of the earlier work -- an extension in as much as they apply to a much more general class of tire-road kinematics; a simplification in that their derivation involves certain assumptions made in the interest of reducing mathematical complexity which, although reckoned totally compatible with the limited goals of the present study, are somewhat less rigorous than those of the original analysis (e.g., the present analysis assumes a uniform lateral deformation of the tire carcass, whereas Fiala computes an approximately parabolic deformation by considering the carcass as an elastically supported beam with a point load at the center of the contact patch).

In conceptual terms, the essential quality of the new tire model is that it assumes two components of elastic deformation, each of which increases linearly from a zero value at the contact patch leading edge to a maximum at a point in the patch where the resultant shear stress due to elastic deformation equals the normal pressure times the interfacial friction coefficient, and the tread begins to slide. At low values of side and longitudinal slip, no contact patch sliding occurs and the tire forces are linearly related to the slip variables. At higher slip values, contact patch sliding becomes appreciable, and the rate of increase of the tire forces with increases in the slip variables becomes less than linear and, ultimately, negative as a result of the decrease in friction coefficient associated with increasing sliding speed.

2.4. COMPARISON WITH AVAILABLE DATA

2.4.1. FREE ROLLING. Under conditions of zero longitudinal slip and inclination angle, the tire side force equation (equation A-21) may be written in the form

$$-\frac{F_{yw}}{\mu F_z} = \begin{cases} \bar{\alpha}, & \text{for } -.5 \leq \bar{\alpha} \leq .5; \\ 1 - \dfrac{1}{4\bar{\alpha}}, & \text{for } |\bar{\alpha}| > .5; \end{cases} \tag{7}$$

where $\bar{\alpha}$, the normalized sideslip angle, is given by

$$\bar{\alpha} = \frac{C_\alpha \tan\alpha}{\mu F_z}, \tag{8}$$

with C_α, the tire cornering stiffness, defined in accordance with convention [24] as

$$C_\alpha \equiv -\left.\frac{\partial F_{yw}}{\partial \alpha}\right|_{\alpha=0}, \tag{9}$$

and μ , the interface friction coefficient, given by

$$\mu = \mu_o(1 - A_s V_s) \tag{10}$$

V_s is the sliding velocity of the tire rubber and μ_o is the value of the interface friction coefficient at $V_s = 0$. The sliding velocity is given by

$$V_s = u_w \tan\alpha \tag{11}$$

The normalized form of the side force equation for the free-rolling tire (equation 7) is depicted graphically in Figure 2a. Figure 2b is a "carpet plot," i.e., a graph showing the dependence of F_{yw} on the dimensional variables α and F_z, constructed using equation 6 and the parameter values shown on the figure. A carpet plot derived experimentally from measurements with a representative automotive tire [25] is given in Figure 2c.

The excellent qualitative agreement between calculated and measured side force characteristics for the freely rolling tire is apparent from a comparison of Figures 2b and 2c. The principal discrepancy between the two plots is attributable to the model's assumption that the effect of tire normal load (F_z) on cornering stiffness (C_α) is negligible. Within the context of the present analysis, the inaccuracy associated with this simplification is regarded as insignificant. For other applications requiring greater accuracy, revision of the model to take appropriate account of the influence of F_z on C_α is indicated.

2.4.2. STRAIGHT RUNNING. Under conditions of zero sideslip and inclination angles, the longitudinal tire-force equation (equation A-20) may be written as:

$$-\frac{F_{xw}}{\mu F_z} = \begin{cases} \bar{s}, & \text{for } -.5 \leq \bar{s} \leq .5; \\ 1 - \dfrac{1}{4\bar{s}}, & \text{for } |\bar{s}| > .5; \end{cases} \tag{12}$$

(a) Plot of Normalized Side Force Equation (Eq. 7)

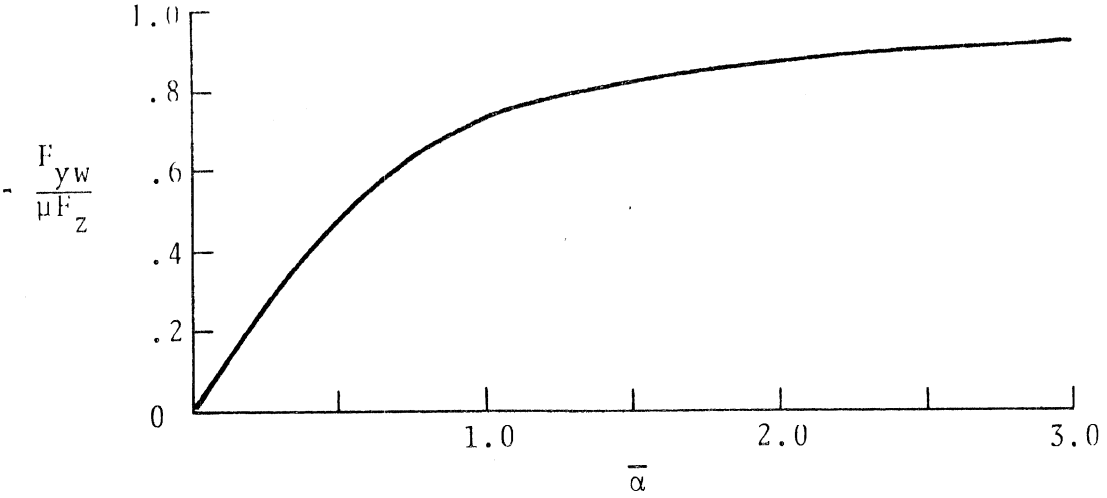

(b) Carpet Plot Computed Using Above Side Force Equation

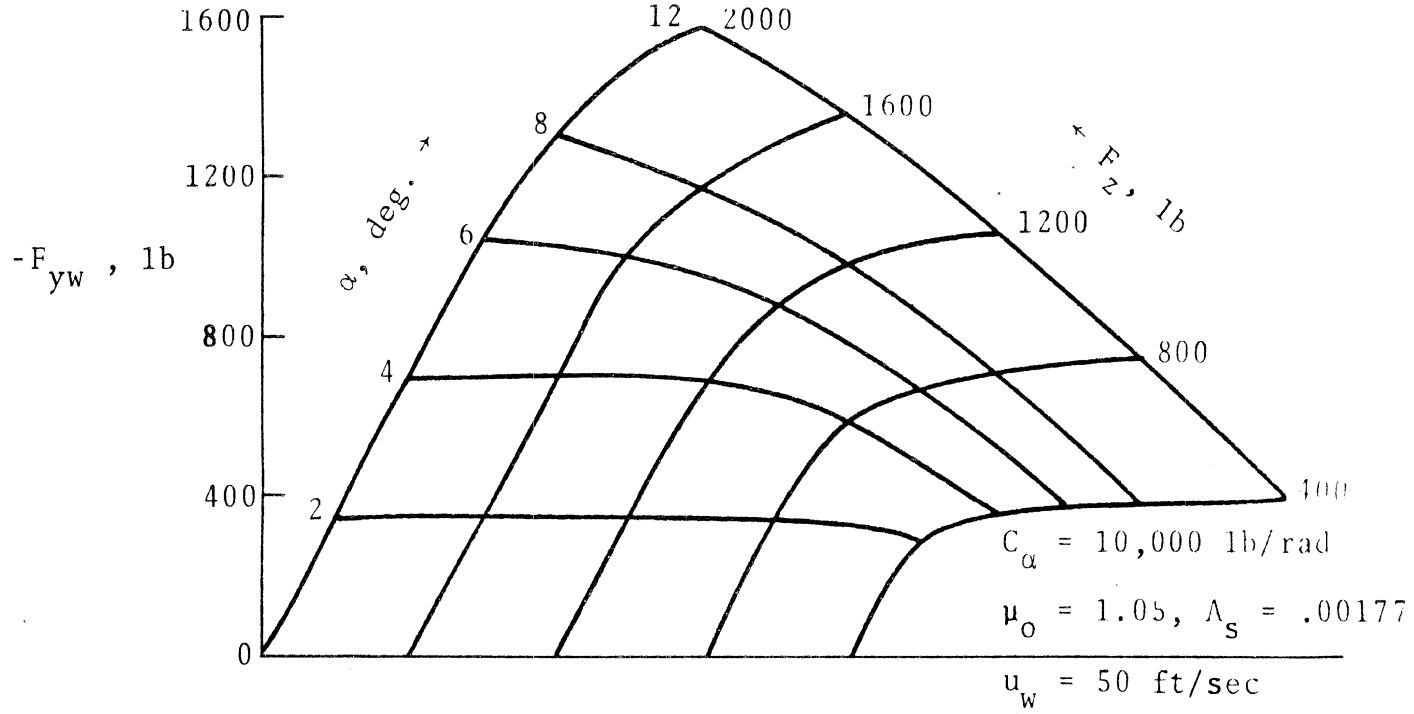

(c) Typical Experimentally Derived Carpet Plot (Ref. 25)

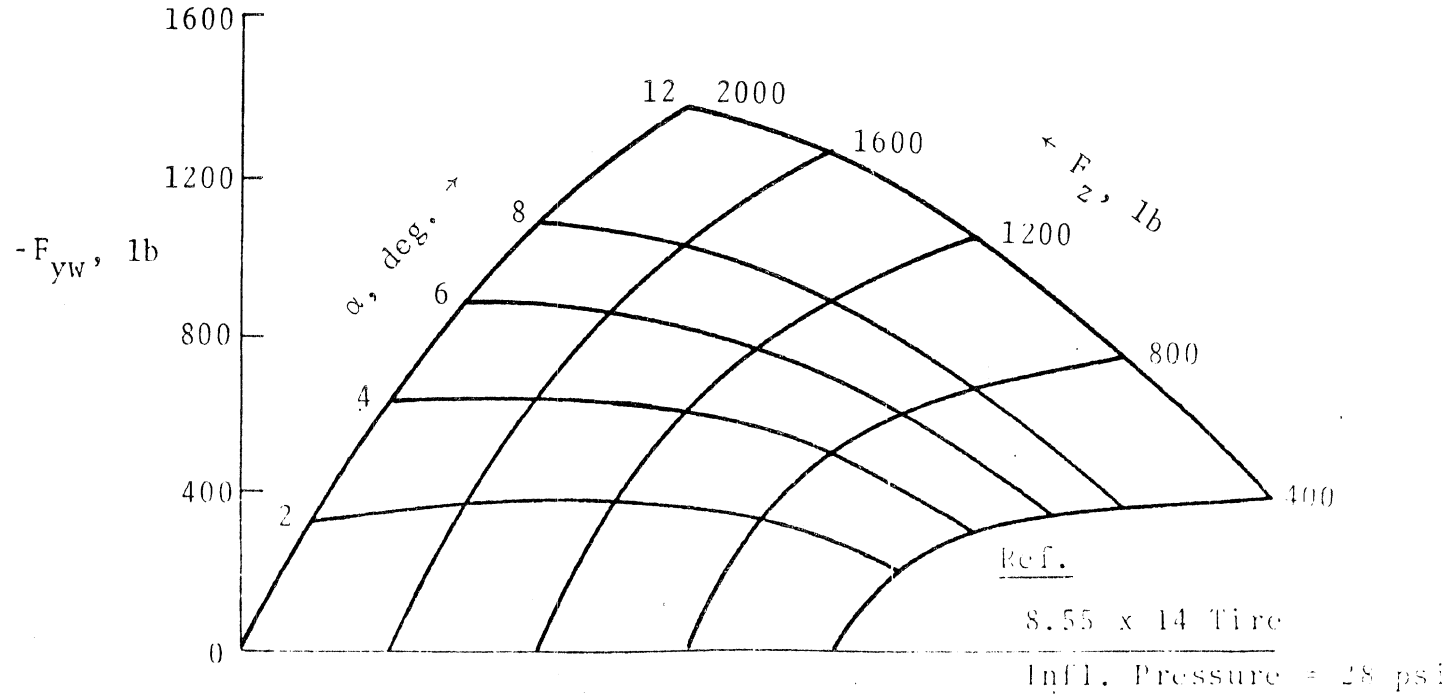

FIGURE 2. FREE ROLLING TIRE SIDE FORCE CHARACTERISTICS

where

$$\bar{s} = \frac{C_s s}{\mu F_z (1-s)} \quad , \tag{13}$$

$$C_s \equiv - \left. \frac{\partial F_{xw}}{\partial s} \right|_{s=o} \tag{14}$$

with μ again given by equation 10, but with the sliding velocity in this case given by

$$V_s = u_w s \quad . \tag{15}$$

The analogy between C_s, the tire longitudinal stiffness, and C_α, the lateral stiffness (see equation 9), is apparent.

The normalized form of the straight-running longitudinal tire force equation (equation 12) is depicted graphically in Figure 3a. (It will be noted that the functions depicted in Figures 2a and 3a are identical--compare equations 7 and 12.) Figure 3b is a plot of F_{xw}/F_z versus s, for two different values of u_w, computed using equation 12 and the parameter values indicated on the figure.

Examination of the curves shown in Figure 3b reveals that equation 12 is certainly in agreement with generally accepted conceptions of the "typical" brake force/slip characteristic [e.g., 26,27]. The predictions also compare very favorably with particular experimental data to be found in the literature--see, for example, curves (1) and (2) of Figure 3c. On the other hand, experimental data may also be found which differ rather markedly in character from the calculated results--for example, see curves (3) and (4) of Figure 3c. There are many possible explanations for these differences, including, of course, experimental inaccuracies. However, the most likely explanation involves the relationship between the tire-road friction coefficient and speed. The calculated curves (Figure 3b) are based on a linear μ-V_s relation (equation 10) and a particular value chosen for its slope.

(a) Plot of Normalized Longitudinal Force Equation (Eq. 12)

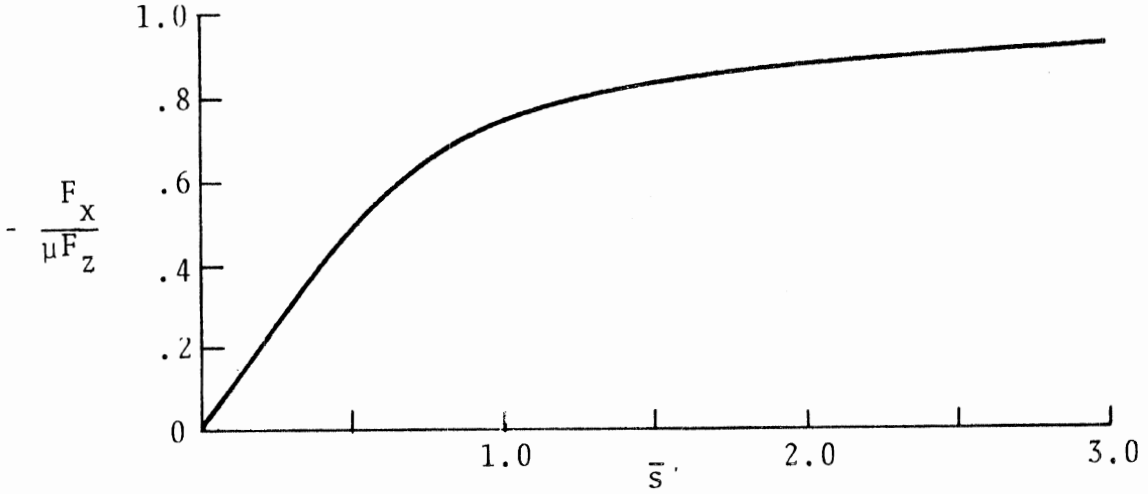

(b) Plot of F_{xw}/F_z vs. s Computed Using Above Equation

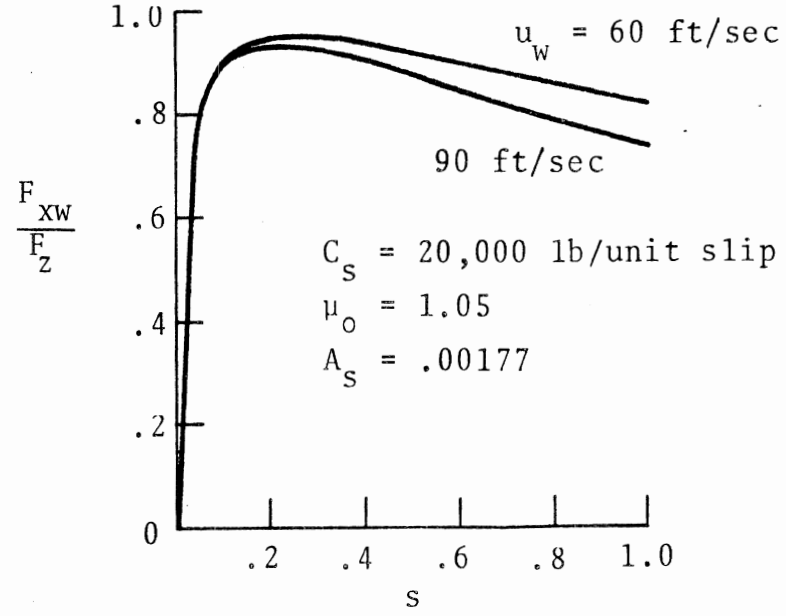

(c) Experimentally Derived Plots of F_{xw}/F_z vs. s

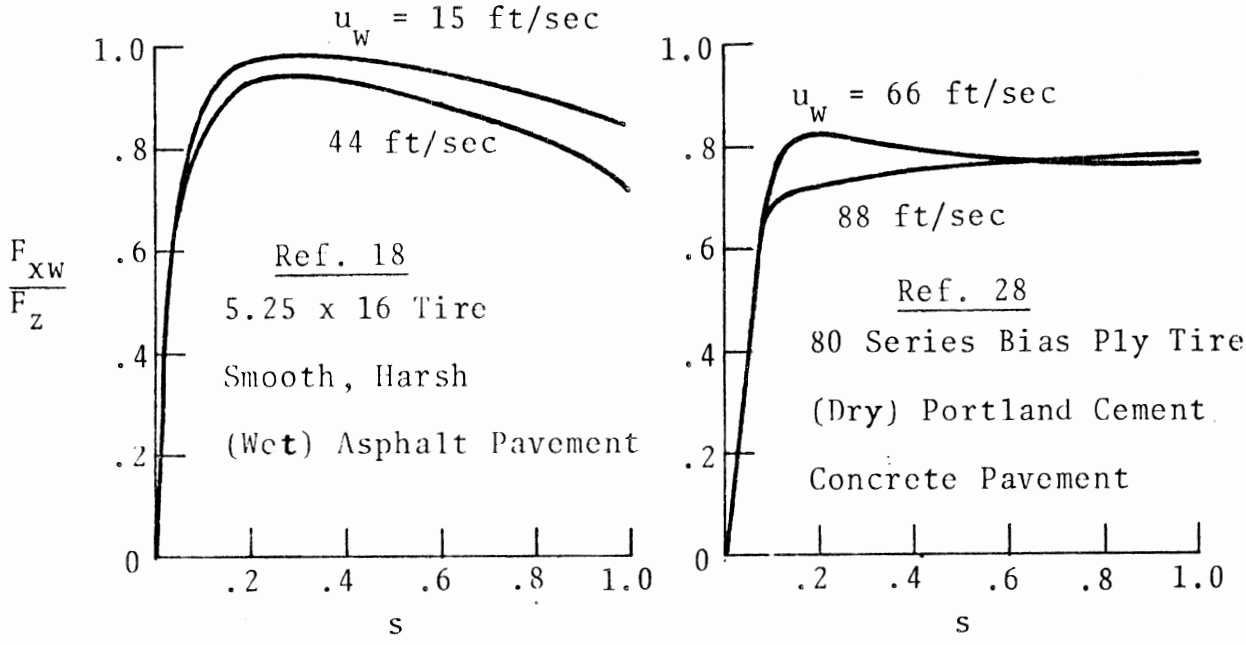

FIGURE 3. STRAIGHT RUNNING LONGITUDINAL TIRE FORCE CHARACTERISTICS

Merely changing the value of the μ-V_s slope can produce a rather substantial change in the nature of the force slip curve (see Figure 4). A change in the basic form of the μ-V_s relation can produce even more pronounced effects (see Figure 4 again). As noted in the model derivation (Appendix A), the assumption of the linear μ-V_s relation is a pragmatic one, made, in the absence of substantial experimental data, in keeping with the pragmatic philosophy of the present study. Additional work to develop a more general μ-V_s relation, which might account for a broad range of experimentally observed force-slip characteristics, represents a promising line of inquiry for future research. For purposes of the present study, however, it is felt that the linear approximation agrees sufficiently with the qualitative aspects of experimental findings to justify its adoption.

2.4.3. COMBINED SIDE AND LONGITUDINAL SLIP. Figure 5 compares calculated and measured values of F_{xw}/F_z and F_{yw}/F_z under conditions of combined side and longitudinal slip. Figures 5a and 5b, respectively, are typical theoretical and experimental curves of F_{xw}/F_z versus s, for $\alpha = 0°, 4°, 10°$. Figures 5c and 5d are similar curves of F_{yw}/F_z versus α, for $s = 0.1, 0.2, 0.4, 1.0$. All of the experimental data shown are from the recent paper by Holmes and Stone [17].

The results depicted in Figure 5 speak for themselves. The discrepancies between the calculated and measured results can be attributed to anomalies in the structure or testing of the particular tire employed in the experiment, rather than to a basic incompatibility between the model and the actual performance of pneumatic tires. Accordingly, the derived equations for F_{xw} and F_{yw}, equations A-19 through A-21 appear to constitute a tire mechanics model which agrees qualitatively with available experimental data, and represents concisely the complex phenomena of influence in terms of a limited number of basic parameters, each having an effect on gross vehicle response that is amenable to systematic study through computer-aided analysis.

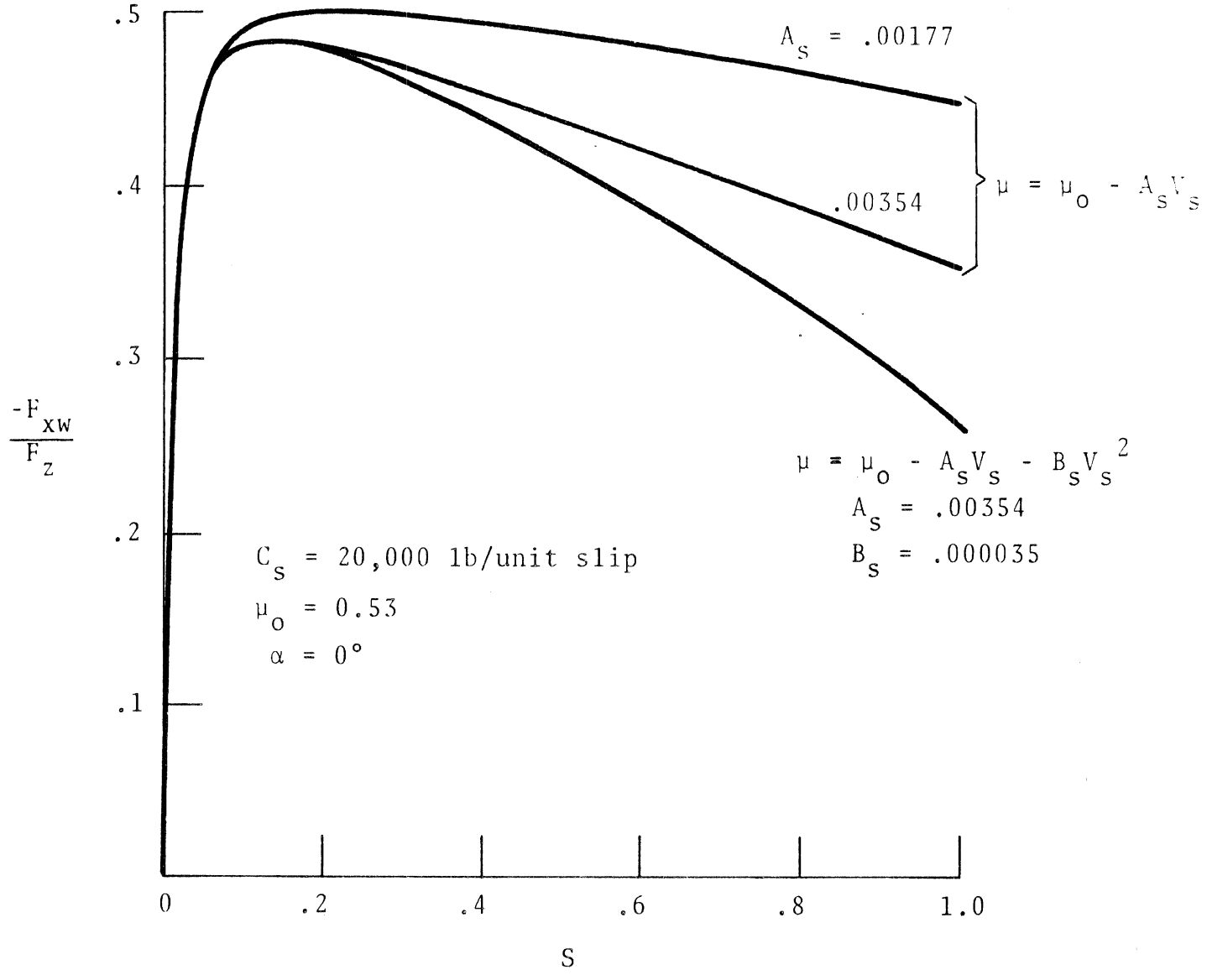

FIGURE 4. INFLUENCE OF FRICTION/VELOCITY RELATIONSHIP ON LONGITUDINAL TIRE FORCE CHARACTERISTICS COMPUTED FROM EQUATION 12

(a) Computed from Equations A-19 through A-21

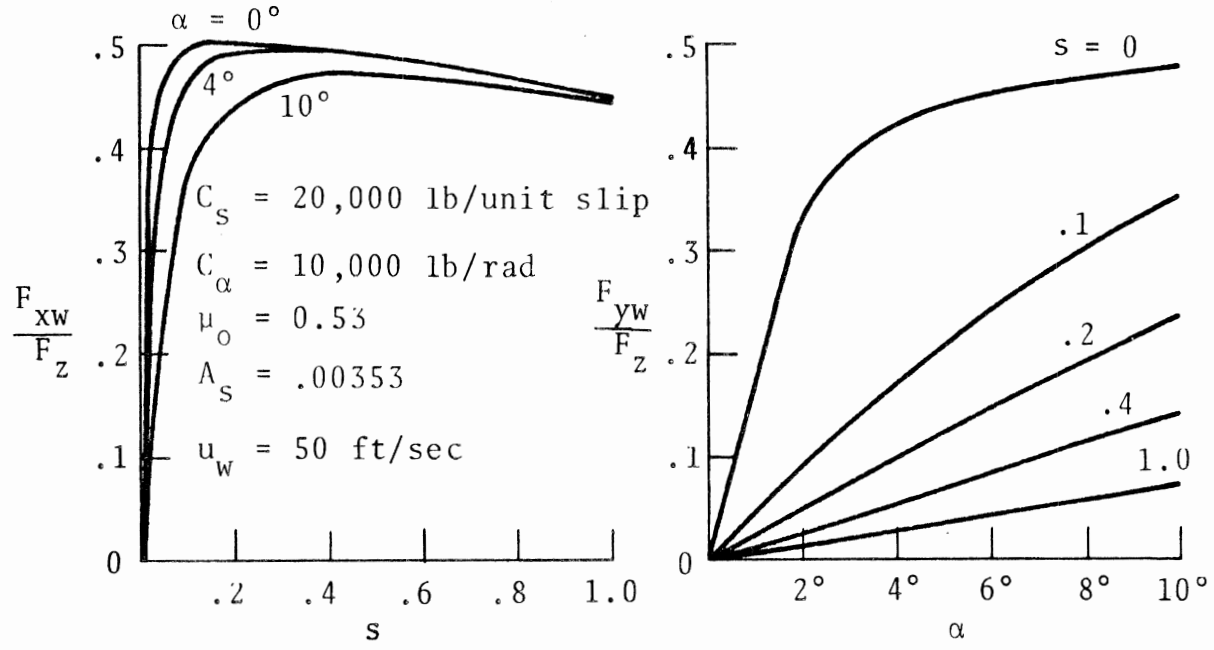

(b) Experimental Data From Holmes and Stone [18]

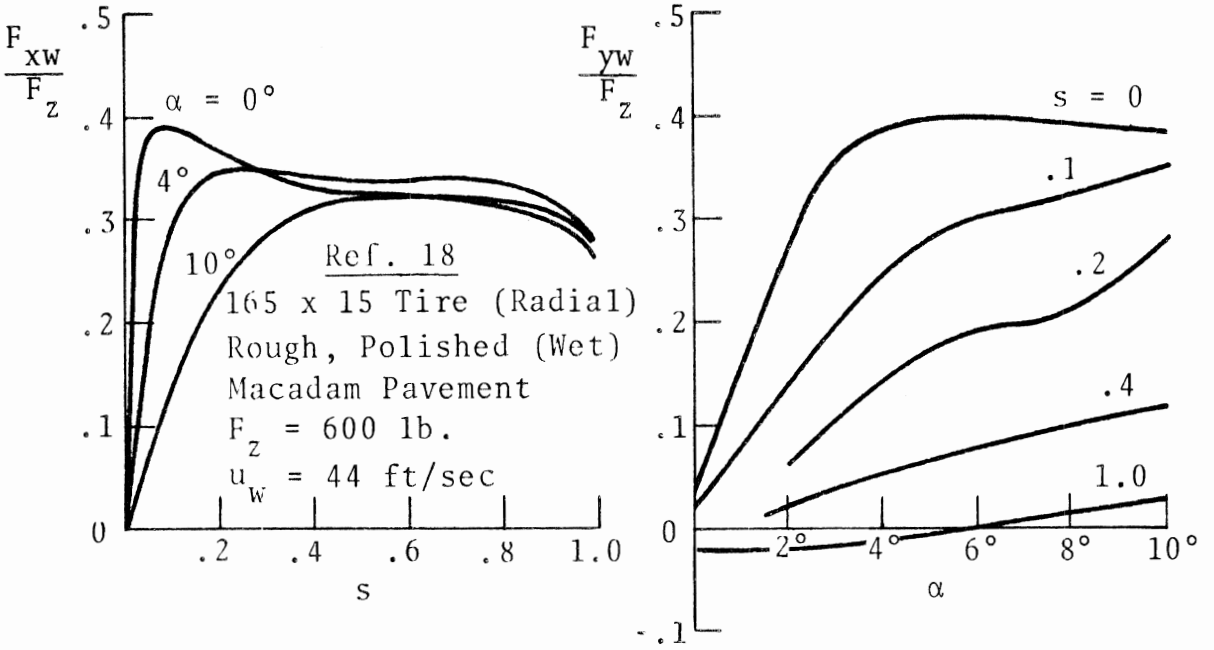

FIGURE 5. TIRE FORCE CHARACTERISTICS - COMBINED SIDE AND LONGITUDINAL SLIP

3. DEVELOPMENT AND APPLICATION OF THE ANALOG SIMULATION

3.1. VEHICLE MECHANICS REPRESENTATION

Figure 5A is a block diagram of the horizontal plane simulation model developed for this study. Everything outside of the "tire mechanics" block in the lower center of the diagram comes under the heading of "vehicle mechanics."

As explained in the Introduction, the direction of primary emphasis in the model formulation was towards complete characterization of the tire's traction mechanics. Given the inevitable limitations on total simulation "size" associated with available computer capacity, this priority decision imposed a rigid constraint on the degree of complexity in the representation of the mechanics of the vehicle. In spite of this, the model represents a very sizeable simulation, involving vehicle dynamics, vehicle statics, wheel rotation dynamics, tire kinematics, trajectory kinematics, steering system dynamics, aerodynamics, and force and moment component resolution. The equations of motion and kinematic relationships employed to describe the mechanics of the vehicle are presented in full in Appendix B.

The major simplification in the vehicle dynamics analysis is the assumption that the vehicle is a rigid mass constrained to move in a horizontal plane. This simplication was not taken lightly because it is known that the influence of roll and pitch dynamics on the directional response of automotive vehicles can be important [23]. One such manifestation is the "load transfer effect," where inertia-induced changes in vertical tire loading couple with nonlinear mechanical properties of the tire to produce significant variations in lateral and longitudinal forces produced at the tire-road interface. Although the analysis does not completely account for roll and pitch dynamics, the load transfer process is approximated by quasi-static relationships (similar approximations have been made in the past by other investigators, e.g., Goland and Jindra [28]).

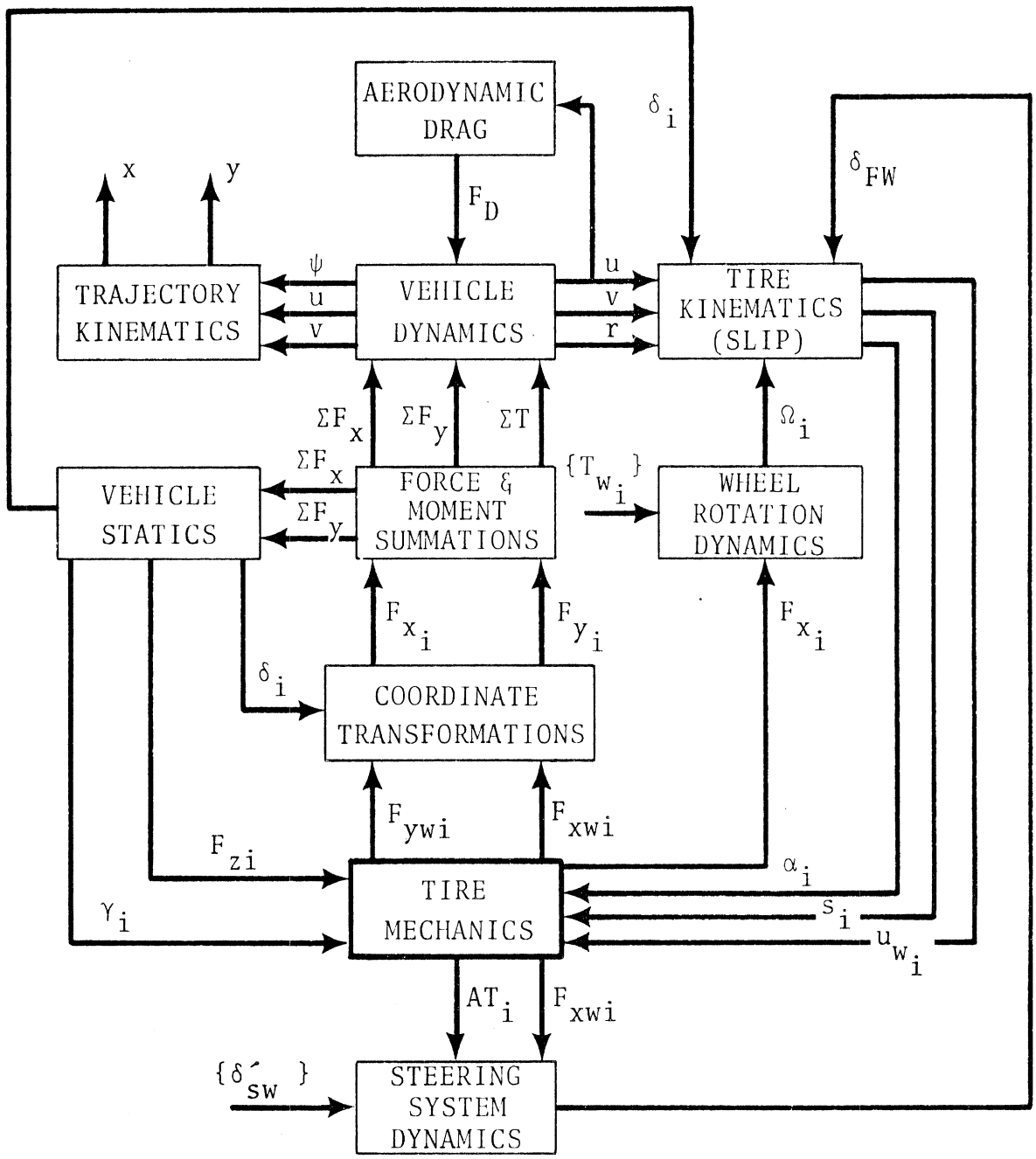

FIGURE 5A. BLOCK DIAGRAM OF HORIZONTAL PLANE SIMULATION

A second class of roll-pitch-yaw coupling effects exerting significant influence on the directional response of the motor vehicle are the variations in tire-road interface kinematics due to vehicle roll and pitch. A procedure employed here to compensate for the neglect of sprung mass roll dynamics consists of quasi-static calculations to account for (1) wheel roll-steer and (2) wheel camber effects. Hales [30] has demonstrated the validity of quasi-static approximation to account for these effects in both steady-state and dynamic response calculations.

The wheel rotation degrees of freedom have not been considered in previous vehicle handling analyses [e.g., 19-21, 31-35]. As discussed in Section 2.2, the objectives of the present study demand this extension of the state of the vehicle simulation art. Accordingly, the vehicle mechanics representation includes equations describing the rotational dynamics of each wheel, which permit the computation of instantaneous values of longitudinal slip ratio for each tire when either braking or driving torques are applied.

3.2. COMPUTER MECHANIZATION

The equations and functions representing the vehicle-tire system were mechanized on an Applied Dynamics AD4 analog computer (half-expanded) with extra summers and multipliers. In order to minimize computer equipment needs, the analog circuits for calculating tire forces were time-shared using the track-store integrators, electronic switches, and logic elements available on the AD4. Each computed tire force was updated every 4 milliseconds, i.e., 250 times per second (this update frequency appears to be adequate for representing continuous phenomena occurring at frequencies up to approximately 40 Hertz). In all other respects the analog mechanization was conventional in that the computing elements operated in parallel in producing a real-time solution.

3.3. MODEL VALIDATION

The scope of this study did not allow for any testing to experimentally validate the developed simulation. It was possible, however, to compare the present simulation results with results

obtained previously by other investigators. Figure 6 is one example of such a comparison. The data shown are equilibrium values of path curvature as a function of steer angle and applied drive torque (or thrust), computed (1) by Radt and Pacejka [36], and (2) by us, using the developed simulation with corresponding values for all input data.

Comparisons have also been made with results produced by a digital mechanization of a mathematical model developed by McHenry, et al. [37]. The digital model includes a suspension system, unsprung-mass degrees of freedom, and roll, pitch, and bounce dynamics. Figure 7 is a comparison of trajectories and yaw-rate time histories produced by the respective models for a rapid lane-change maneuver. The two sets of results are nearly identical. Similar comparisons for calculations of response to moderate step inputs of front wheel angle and brake torque also demonstrate close agreement. For brake inputs large enough to cause one wheel to lock, however, the responses predicted by the two models are considerably different; the results produced by the digital simulation model are characterized by lower yaw rates and sideslip velocities, i.e., less tendency to spin (see Figure 8). Undoubtedly, the wheel degree of freedom and the difference in the method of computing tire forces are the main reasons for the discrepancy. Vehicle testing is required to evaluate the accuracy of the model in predicting "skidding" behavior when one or more wheels lock.

3.4. ON THE SCOPE OF THE PARAMETRIC STUDIES

The generation of a mathematical model of a motor vehicle and its tires and its subsequent mechanization for computer solution is basically a straightforward task from a conceptual point of view. Admittedly, judgements must be made as to details to be included in the model so the developed simulation will be sufficiently broad in scope and accuracy to justify the conclusions drawn. However, it is much more difficult, in both conception and execution, to utilize the generated simulation to acquire results amenable to meaningful interpretation.

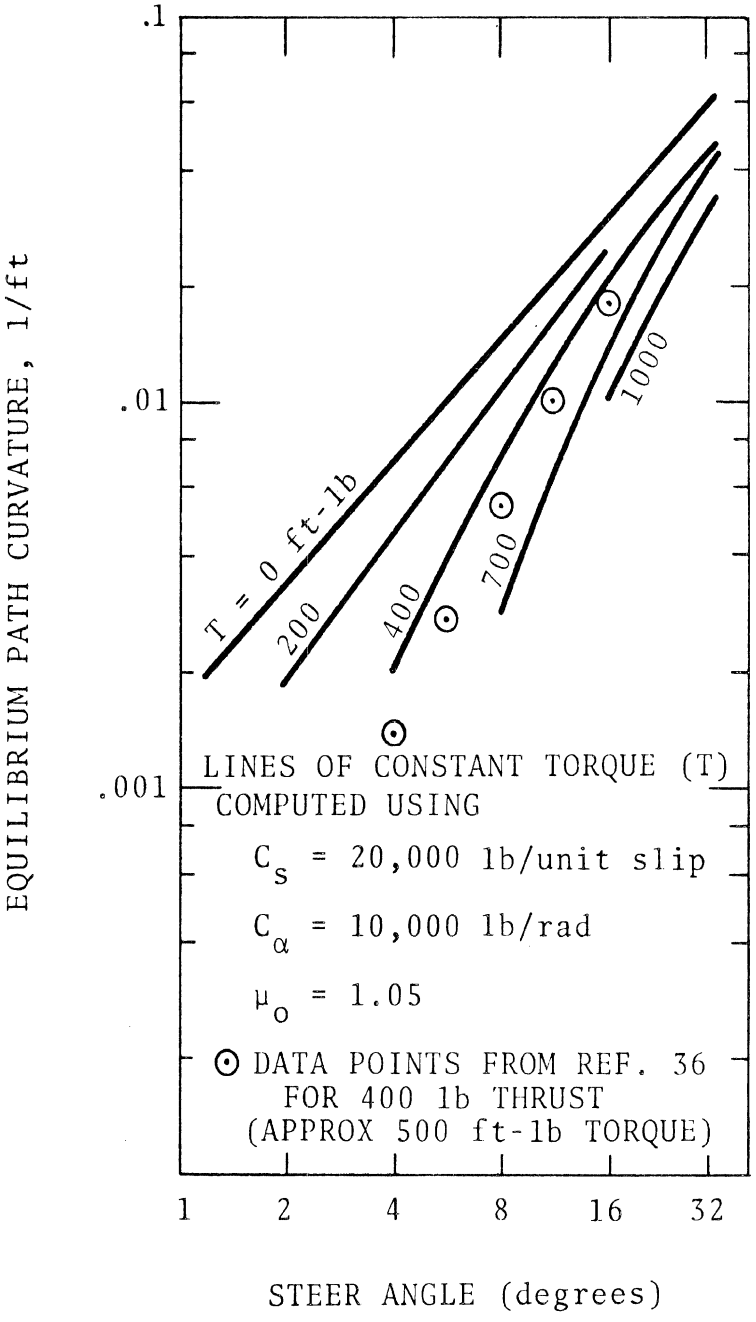

FIGURE 6. COMPARISON OF STEADY TURNING PREDICTIONS WITH RESULTS FROM RADT AND PACEJKA [36]

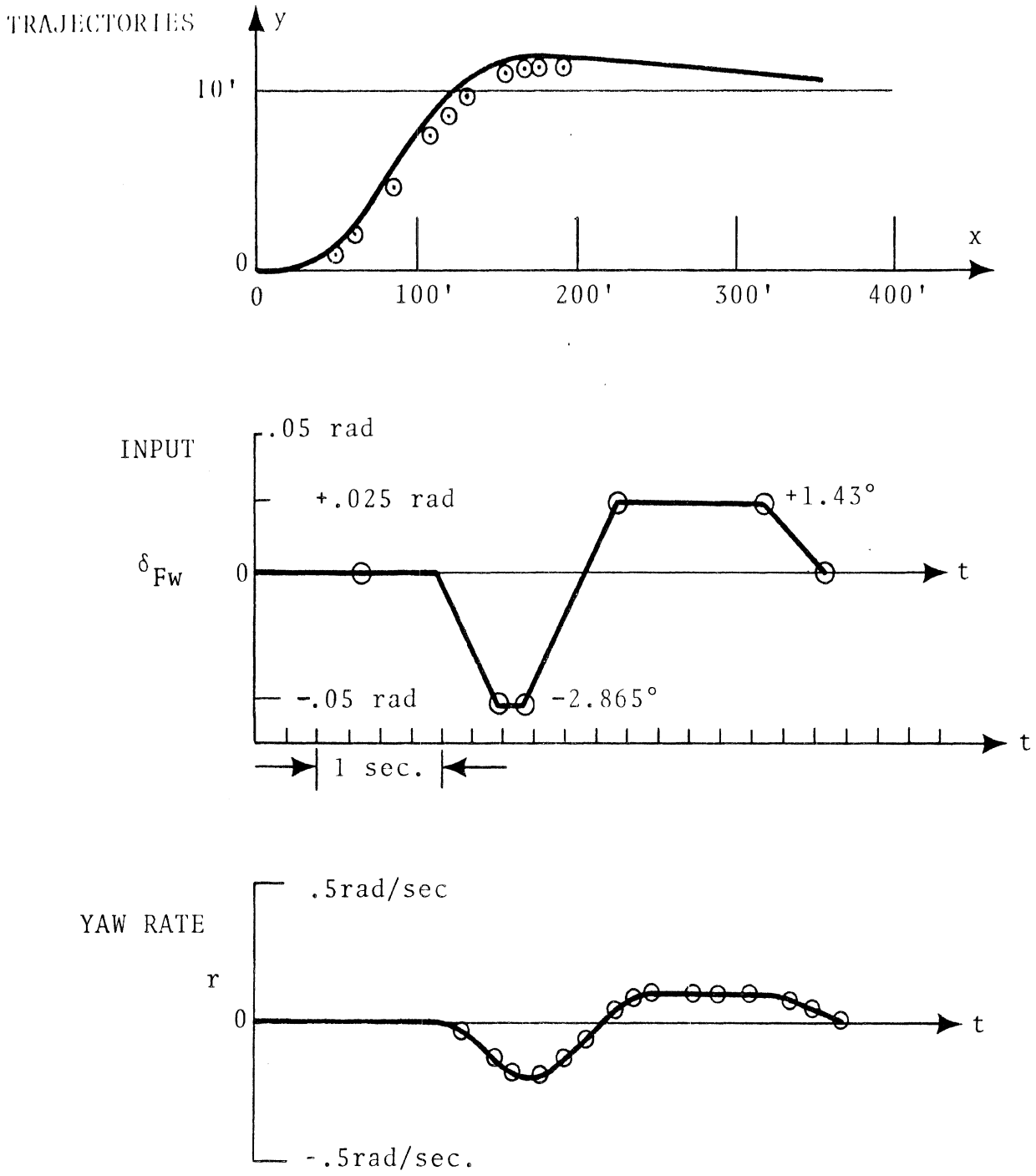

FIGURE 7. COMPARISON OF LANE CHANGE MANEUVER CALCULATIONS: HSRI ANALOG SIMULATION AND CORNELL DIGITAL SIMULATION [37]

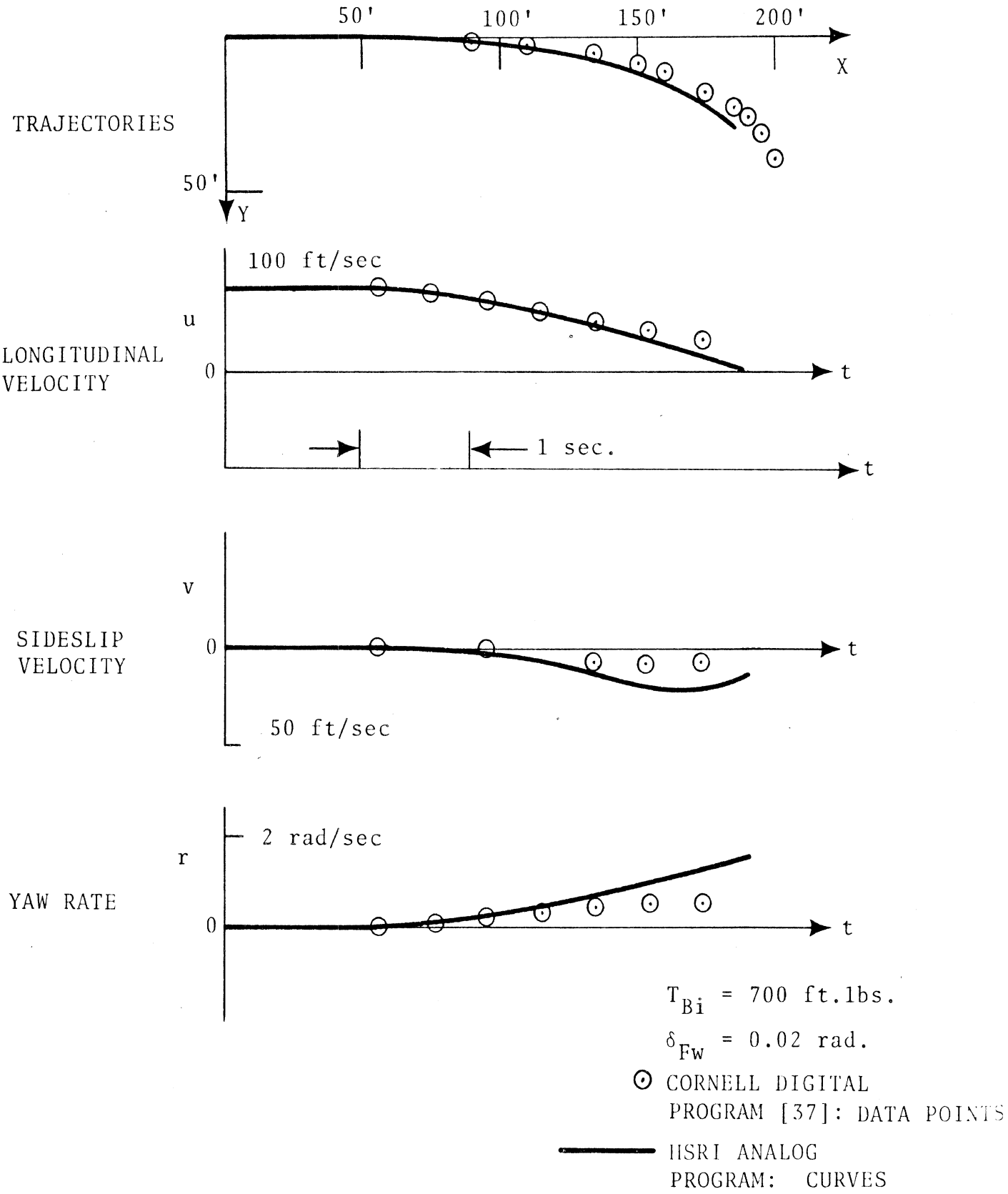

FIGURE 8. COMPARISON OF COMBINED STEERING/BRAKING MANEUVER CALCULATIONS: HSRI ANALOG SIMULATION AND CORNELL DIGITAL SIMULATION

This problem, which involves making value judgements about vehicle behavior (good, bad, or indifferent), has perplexed many investigators [c.f., 38-40]. Its inherent difficulty stems from the lack of merit-criteria applicable either to matters of highway safety or to matters involving control quality and control optimization. Given the absence of established criteria for evaluating the performance of either the driver-vehicle-tire system or the vehicle-tire system, and the understanding that the development of such criteria would constitute a major research activity far beyond the scope of the investigation, it was necessary to improvise in this study.

To a certain extent the criterion problem was sidestepped by restricting the objectives of the study. As stated in the Introduction, the third task consisted of a parametric investigation "to examine the extent to which a vehicle's responses to various specified combinations of brake, throttle, and steering control inputs are affected by realistic variations in the values of principal tire mechanical characteristics." Thus, we have restricted the study to a determination of the influence of tire-traction parameters on a variety of open-loop vehicle maneuvers whose specification and selection were not established a priori but rather evolved through a process relying heavily on the judgement of the researchers involved. To a certain extent, a pragmatic viewpoint was adopted. It appeared logical to select maneuvers that involve physically realistic steering wheel angle and braking- or driving torque inputs such as are required to execute extreme turns, lane changes, and rapid stops. An attempt was made to define these maneuvers by a systematic process employing: (1) subjective formulation by a panel of researchers; and (2) experimental efforts utilizing an instrumented vehicle. In the final analysis, however, the maneuvers employed to develop the findings discussed below derive from a combination of the efforts mentioned above, plus substantial trial and error, supplemented by knowledge of vehicle dynamics and just plain reasoning.

Since this study was conceived as a preliminary step in defining tire-traction parameters and relating them to the pre-crash "safety quality" of a motor vehicle, attention was centered on situations in which the vehicle is pushed to the limit imposed by the frictional couple prevailing at the tire-road interface. This view is equivalent to defining how tire-traction parameters (1) influence the development of a "skid" and (2) determine "skidding" behavior following its initiation. This is a concise but rather unscientific statement of the study objective, since the term "skid" has yet to be given a precise meaning.

From the lay driver's point of view, a "skid" is a condition in which the controls of his vehicle suddenly lose their effectiveness. The driver also associates uncontrollable vehicle spinning and sideslipping with the skidding condition. Such a definition is relative, however, since the more highly skilled the driver, the further the boundary between control and loss of control will be moved into the "skidding" regime. Further, the trajectory (or path) of a motor vehicle is extremely sensitive to the manner and rate with which the condition of maximum shear force is approached. For example, there are combinations of steering wheel displacement and drive thrust which if applied suddenly would cause the vehicle to respond in a highly undesirable manner, whereas if they are applied slowly the vehicle achieves an equilibrium turning condition.

Time, funds, and ingenuity did not permit a thorough investigation of this highly nonlinear phenomenon, namely, "skidding." Rather the objectives of the study and the pragmatism of the approach restricted the investigation to consideration of four maneuvers:

1. Steady-state turning
2. Braking from a steady turn
3. Response to a steering increment at high lateral accelerations
4. A combined lane-change and braking maneuver

The influence of tire-traction parameters on the performance of a prototypical vehicle undergoing each of these maneuvers is discussed in Section 4.

3.5. VARIATION OF TIRE-TRACTION PARAMETERS

The generalized functional forms of the tire-traction relationships, equations 3 through 5, involve the kinematic variables, F_z, α, s, γ, V; the nominal tire-road friction coefficient, μ_o; and an unspecified number of variables describing the properties of the tire, $t_1,\ldots,t_n$, denoted as "tire mechanics characteristics." Reference to equations A-20 through A-29 of Appendix A reveals that the specific tire-traction relationships derived therein involve a total of five tire mechanics characteristics, C_α, C_s, C^*_γ, x_p, and A_s (in addition to μ_o). These are not the only tire properties influencing the directional response of the automobile; the equations describing wheel rotation dynamics presented in Appendix B involve four others, C_z, C_x, R, and RR, each of which affects wheel slip, and thus, indirectly influences the tire shear force components.

Stringent limitations on time and funds made it necessary to restrict the domain of the parametric studies to a small portion of the overall multi-dimensional "space" defined by the real-world variability of each of these independent variables. Based on (1) judgements of the relative importance of each potential variable with respect to gross trajectory response, and (2) availability of experimental data from which realistic variation levels and bounds could be established, it was decided to concentrate on studying the influence of the two stiffness parameters, C_α and C_s, and the nominal friction coefficient, μ_o.

Three levels were chosen for each of the stiffness parameters, the middle value corresponding to a "typical" value for conventional passenger tires of U.S. manufacture, and the end points designed essentially to bracket the ranges of values for real or

practical tires. The values of C_α were based on data from [5, 15, 32, 41, 42]; those for C_s on data from [11-14, 43]. Figures 9 and 10 illustrate how variations over the ranges selected for C_α and C_s, respectively, influence overall traction performance of a tire operating with combined lateral and longitudinal slip.

Calculations were made for nominal friction coefficients of 0.53 and 1.05. Originally calculations were also to be made for friction coefficients much lower than $\mu_o = 0.53$, but substantial scaling difficulties were encountered and time did not permit reworking the computer mechanization to accomplish this objective.

Values for all other tire mechanics characteristics were fixed throughout the simulation program, as indicated in Table 1. These values are intended to be representative of typical U.S. tires, estimated on the basis of available data.

TABLE 1.
VALUES OF TIRE MECHANICS CHARACTERISTICS EMPLOYED IN SIMULATION STUDY

SYMBOL	NAME	VALUE(S)
C_α	Cornering stiffness	6,000; 10,000; 14,000 lbs/rad
C_s	Longitudinal stiffness	5,000; 20,000; 40,000 lbs/unit slip
μ_o	Nominal friction coefficient	0.53, 1.05
C^*_γ	Relative camber stiffness	0.167
x_p	Pneumatic trail	0.1 ft.
A_s	Friction reduction factor	0.00335 sec/ft
C_z	Vertical deflection rate	0.001 in/lbs
C_x	Vertical force offset rate	0.0005 in/lbs
R	Nominal tire radius	1.145 ft.
RR	Rolling resistance factor	0.02

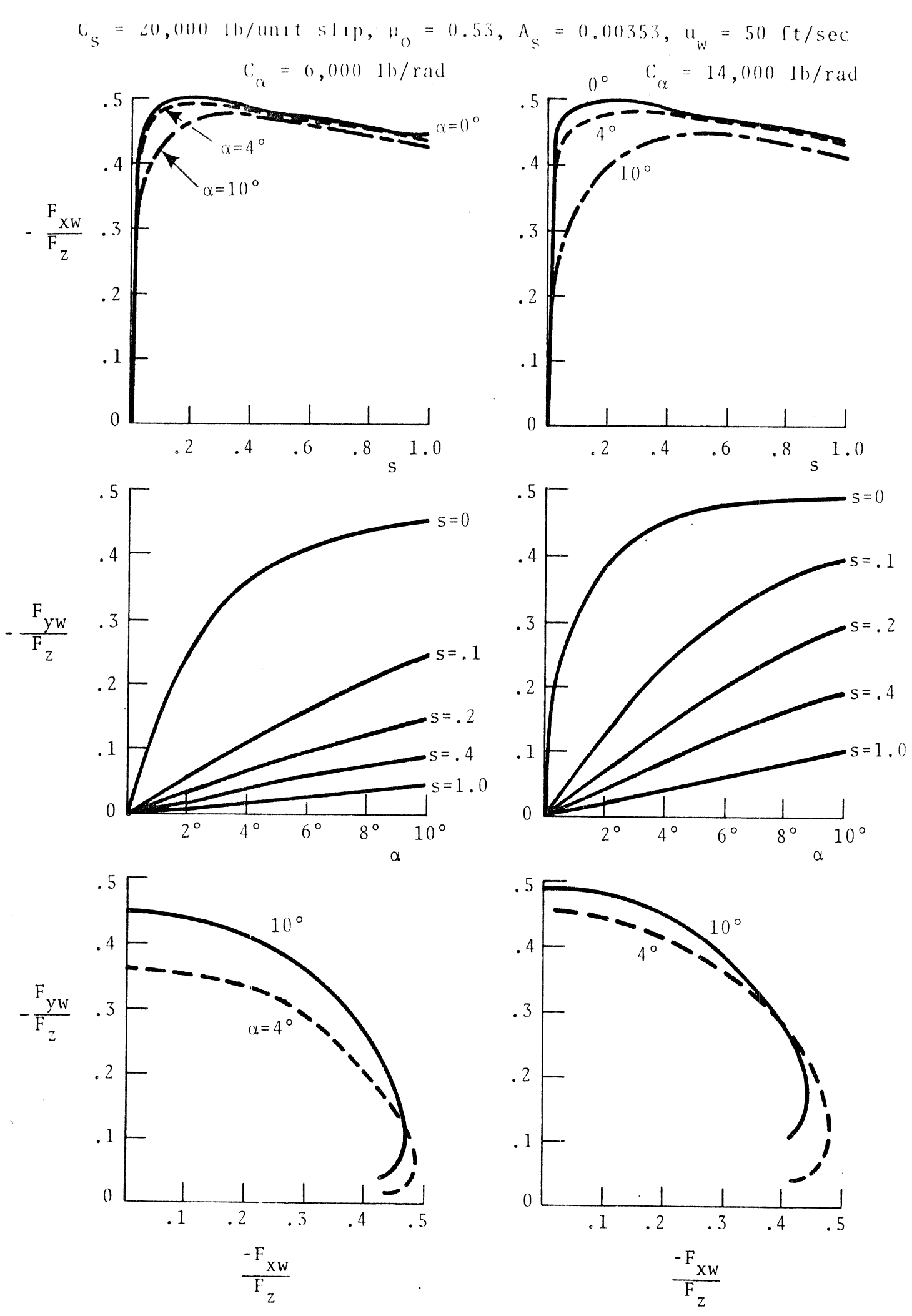

FIGURE 9. INFLUENCE OF VARIATION OF C_α ON TIRE TRACTION PERFORMANCE AS COMPUTED FROM EQUATIONS A-19 THROUGH A-21

C_α = 10,000 lb/rad, μ_o = 0.53, A_s = 0.00353, u_w = 50 ft/sec

C_s = 5,000 lb/unit slip

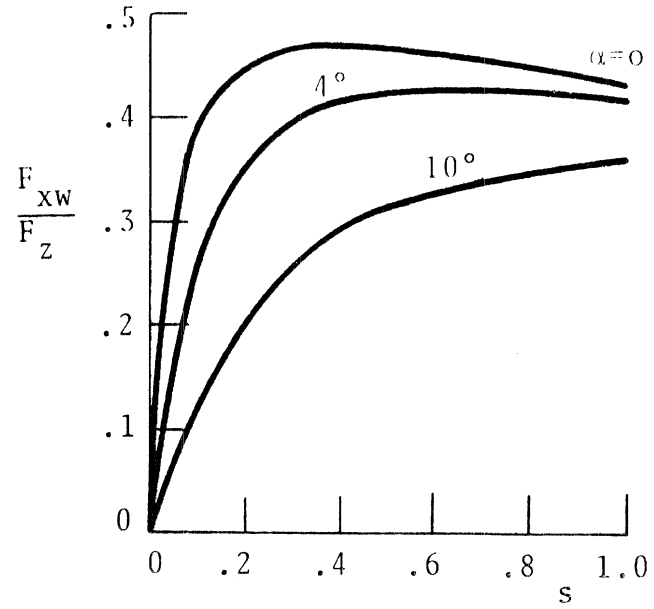

C_s = 40,000 lb/unit slip

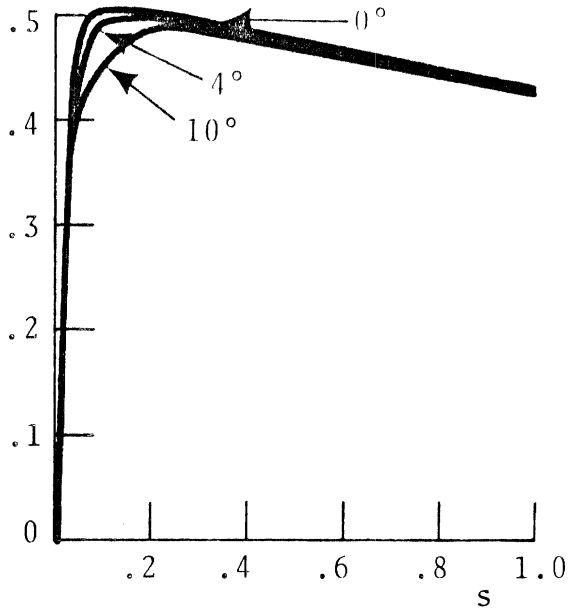

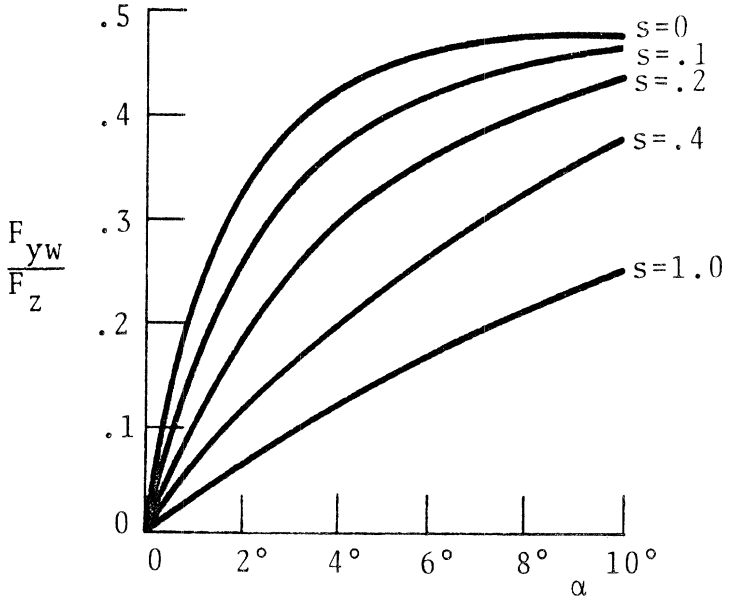

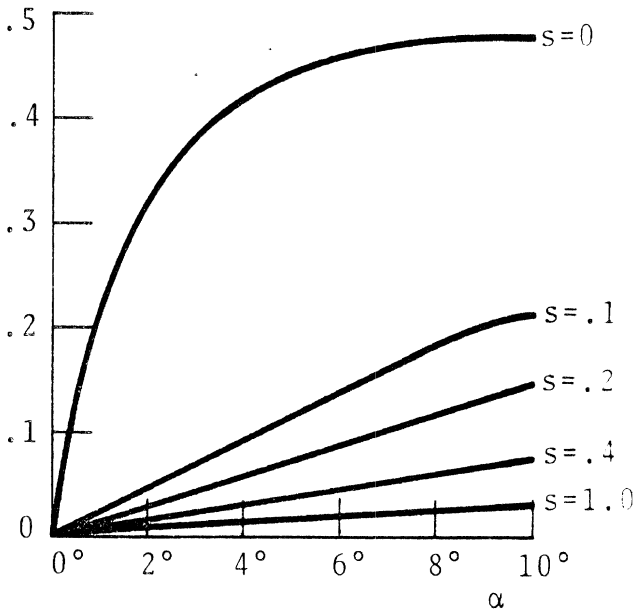

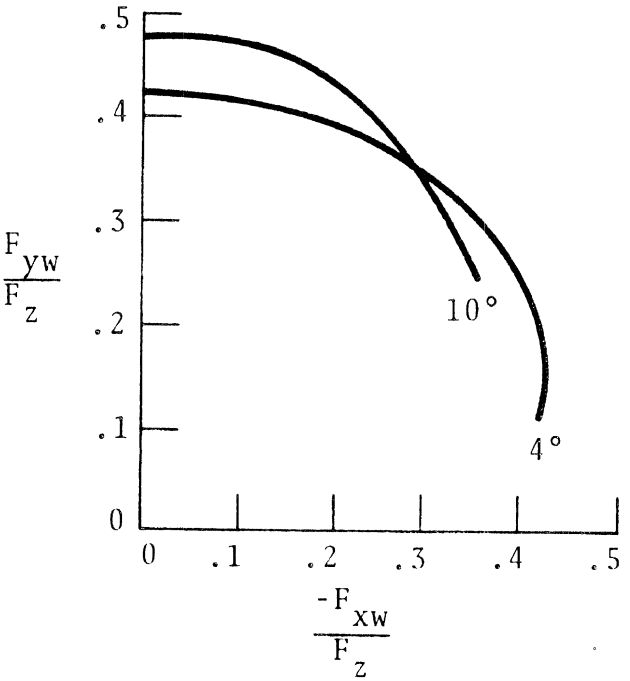

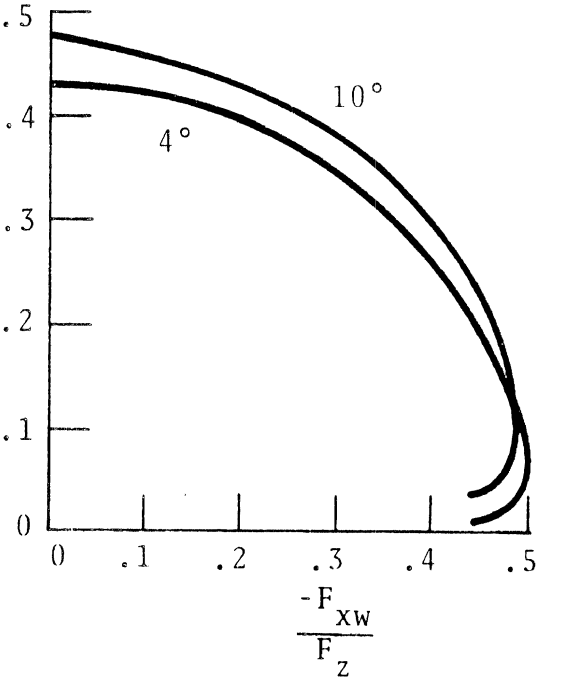

FIGURE 10. INFLUENCE OF VARIATION OF C_s ON TIRE TRACTION PERFORMANCE AS COMPUTED FROM EQUATIONS A-19 THROUGH A-21

3.6. VEHICLE PARAMETERS

Values of all vehicle parameters involved in the simulation were selected to be representative of a typical full-size American sedan. The values used are given in Table 2.

TABLE 2.
VALUES OF VEHICLE CHARACTERISTICS
EMPLOYED IN SIMULATION STUDY

SYMBOL	NAME	VALUE
m	Mass	124 slugs
t	Half tread	2.5 ft
a	Distance, CG to front axle	4.5 ft
b	Distance, CG to rear axle	5.5 ft
I	Yaw moment of inertia	3000 slug-ft^2
h	CG height	2.0 ft
$K_{f\phi}$	Front roll stiffness	24,000 ft-lb/rad
K_{ss}	Steering stiffness	6,000 ft-lb/rad
I_{wz}	Wheel inertia about kingpin	0.75 slug-ft^2
K_p	Kingpin offset	0.2 ft
C_f	Steering damping	20 ft-lb/rad/sec
C_{sR}	Rear roll steer coefficient	0.04
$K_{r\phi}$	Rear roll stiffness	12,000 ft-lb/rad
I_{wy}	Wheel inertia about axle	1.5 slug-ft^2
K_f	Front spring rate	4,000 lbs/ft.
C_D	Drag coefficient	0.45
A_D	Cross-sectional area	25.5 ft^2
C_w	Wheel damping	0.15 ft-lbs/rad/sec.

4. RESULTS OF THE PARAMETRIC STUDY

4.1. INFLUENCE OF TIRE-TRACTION PARAMETERS ON STEADY AND MAXIMUM TURNING PERFORMANCE

The most complete published analysis of the steady state turning performance of an automotive vehicle is presented by Radt and Pacejka [36]. These researchers investigated the performance of a prototypical vehicle configuration defined by one particular set of vehicle-tire properties. Although the study does not permit one to draw specific conclusions relating to the influence of the shear-force characteristics of pneumatic tires, the results do serve to define the "anatomy" of a steady turn. It is possible to observe the locus of the turn center moving forward with increased drive torque and steer angle, and to see the origin of the "drag" force occurring at high lateral accelerations. In this manner, the large reductions in the trim value of longitudinal velocity accompanying a tight turn are fully explained. In addition, the analysis illustrates the understeer effect associated with the large lateral load transfer on the front wheels (caused by the existence of a roll stabilizer bar) and the oversteer effect resulting from rear-axle drive.

As a result of the requirement for examining the influence of tire traction parameters on steady turning behavior, calculations have been performed in this investigation that constitute, in effect, an extension of the scope of the study pursued by Radt and Pacejka. Specifically, calculations have been made demonstrating how the tire traction parameters C_α, C_s, and μ_o influence the following:

1. Vehicle "cornering efficiency," a performance measure defined herein as the maximum obtainable lateral acceleration (in g units) ratioed to the friction coefficient, μ_o
2. Path curvature response, and
3. The limit turn condition beyond which it is not possible to maintain the vehicle on a path of fixed curvature.

Figure 11 is a plot of calculated values of steady state path curvature achieved by a vehicle on a surface with $\mu_o = 1.05$, as a function of steering-wheel displacement and rear-wheel drive torque. The curves show the influence of the selected values of cornering stiffness (C_α = 6,000; 10,000; 14,000) when longitudinal stiffness is held fixed (C_s = 20,000). The reduction of path curvature with increased drive thrust, typically associated with the understeer vehicle, is seen to be accentuated by increases in the cornering stiffness of the tire. The influence of C_α on path curvature is negligible at the lower levels of drive torque. In this region it is the static margin and not the total cornering stiffness that is the controlling factor [23]. We may conclude that the nonlinear tire mechanics associated with increased cornering stiffness produce increased understeer with increased thrust until a level of drive thrust is reached at which increased thrust produces an increase in the path curvature. This phenomenon is depicted by the curves associated with δ'_{SW} = 16 degrees. Note that the oversteer tendency produced at high levels of drive torque (a phenomenon discussed in [36]) is sharpest for the vehicle with the tires having the high cornering stiffness. Further, the vehicle with tires having the highest value of C_α (14,000 lb/rad) reaches the limit-turn condition* at a lower drive torque than those torques attained at the turn limits when C_α = 10,000 or 6,000. These findings indicate that the lower the cornering stiffness, the lower the understeer quality at large lateral accelerations, and the more gradual the change to oversteer as the limit-turn condition is approached; the greater the cornering stiffness, the

---

* The limit-turn condition is that point at which the inside rear wheel of a turning vehicle becomes so unloaded that any attempt to obtain increased drive thrust through a torque-dividing differential causes the unloaded rear wheel to spin. This condition cannot be reached if the engine is unable to deliver the necessary torque.

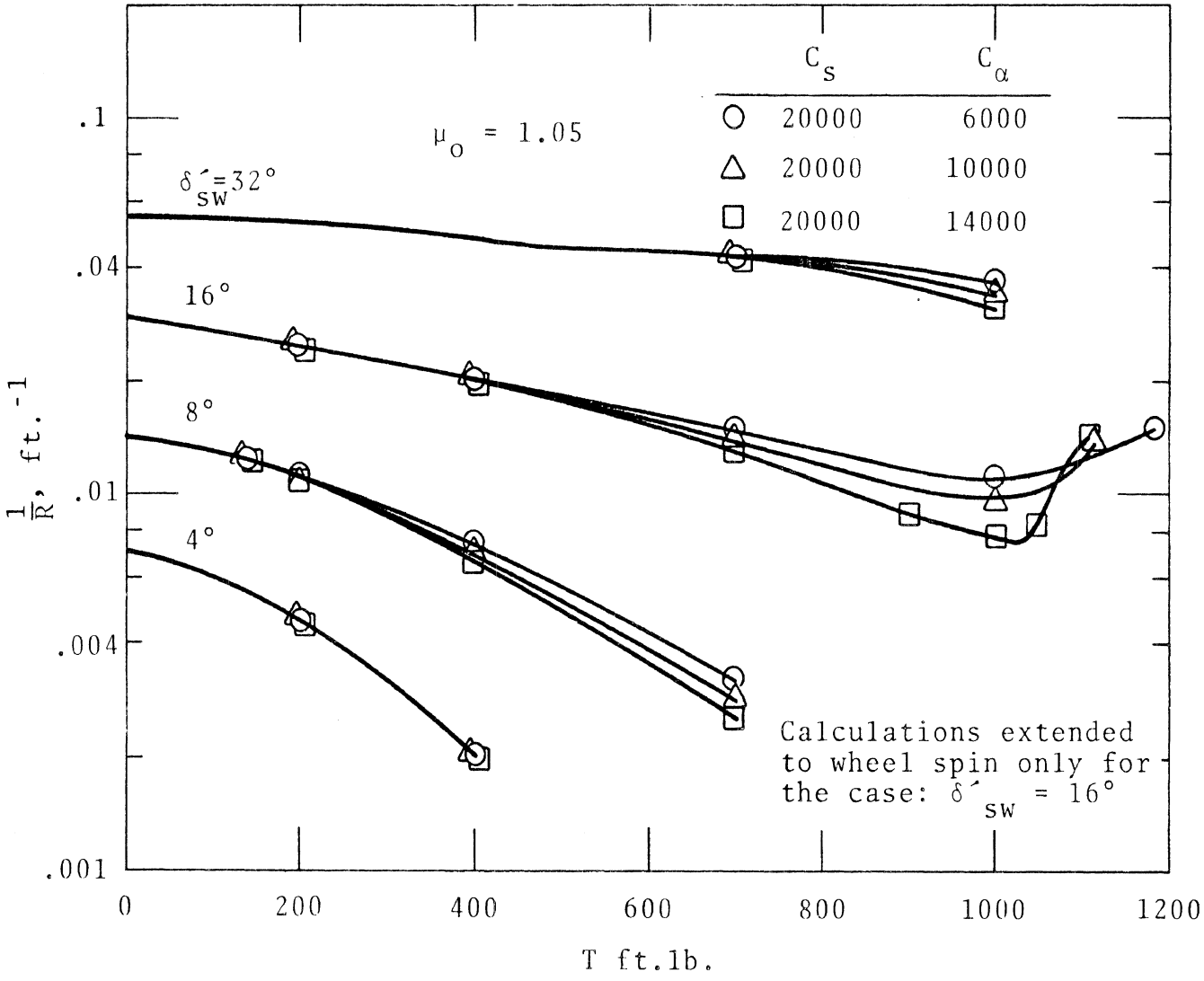

FIGURE 11. STEADY-STATE PATH CURVATURE VS DRIVE TORQUE; INFLUENCE OF C_α

greater the understeer quality at large lateral accelerations and the sharper the change to oversteer as the limit-turn condition is approached.

Similar results are obtained when C_α is held fixed and C_s is varied. Figure 12 shows that, in general, C_s has less influence on the steady turning performance of a motor vehicle than C_α. Significant differences due to C_s are observed for $\delta'_{sw} = 16$ degrees and it appears that reduced braking stiffness has an effect comparable to reduced cornering stiffness.

Based on the findings of Radt and Pacejka, we would expect that increasing the cornering stiffness of all four tires would result in increased speeds in a steady turn established by a given thrust and steer angle. This expectation is borne out by the results plotted in Figure 13. Further, this result holds when tires are being operated at, or near, their friction limit. In Figure 13, the speed, V, established in a steady turn, is plotted as a function of C_α and C_s for a steering wheel angle of 16 degrees and a drive torque of 1000 ft-lbs ($\mu_o = 1.05$). Maximum velocity is achieved when C_α and C_s are at their maximum values. A minimum velocity is achieved when C_α and C_s are at their lowest values.

For the vehicle studied here (and for the range of tire parameters considered) steady-state calculations (see Figure 14) show that the centripetal acceleration, $\left(\frac{Vr}{g}\right)$, achieved when the steering input (δ_{sw}) is 16 degrees is very close to the peak centripetal acceleration attainable for any steer angle. Thus it becomes practical to use this steer displacement value for evaluating the influence of C_α, C_s, and μ_o on the maximum steady turning capability of the simulated motor vehicle. Variations in braking stiffness, C_s, have, practically speaking, no effect on the variable Vr/g plotted as a function of drive torque T. On the other hand, variations in C_α and μ_o produce the results shown in Figure 15. As expected, higher cornering stiffnesses produce higher centripetal accelerations, at the lower values of drive torque. Note, however, that this finding holds for all drive-torque

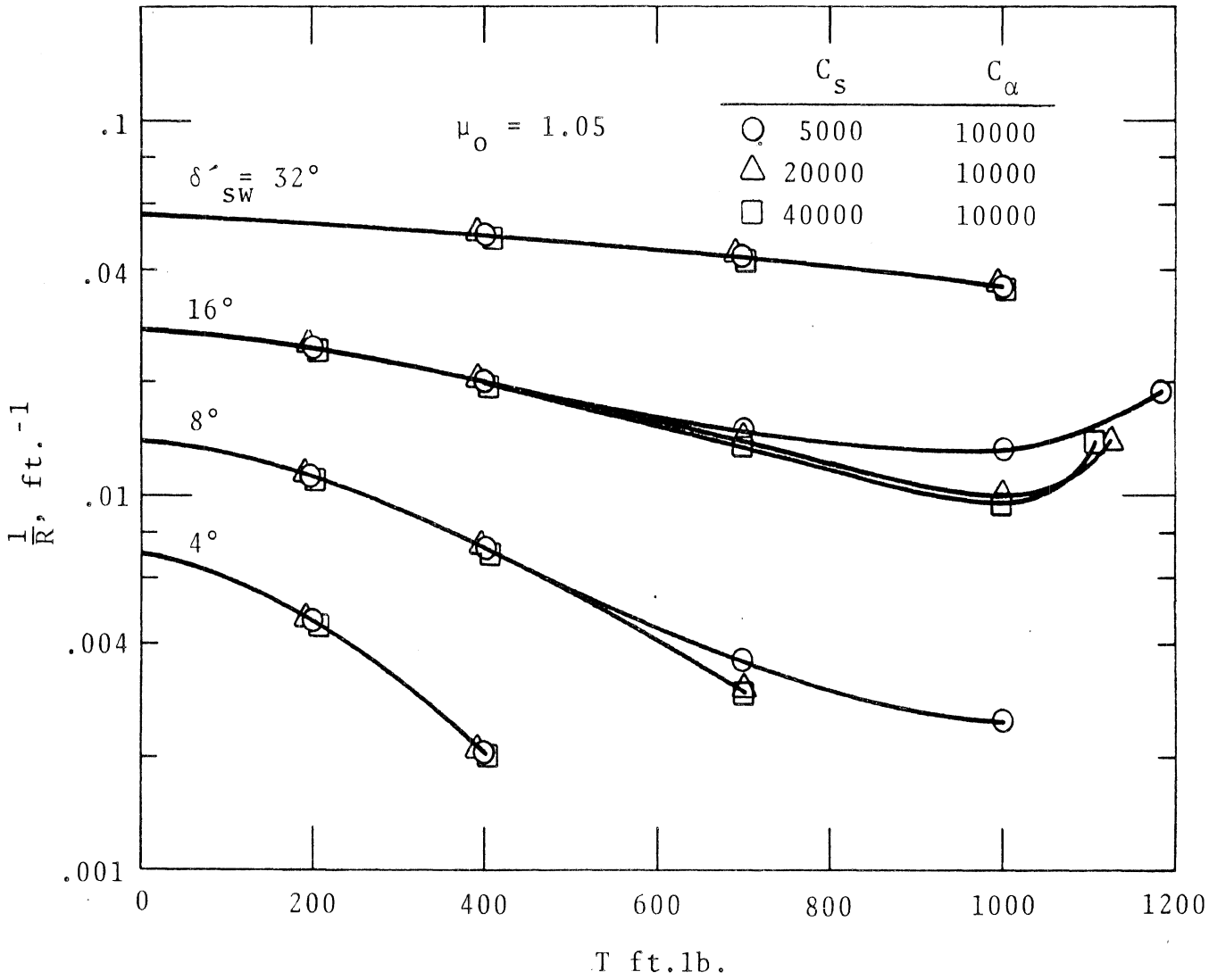

FIGURE 12. STEADY-STATE PATH CURVATURE VS DRIVE TORQUE; INFLUENCE OF C_s

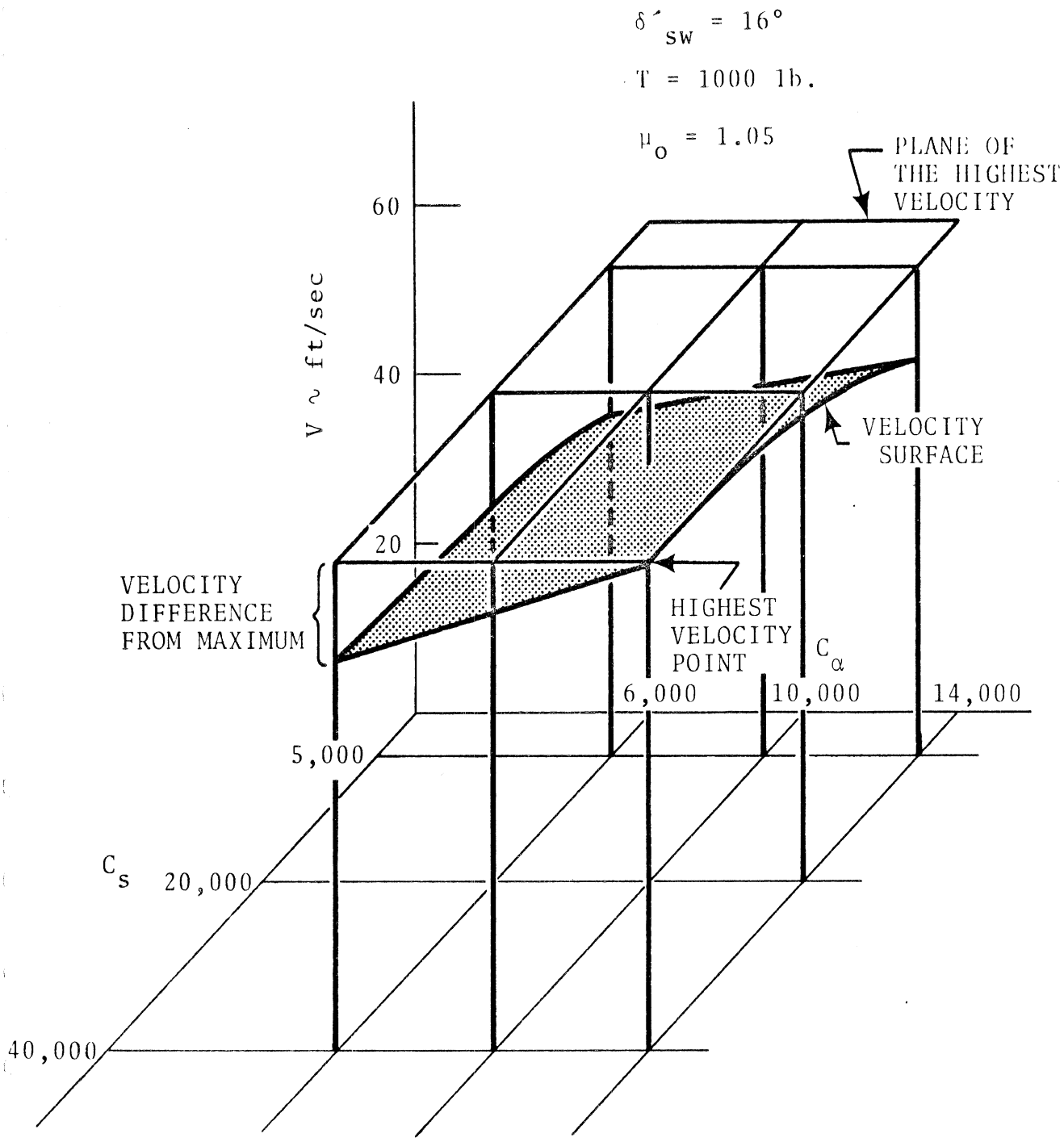

FIGURE 13. INFLUENCE OF TIRE STIFFNESS ON THE VELOCITY PRODUCED IN A STEADY TURN

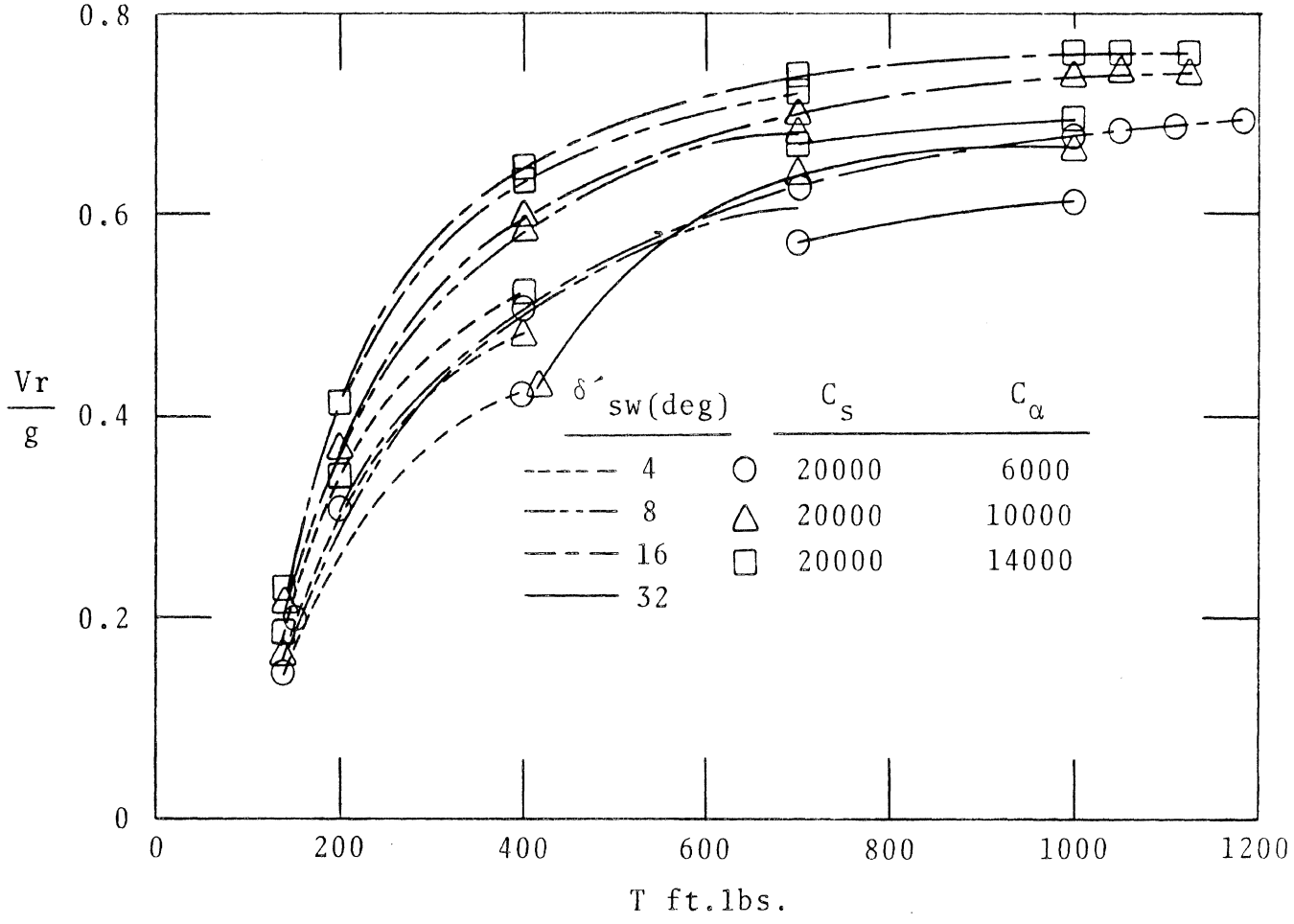

FIGURE 14. Vr/g VS. TORQUE FOR δ'_{sw} = 4°, 8°, 16°, 32° AND μ_o = 1.05

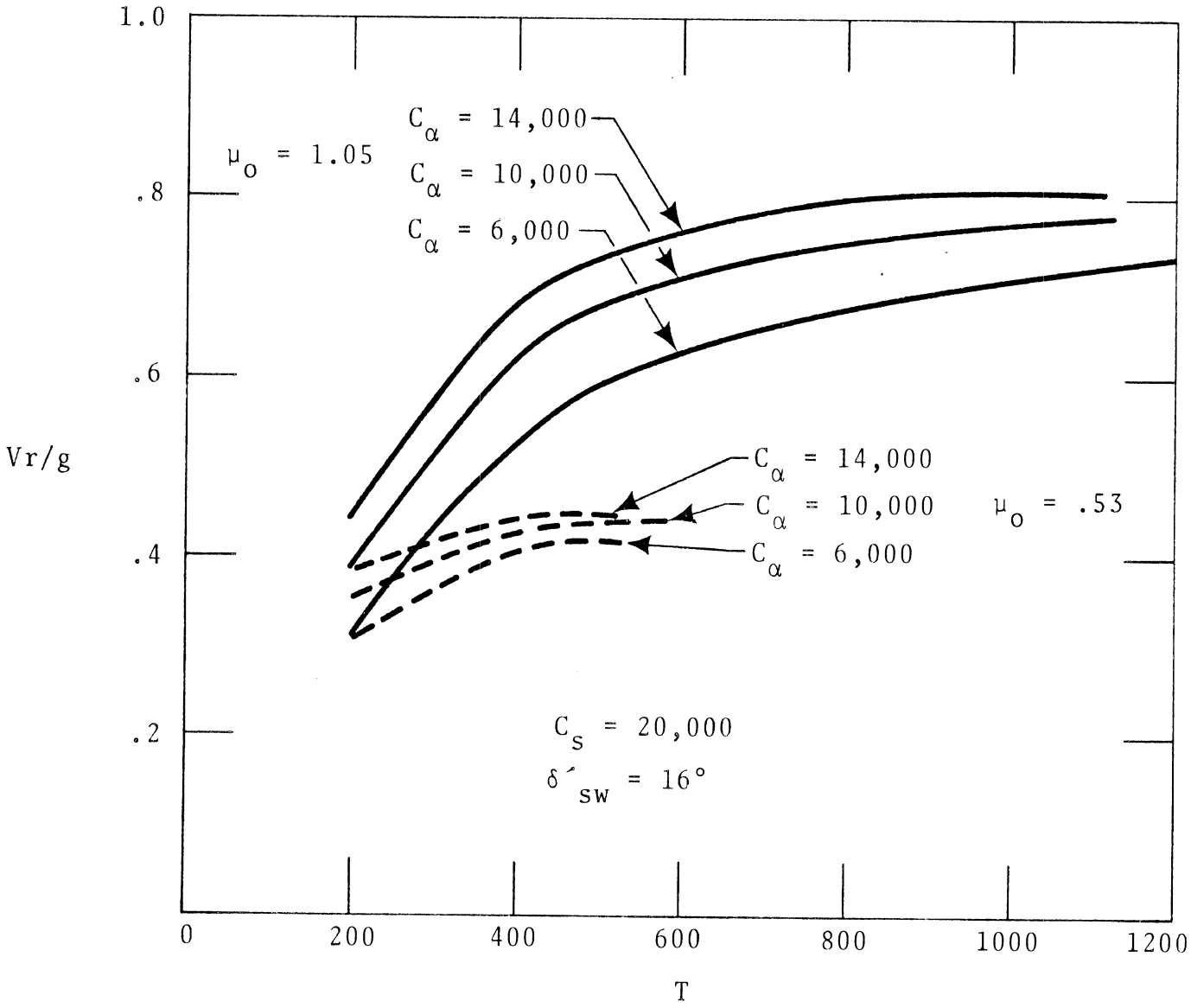

FIGURE 15. STEADY-STATE CENTRIPETAL ACCELERATION (FOR δ'_{sw} = 16 DEG.) AS INFLUENCED BY C_α AND μ_o

values up to the point at which the equilibrium turn limit is reached. For the present, we must conclude that increased cornering stiffness produces increased turning capability for a given δ'_{sw} and T, even when the tires are operating near their friction limit. Until additional studies are made to investigate the influence of load transfer on the cornering stiffness parameter, C_α, this conclusion seems warranted for tires exhibiting little change in cornering stiffness with change in vertical load.

Plotting the centripetal acceleration, Vr/g, achieved during steady turns on the lower friction surface ($\mu_o = 0.53$) shows the same trends obtained on the higher friction surface (see Figure 15). If, however, we introduce the concept of cornering efficiency (i.e., the ratio of lateral acceleration in g units to the prevailing friction coefficient) and normalize the drive torque, T, we obtain Figure 16. It is apparent that the vehicle is able to achieve a higher cornering efficiency and a higher normalized drive torque on the surface with the lower friction coefficient. Specifically, for the tire stiffness parameters indicated, the vehicle achieves a cornering efficiency equal to approximately 74 percent on the $\mu_o = 1.05$ surface, whereas it exhibits an efficiency of 84 percent on the $\mu_o = 0.53$ surface. Consequently, the turning capability of a pneumatic-tired vehicle does not decrease in direct proportion to reductions in the coefficient of friction for the tire-road interface. It should be understood, however, that this statement is restricted to the case of smooth roads with additional analyses and measurements required to extrapolate these results to a real world environment possessing typical levels of road roughness.

4.2. THE PATH RESPONSE PRODUCED BY BRAKING IN A STEADY TURN

4.2.1. INTRODUCTORY REMARKS. In contrast to the steady-turning state produced by a steering-wheel displacement and rear-wheel drive torque, no equilibrium state results when the

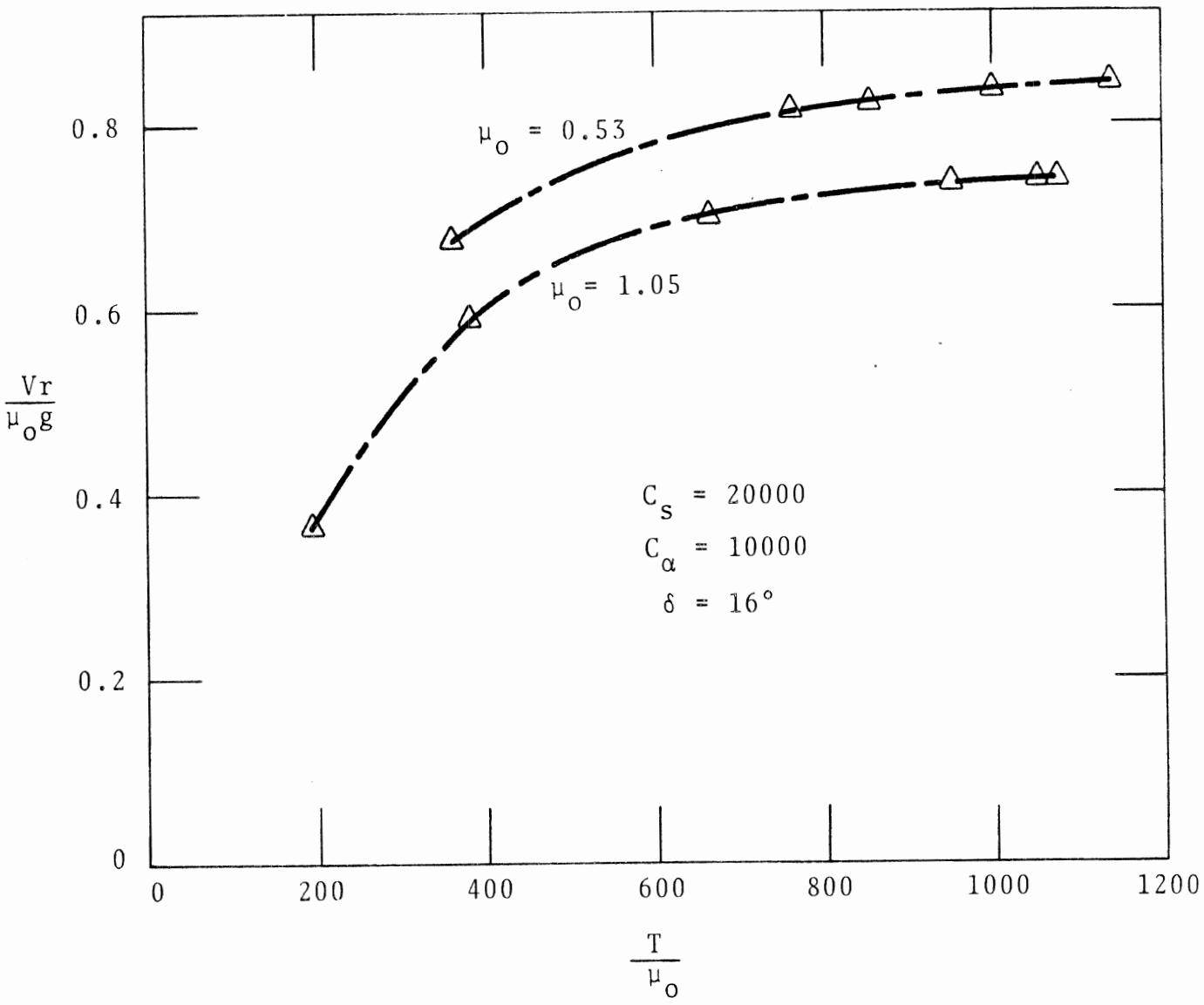

FIGURE 16. NORMALIZED CENTRIPETAL ACCELERATION VS. NORMALIZED TORQUE AS A FUNCTION OF μ_o

torque on the rear wheels is reversed to produce a braking thrust instead of a driving thrust. Consequently, a comparison of the behavior of vehicles influenced by brake thrust requires that the motions (trajectories) produced in response to a specified braking action be compared. Two problems arise. One involves the selection of the initial state of motion from which braking is initiated. The second concerns the selection of the braking input itself.

With respect to the first selection, there are three general possibilities. One procedure involves purely symmetric braking resulting in straight line motion, as generally occurs when the steering wheel is trimmed to produce a zero turning input. A second procedure is to brake from the initial turning state established by steering wheel displacement and drive thrust. A third possibility utilizes a maneuver in which both braking and steering inputs are imposed on a vehicle which is initially proceeding in straight line motion. To the extent that any of these open-loop maneuvers correspond to real-world emergencies in which the tires are forced to operate at, or near, the friction limit, it is appropriate to consider them for this study. Accordingly this investigation attempts to evaluate the effects of the tire traction parameters C_α, C_s, and μ_o on:

- Straight-line braking efficiency
- The trajectory resulting from braking in a curved path
- An open-loop lane change maneuver with a simultaneous deceleration.

The first study constitutes an investigation of the extent to which the braking-stiffness parameter influences the degree to which a motor vehicle can utilize the available friction without experiencing wheel-lockup on either axle. The analysis proved trivial in that very little effect was found. For the interested reader, a brief summary of the methodology and the findings is

given in Appendix C. The second study is reported in this section of the report and the third study is treated in a subsequent section.

Braking to zero velocity while tracking a curve of fixed radius can be necessary in real-life situations. In general, tracking such a curve during a braking maneuver requires making steering corrections. Thus, the amount of steering required to produce a trajectory of constant curvature could be used to measure the extent to which braking action interferes with curve tracking. Since we cannot determine the steering required to correct for the influence of braking unless we structure a closed-loop analysis, the departure of the open-loop vehicle from the desired trajectory is used as a measure of the influence exerted by the various tire traction parameters. Further, this maneuver produces a strong tendency for "spin down" and "lockup" of the right rear wheel resulting from the unloading of this wheel during combined lateral and longitudinal acceleration. The simulations showed that the lockup tendency could be made as marginal as desired by modifying either the initial turn condition or the level of the braking input.

The path-curvature response produced by braking (with steering wheel held fixed) is influenced by a number of factors. First, the path curvature will tend to increase beyond the initial value of curvature since braking causes the forward velocity to decrease with time, and the normal static directional stability of the vehicle causes the path curvature to increase as the speed of the vehicle decreases [23]. This understeer effect occurs in all vehicles having a positive static margin which, of course, is usual design practice. Added to this understeer phenomenon, is the influence of the nonlinear mechanics of the tires. Since the tires are being forced to operate in the vicinity of the friction limit, braking in a turn may be expected to produce trajectories highly sensitive to the nonlinear mechanical characteristics of pneumatic tires.

4.2.2. DISCUSSION OF RESULTS. After making some preliminary runs, two initial turning states were selected for this braking maneuver. The first turn state had a curve radius of 357 feet. With velocity prior to braking equal to 70 ft/sec (48 mph), lateral acceleration normal to the path was 0.426 g, indicating a rather severe turn. The second turn state had a 256 foot curve radius. With velocity prior to braking equal to 49.5 ft/sec (34 mph), lateral acceleration was 0.297 g, which on a high friction surface is approximately the limiting maneuver condition at which it is valid to describe the vehicle and its tires by linearized equations of motion [23]. This second turn state was selected, however, to examine vehicle behavior when operating on a surface having a friction coefficient of 0.53. The tires of a vehicle turning with a lateral acceleration of 0.3 g on a surface with $\mu_o = 0.53$ operate in a regime in which their mechanical characteristics are highly nonlinear.

A series of eleven braking runs was made, including seven on the larger radius curve and four on the smaller radius curve. The assumed values of tire traction parameters (C_α, C_s, and μ_o) and the steer displacement and drive thrust required to establish the desired equilibrium state are tabulated for each run in Table 3. It will be noted that the tabulated set of motion variables vary slightly for each run. This variation derives from the necessity to iterate, starting from estimates based on the steady turn analyses, to the final values of δ'_{sw} and T required to achieve the desired equilibrium state. For each run, the steer angle was held fixed, the driving thrust was terminated, and brake torque was applied during a 0.5 second interval as shown in the sketch below.

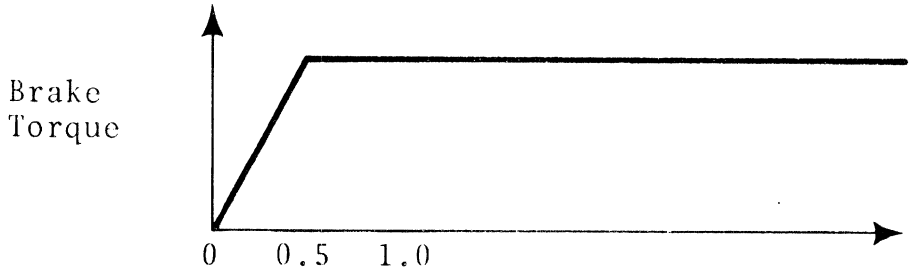

TABLE 3. STEADY TURN CONDITIONS PRIOR TO BRAKING

Tire Traction Parameters				Control Inputs		Motion Variables					
Run #	μ_o	C_s	C_α	δ'_{sw}	ft/lb T	ft/sec u	ft/sec v	rad/sec r	ft/sec V	$\frac{1}{R}$	$\frac{Vr}{g}$
1	1.05	20,000	6,000	4.12°	345	69.77	-3.16	.1956	69.84	.0028	0.4249
2	1.05	20,000	10,000	3.66°	292	70.32	-1.40	.1956	70.33	.0028	0.4275
3	1.05	20,000	14,000	3.44°	266	70.24	-0.63	.1954	70.24	.0028	0.4270
4	1.05	5,000	6,000	4.01°	348	70.22	-3.29	.1954	70.29	.0028	0.4273
5	1.05	5,000	10,000	3.61°	292	70.32	-1.45	.1956	70.33	.0028	0.4275
6	1.05	5,000	14,000	3.61°	291	70.00	-1.43	.1956	70.01	.0028	0.4251
7	.53	20,000	10,000	4.52°	370	69.67	-3.83	.1930	69.77	.0028	0.4130
8	.53	20,000	6,000	4.52°	225	49.44	-1.11	.1904	49.45	.0039	0.2825
9	.53	20,000	10,000	3.61°	195	49.44	-0.22	.1894	49.44	.0038	0.2901
10	.53	20,000	14,000	3.50°	184	49.50	+0.17	.1908	49.50	.0039	0.2941
11	.53	5,000	10,000	3.61°	196	49.50	-0.23	.1912	49.50	.0029	0.2940

A typical value for front-to rear-axle brake distribution (viz.; 60 percent, front; 40 percent, rear) was assumed in these simulations. For the surface with the high coefficient of friction, the total applied brake torque was 2500 ft-lbs; for the low friction surface, the applied brake torque was 1700 ft-lbs. With these input conditions, the applied brake torque was just sufficient to lock the right-rear wheel and no other wheel in run number 2. (See Table 3).

The transient response of the vehicle, caused by the assumed braking input, can be integrated to determine the trajectory of the center of gravity with respect to an earth reference. On so doing, one obtains the trajectories plotted in Figure 17 for runs one through three.

Figure 17 shows that during the latter portion of this turning-braking maneuver, the trajectory of the center of gravity lies inside the curved path which would be traced by the vehicle if braking were not taking place. As mentioned earlier, this result would be anticipated because of the increased path curvature accompanying a reduction in the longitudinal velocity. As a result of braking, we might also expect the vehicle to change its attitude with respect to its total velocity vector. If large angles of sideslip occur, a vehicle will extend beyond its lane of travel even if the path curvature remains constant.

Figure 18 presents plots versus time of the instantaneous radii of curvature and vehicle sideslip angles that are produced by three values of cornering stiffness, when C_s = 20,000 and μ_o = 1.05. (Figures 17 and 18 apply to runs one through three.) With the tires of low cornering stiffness (C_α = 6,000), the vehicle experiences an angle of sideslip approaching 16 degrees near the end of the maneuver. The higher the cornering stiffness, the smaller the sideslip angle in the steady turn and the smaller the increase or departure from the initial sideslip trim value as the maneuver progresses and the vehicle comes to a stop. The path radius initially increases and then decreases as the vehicle slows down in the braked turn. For the two lower values of

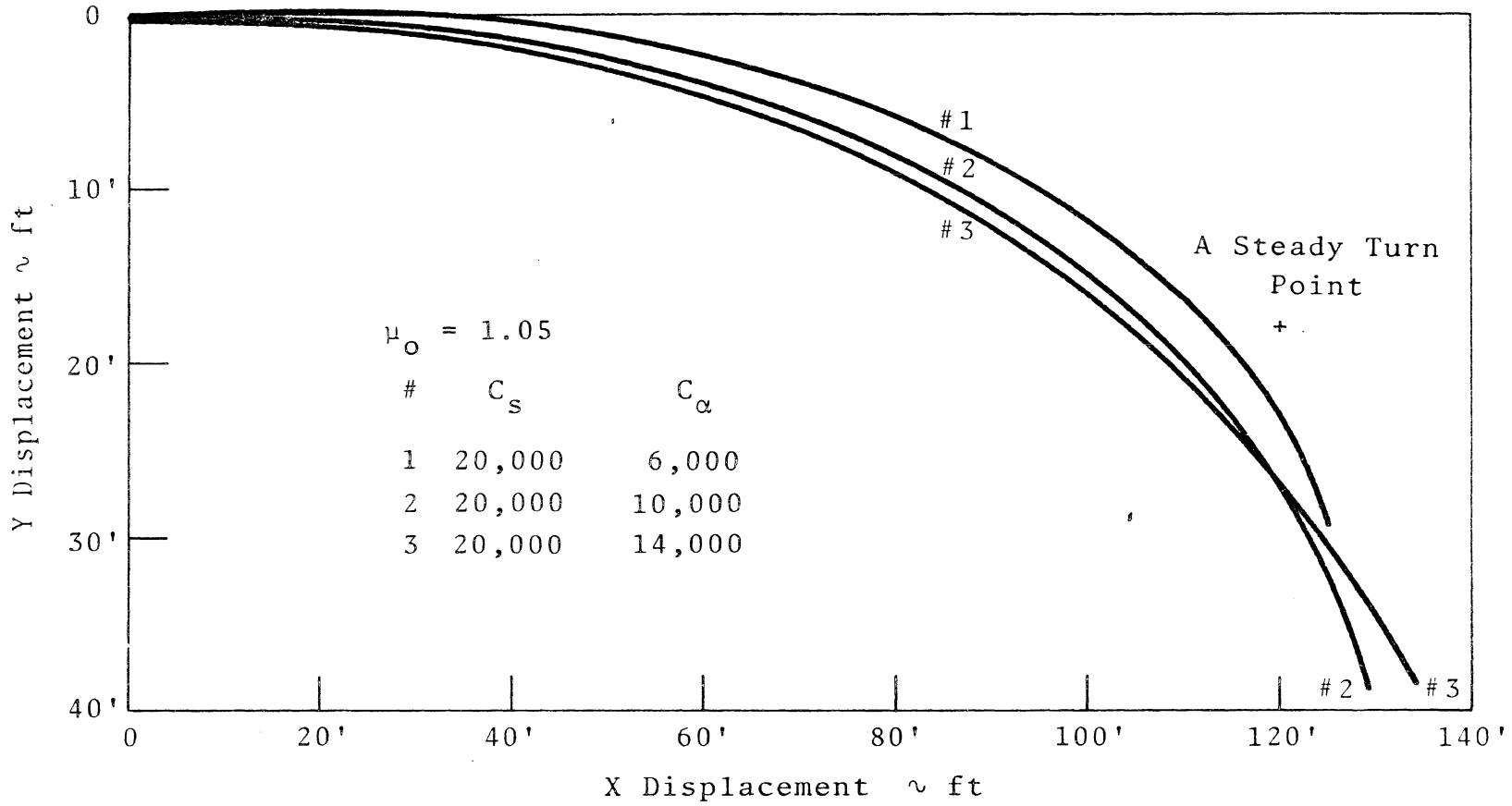

FIGURE 17. PATH TRAJECTORIES FOR RUNS 1, 2, AND 3

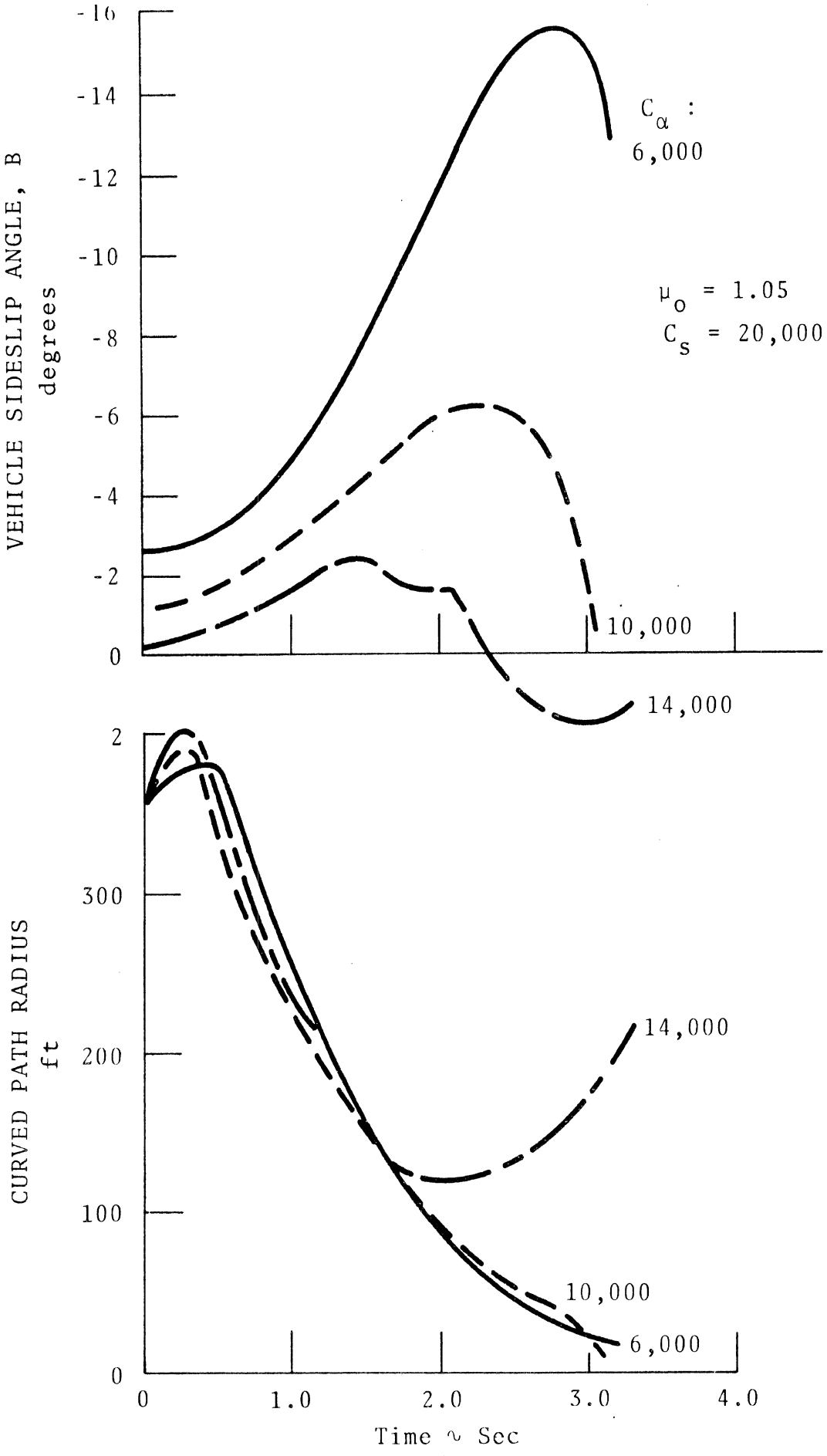

FIGURE 18. PATH RADIUS AND SIDESLIP ANGLE PRODUCED BY BRAKING IN A TURN

cornering stiffness (C_α = 6,000; 10,000), extremely short turning radii are encountered at the end of the maneuver. The larger value of cornering stiffness (C_α = 14,000) not only prevents the sideslip angle from getting large but also mitigates against any final tendency to turn more and more sharply.

Figure19 presents data (similar to that in Figure 18) for that case in which the braking stiffness is small (C_s = 5,000) and the vehicle is assumed to be operating on a high friction surface (μ_o = 1.05). The detailed time histories produced in the simulation show that only in run four (C_α = 6,000) does the right-rear wheel lock up. Further, they show that a reduction in braking stiffness tends to retard the tendency for wheel spin down to a lockup condition. This tendency towards less spin down is responsible for the smaller values of sideslip angle that result when C_s = 5,000, as compared with the sideslip angles produced when C_s = 20,000 (see Figure 18). A smaller braking stiffness also produces a significant improvement in the path radius response, in that there is a much reduced tendency for "windup" near the end of the stop. Increases in cornering stiffness, on the other hand, cause the reduction in path radius with time to decrease. It would appear that, in this particular maneuver on a high friction surface, there are advantages in having tires with a high cornering stiffness and a lower braking stiffness. A direct comparison of the influence of C_s, for fixed C_α, is given in Figure 20.

Run seven is comparable to run two except the friction coefficient, μ_o, was reduced from 1.05 to 0.53. Since the trim centripetal acceleration of the vehicle, in g units, ratioed to the friction coefficient, μ_o, is approximately 0.8, (see Table 3), it is apparent that the tires are operating near their friction limit. When braking is initiated, the path radius approaches infinity and the center of gravity moves approximately in a straight line. The detailed time histories show that all

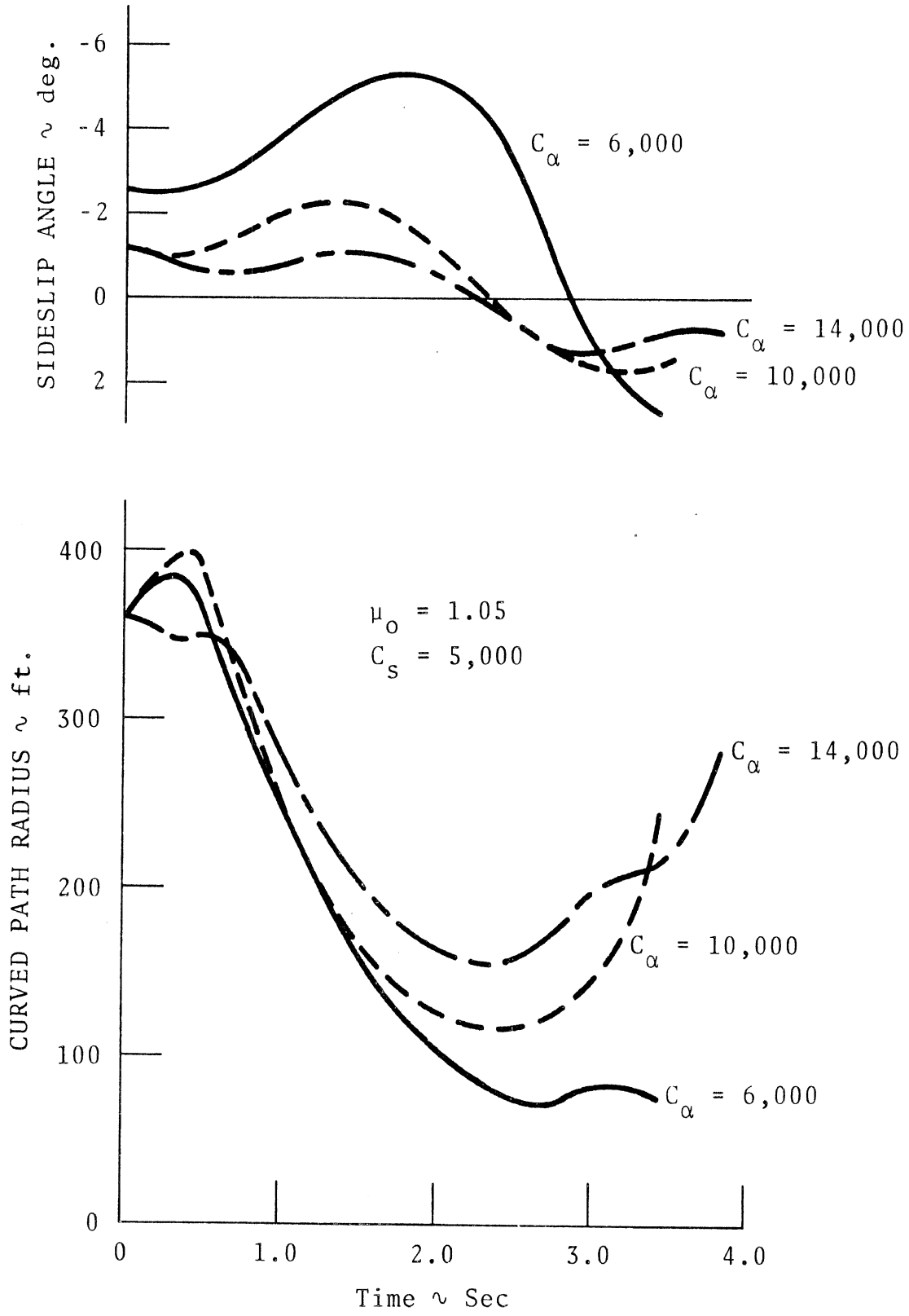

FIGURE 19. PATH RADIUS AND SIDESLIP ANGLE PRODUCED BY BRAKING IN A TURN

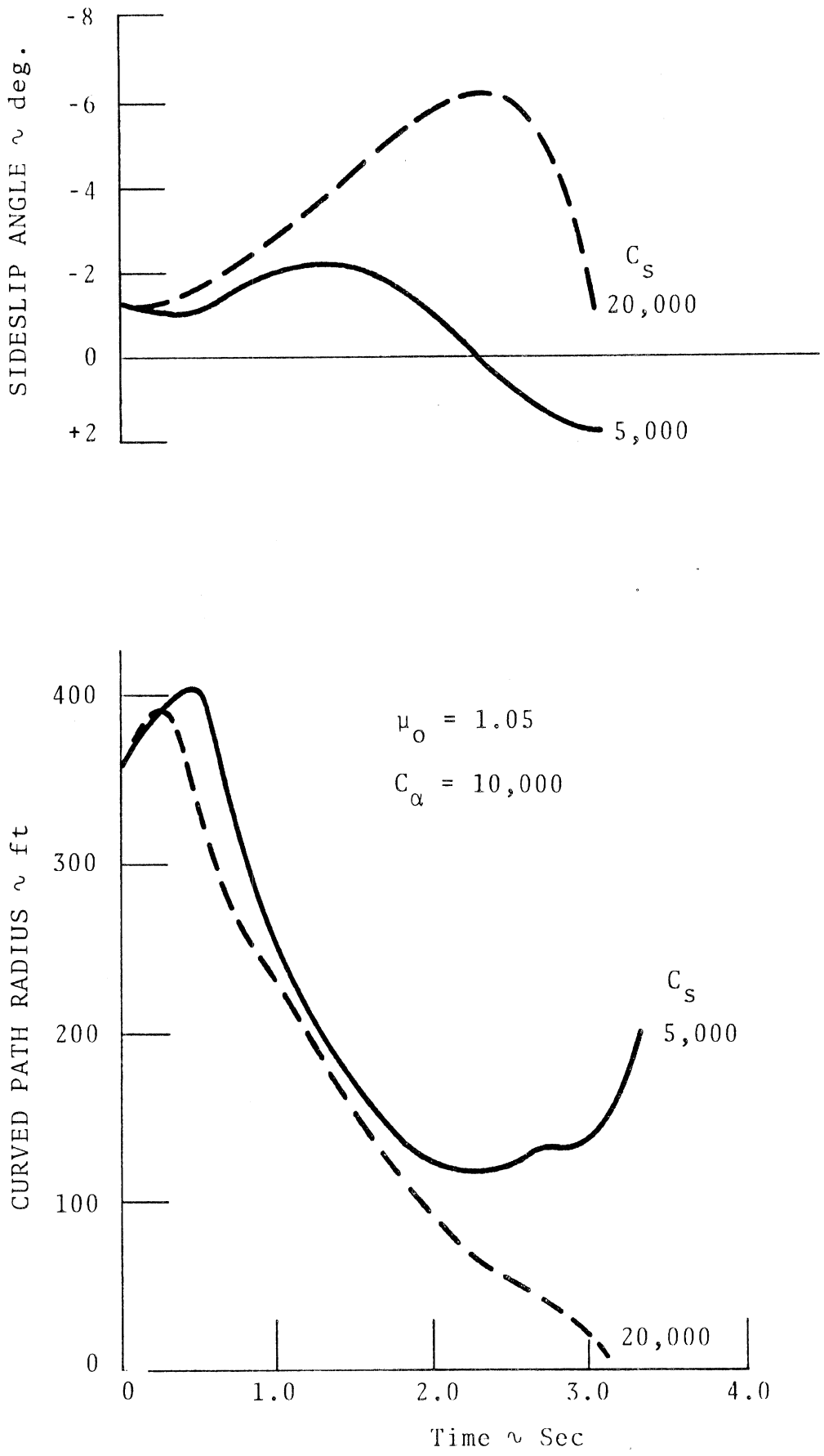

FIGURE 20. PATH RADIUS AND SIDESLIP ANGLE PRODUCED BY BRAKING IN A TURN

four wheels lock and the computation of the trajectory indicates that the vehicle displaces laterally only 2.12 feet from the tangent to the curve at the time braking is initiated. Inspection of the sideslip angle response shows that it exceeds -25 degrees four seconds after the start of the maneuver.

Simulations similar to runs one through six were also made to evaluate the influence of a reduced coefficient of friction when the initial trim state was such that the vehicle would remain in a curved path following the onset of braking. Table 3 shows that the trim value of centripetal acceleration, in g units, is approximately 55 percent of the available friction coefficient for runs eight through eleven in contrast to the 40 percent prevailing in runs one through six. As noted earlier, however, the total braking torque applied in runs eight through eleven was only 68 percent of that applied in runs one through six. In Figure 21 we note results similar to those discussed above, with the exception that, following the onset of braking, the path radius increases much more sharply than on the surface with the higher coefficient of friction prior to the subsequent reduction in path radius with time. Based on the results depicted in Figure 22, it seems reasonable to conclude that lower values of braking stiffness also provide some advantage on a surface with a reduced coefficient of friction.

4.3. VEHICLE TRANSIENT STEERING RESPONSE AS INFLUENCED BY THE NONLINEAR MECHANICS OF TIRES

Before discussing the results of the lane change-braking simulation study, we shall consider some findings obtained from transient steering simulations using the initial conditions selected for the turning-braking maneuvers discussed in Section 4.2. above. The maneuver, as designed, produces results which augment existing understanding of the mechanics of pneumatic-tired vehicles.

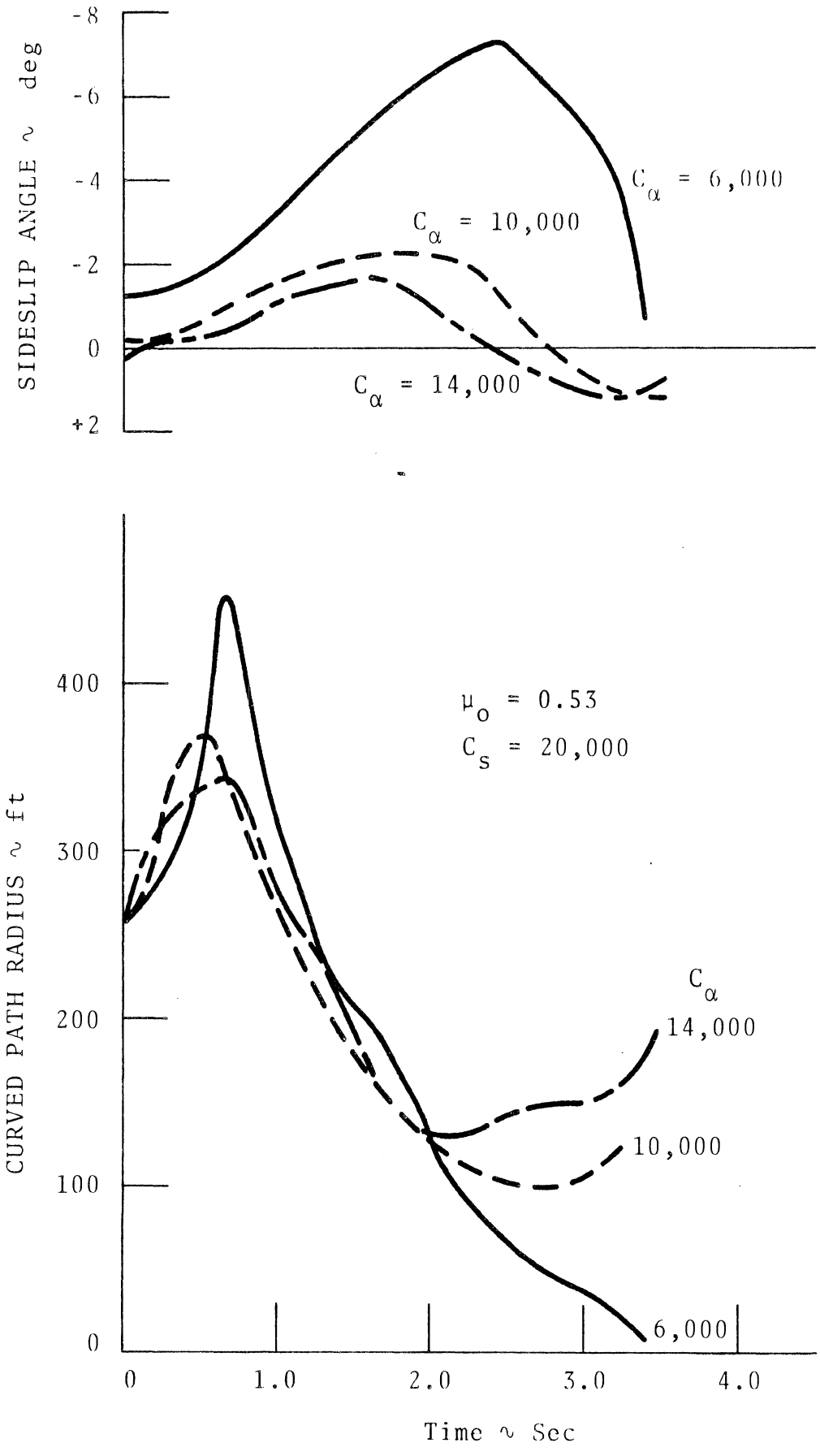

FIGURE 21. PATH RADIUS AND SIDESLIP ANGLE PRODUCED BY BRAKING IN A TURN

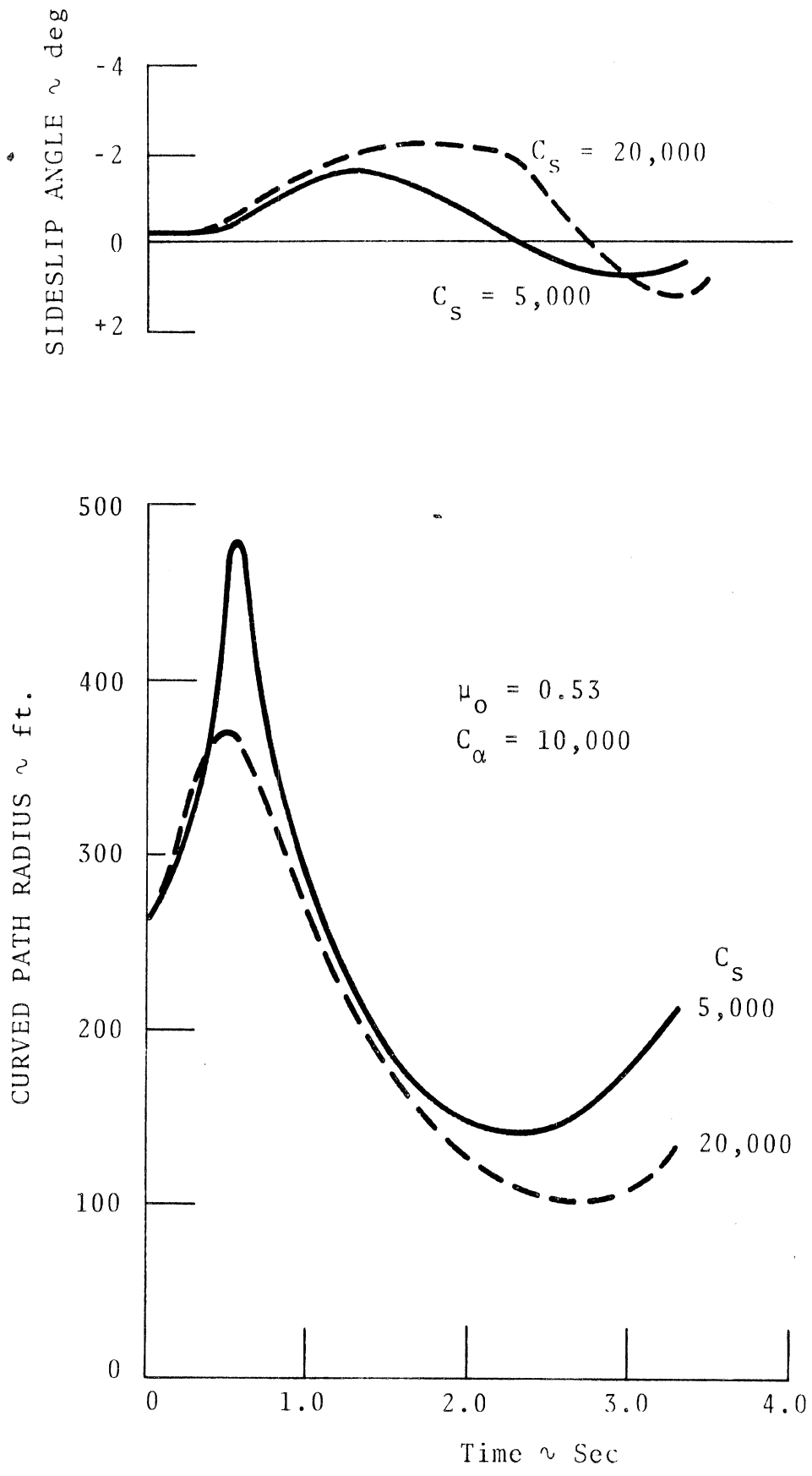

FIGURE 22. PATH RADIUS AND SIDESLIP ANGLE PRODUCED BY BRAKING IN A TURN

The maneuver consists of a vehicle in a steady turn (as produced by fixed steering-wheel displacement and drive thrust) being forced to a new turn condition by a ramp change in steering-wheel displacement. The incremental steering wheel displacement, $\Delta\delta'_{sw}$, is four degrees. The maneuver, as executed, does not force any of the tires to operate very close to the friction limit. Nevertheless, the tires operate in their nonlinear regime and it is possible to gain some insight into the effect of the tire-traction parameters on the transient response of a motor vehicle to steering inputs.

The nonlinear aspects of tire behavior have been emphasized by considering a vehicle to be in either of the two steady turn states identified in Table 3. With the tires modeled in the manner discussed in Section 2, and with the wheel rotation degree of freedom included in the analysis, the computed responses to steering depart substantially from the transient response produced by a similarly-sized step (or ramp) steering input imposed on a non-turning vehicle.

As shown in Table 3, both initial turning states require a steady steering-wheel displacement approximately equal to four degrees. This means that in the maneuver under discussion, the initial steering displacement is approximately doubled. Figure 23 shows the yawing and longitudinal velocity responses produced by a four degree increment in steering-wheel displacement, consisting of a linear increase in steering at a rate of eight degrees per second for half a second. In the maneuver, the driving thrust is held fixed and the vehicle slows down as a result of the increased drag produced by the decreased turn radius and the increased lateral acceleration.

For the case in which $\mu_o = 1.05$, $C_\alpha = 10{,}000$, and $C_s = 20{,}000$, the vehicle initially exhibits the rapid yawing velocity response associated with the directional response mode of the constant-speed vehicle, viz., a mode having a natural frequency of 0.5 cycles

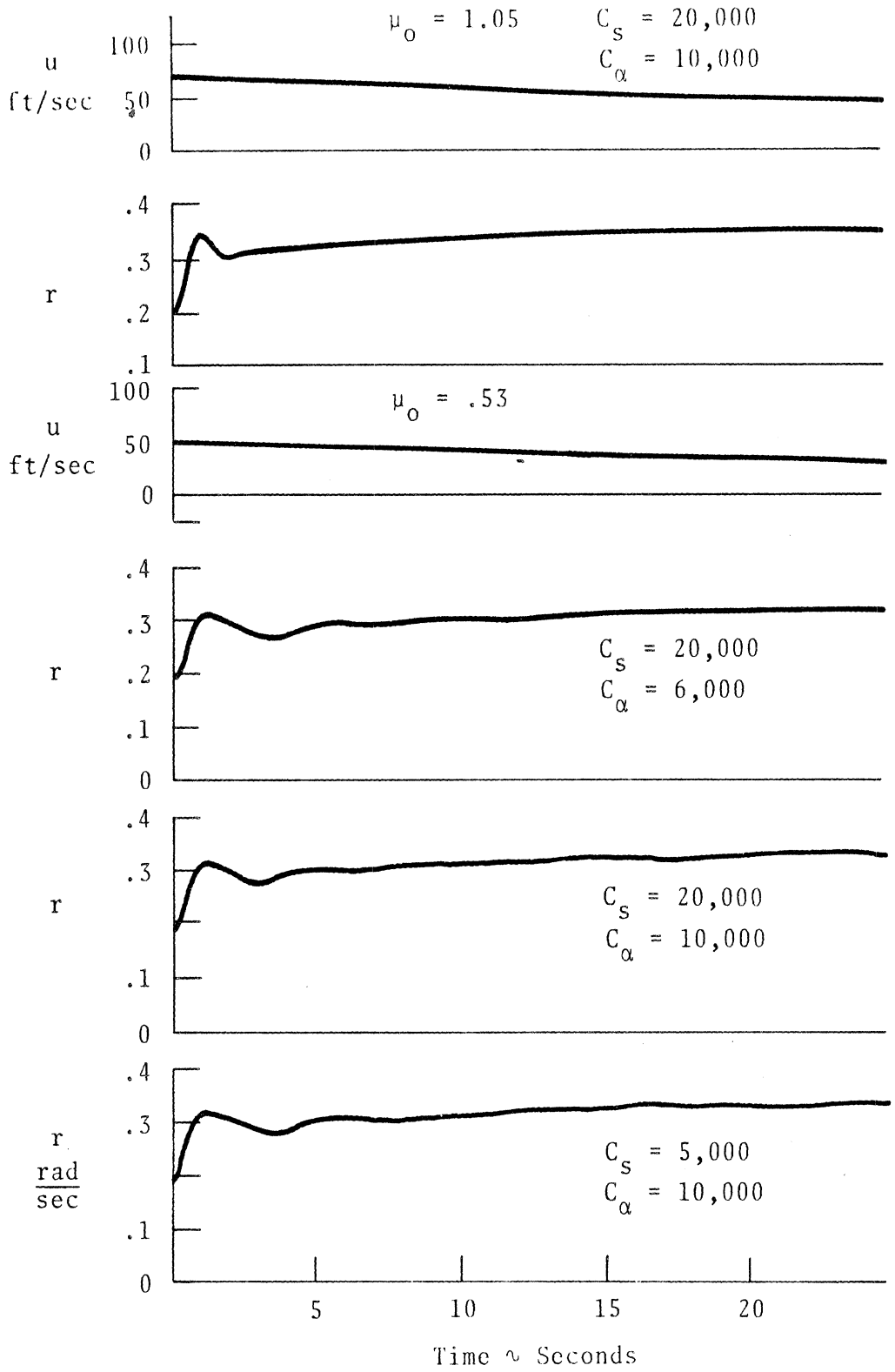

FIGURE 23. RESPONSE TO INCREMENTAL STEER DISPLACEMENT (δ'_{sw} = 4 deg) WITH VEHICLE TRIMMED IN A STEADY TURN [DRIVE THRUST HELD CONSTANT]

per second. A pseudo-steady state is achieved in this short period response whose value (r=0.32 rad./sec.) is significantly less than double the steady turn value (r=0.1956 rad./sec.). Thus the sizeable nonlinearity of the system, attributable primarily to nonlinear mechanics of the tires, is evident. Furthermore, it takes almost 30 seconds to establish a new steady turn condition. During the lengthy period in which the vehicle is slowing down and establishing a new trim longitudinal velocity, the yawing velocity slowly increases producing the increased path curvature required to satisfy the kinematic equilibrium that must be achieved by a vehicle that is basically understeer. In the equilibrium turn achieved 30 seconds after increasing the steering wheel displacement by a factor of 2.09 ($\delta'_{sw_{init.}}$ = 3.66 deg.; $\Delta\delta'_{sw}$ = 4.0 deg.), the speed is decreased from 70.0 ft/sec to 47.5 ft/sec., the yawing velocity is increased from 0.1956 rad/sec. to 0.366 rad/sec., the turn radius is decreased from 357 ft. to 130 ft., and the lateral acceleration is increased from 0.426 g to 0.54 g. These response characteristics contrast markedly with what is obtained when steering inputs are restricted to small magnitudes (such that tire side force is roughly a linear function of slip angle) and the perturbation velocities are sufficiently small so that longitudinal components of the inertial forces and the tire forces (acting on the vehicle) are negligible.

Several other observations should be made. With the friction coefficient given by μ_o = 0.53, such that an initial lateral acceleration of 0.297 g represents an operation closer to the friction limit than the case just treated, the vehicle exhibits a short period response much slower than that obtained on the higher friction surface. With the cornering stiffness of the tire unchanged, i.e., C_α = 10,000, a substantial decrease in the short period frequency is observed. With a decrease in cornering stiffness, i.e., C_α = 6,000, the yawing velocity response on the reduced friction surface is slowed further. Finally, there is

a tendency for the short period oscillation to persist on the reduced friction surface and to be aggravated by a reduction in either the cornering or braking stiffness of the tires.

4.4. THE TRANSIENT RESPONSE TO SIMULTANEOUS STEERING AND BRAKING

A series of lane-change maneuvers, made with and without the application of the brakes, indicates the extent to which this maneuver is sensitive to variations in the tire-traction parameters, C_s , C_α, and μ_o . The simulation study employed a combination of steering and braking inputs selected on the basis of measurements of driver control activity in fast lane-changes and stops. In retrospect, the study might have included more severe combinations of steering and braking in order to produce transient responses in which the vehicle "spins out," that is, exhibits a trajectory and attitude response far removed from the intended maneuver objective. Such an expansion of the study would, however, have imposed very large demands with respect to synthesis and interpretation of the results. At the expense of possibly gaining some insight into the behavior of the vehicle pushed beyond the friction limit, the study objective was restricted to ascertaining the extent to which non-linear tire mechanics (as defined by the selected parameters) govern open-loop response in a typical emergency maneuver.

A lane-change is defined as a maneuver in which a motor vehicle is steered so that it is displaced laterally with its heading in the same direction at the completion of the maneuver as it was before the maneuver began. In theory, this maneuver can be perfectly executed by displacing the wheel first to the left/right and then to the right/left, controlling the steering amplitude and timing to produce the result pictured in Figure 24. Here, two triangular pulses of steering displacement, following each other without delay, produce (a) a yawing response whose integral is zero over the

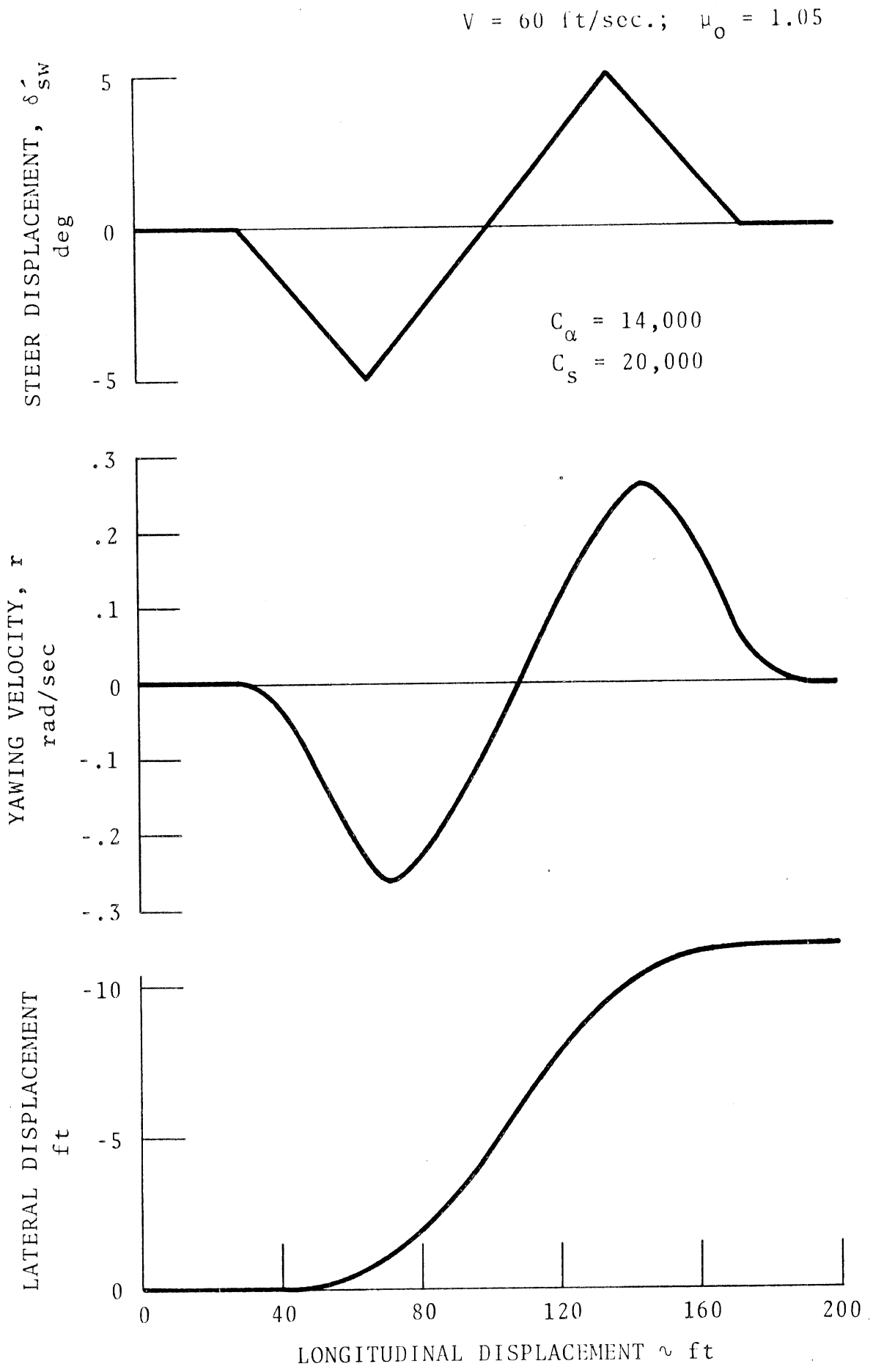

FIGURE 24. LANE CHANGE WITH ZERO BRAKING

maneuver, and (b) a lateral displacement of 11.3 feet. (A lane on a modern highway is typically 12 feet wide.) Note that the maneuver diagrammed in Figure 24 is accomplished in approximately 170 feet of travel with steering activity completed in 2.4 seconds. When accompanied by braking on a reduced coefficient of friction surface, this maneuver becomes marginal in the sense that the tires are forced to operate near their friction limit.

To establish a baseline, the influence of tire-traction parameters on a lane-change maneuver executed at 60 ft/sec without braking is first considered. Figure 25 (a) shows the influence of cornering stiffness on the lateral displacement produced by the steering input diagrammed at the top of Figure 24, on a high coefficient of friction surface (μ_o = 1.05). Essentially perfect lane changes occur even though the magnitude of the lateral displacement is influenced slightly by the cornering stiffness of the tires. Figure 25(b) compares the lateral displacement trajectories achieved on surfaces with a high and moderate coefficient of friction. Almost perfect lane changes are produced in both cases. However, the magnitude of the lateral displacement is slightly less on the lower-friction surface. An examination of the simulation time histories shows that very little speed reduction occurs in these maneuvers when drive thrust is held constant.

On applying a braking input of the following waveform to the front wheels (and on applying brake torques equal to two-thirds of the front-wheel torque to each of the rear wheels), significantly

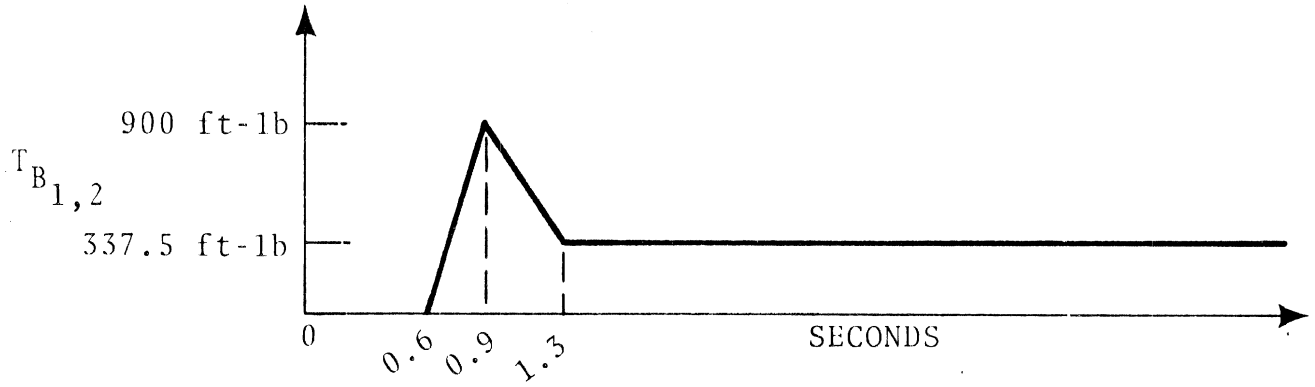

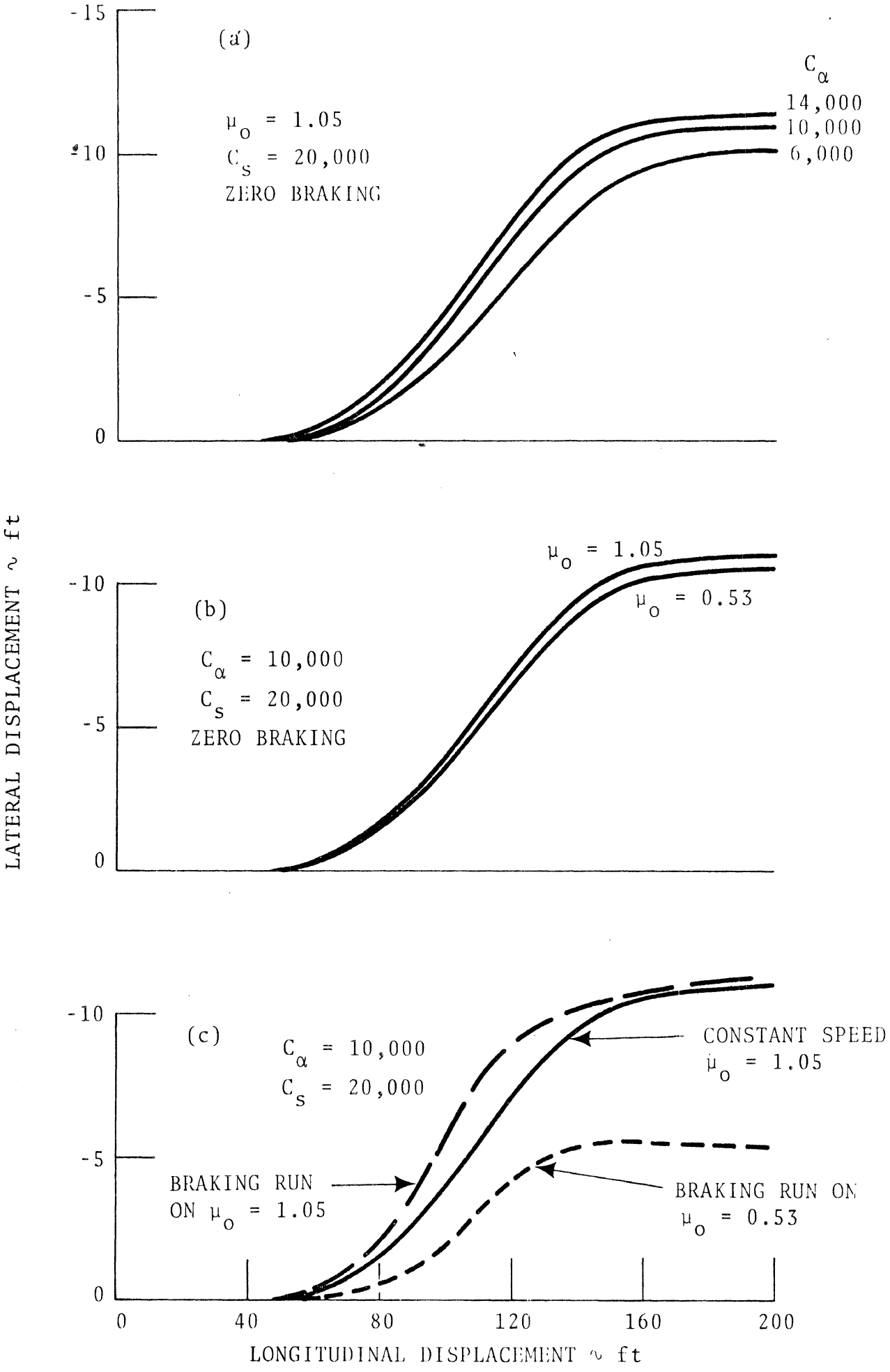

FIGURE 25. LATERAL DISPLACEMENT VS. LONGITUDINAL DISPLACEMENT: A LANE CHANGE MANEUVER

different lateral displacements are obtained for the two coefficients of friction considered in this study. As noted earlier, the assumed braking input is based on waveforms obtained in vehicle tests. This simulated braking action is assumed to begin 0.1 second after the steering input is initiated. Since braking forces reduce the tires' lateral force output, it was found necessary to increase the amplitude of the simulated steering input from 5.0 to 6.87 degrees to obtain essentially the same lateral displacement achieved in the absence of braking on the high friction surface. The timing (i.e., the waveform) of the steering input was unchanged, however, for this combined lane-change and stop maneuver. Whereas, without braking, the assumed steering waveform essentially produced a zero heading change, Figure 25(c) indicates that braking during the lane-change results in a final heading slightly different from the initial heading. With tire stiffness held fixed (C_α = 10,000; C_s = 20,000), a reduction in friction coefficient produces a large change in the lateral displacement achieved when steering and braking are combined.

Figure 26 shows the variation in vehicle trajectories caused by changes in tire traction parameters during a combined steering and braking maneuver. The influence of cornering stiffness on lateral displacement (see Figure 26(a)) is greater when braking than in a constant speed maneuver (see Figure 25(a)). Note, however, that braking and subsequent slowing of the vehicle cause a heading change at the completion of the steering maneuver. Rather than modify the steering waveform to produce a zero heading change, the steering and braking inputs were held fixed, so that the variation in path and other response elements indicate the traction parameters' influence. Whereas the vehicle performs a nominal lane change on a surface with a high coefficient of friction when steering and braking are combined (see Figure 26(a)), Figures 26(b) and 26(c) show that with a friction coefficient of 0.53 widely different trajectories depending on the cornering and braking stiffness of the tires occur.

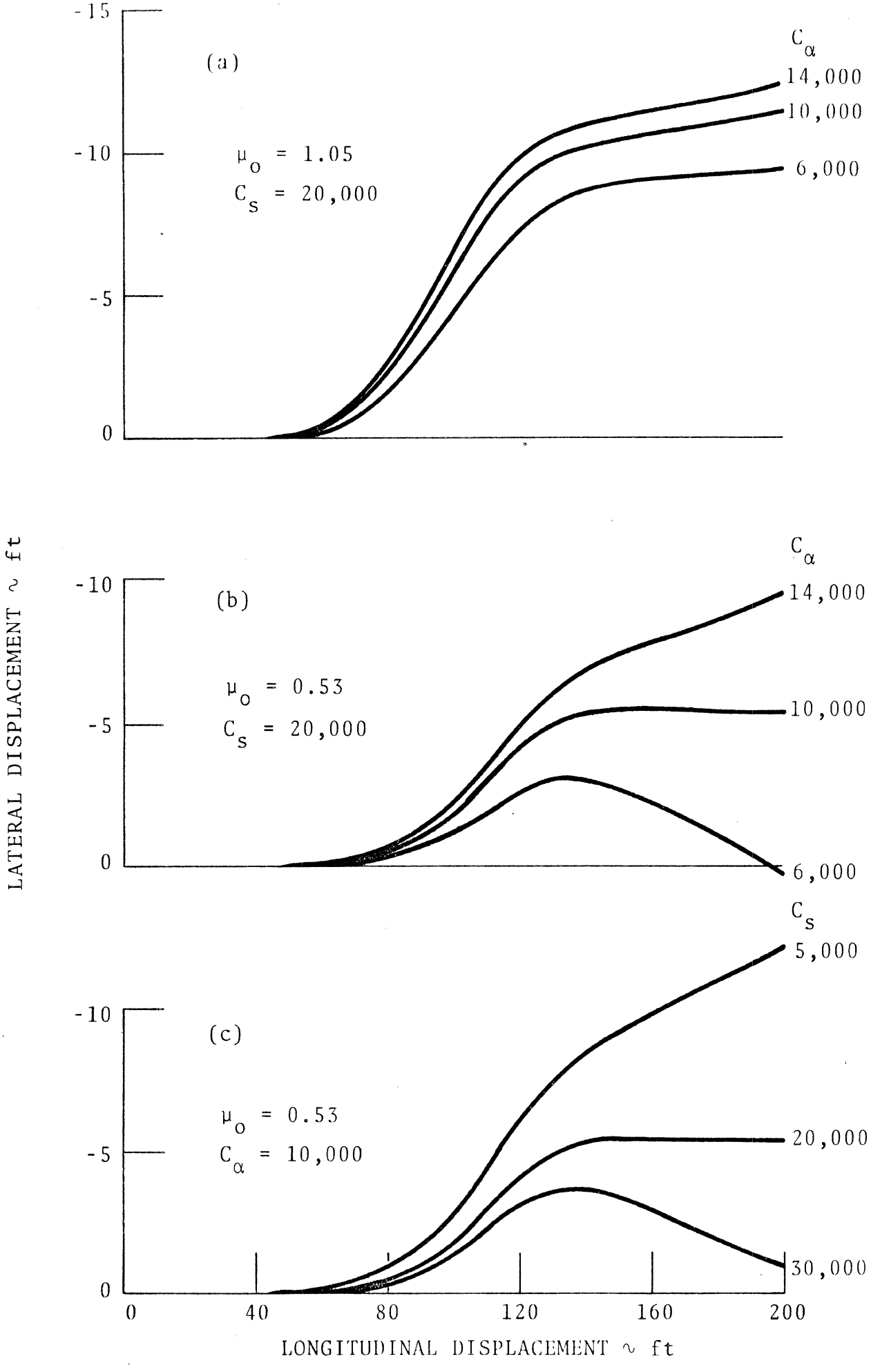

FIGURE 26. LANE CHANGE AND BRAKED STOP
[INITIAL VELOCITY = 60 ft/sec]

It should be noted that the vehicle is not braked sufficiently hard to bring it to a complete stop at the completion of the steering response. (Figure 27 shows that longitudinal velocity is reduced only a little more than half, on both the high- and low-friction surface, at the completion of the steering response.) The longitudinal deceleration in this maneuver is approximately 0.3 g. On a surface of $\mu_o = 0.53$, with this level of longitudinal deceleration and the lateral accelerations associated with the lane change the tires generate forces in the vicinity of their friction limit.

The failure of the vehicle to produce a lateral displacement on the lower-friction surface approximately equal to that achieved on the higher-friction surface, plus the failure to produce a zero heading change on the lower-friction surface, can be understood by examining the detailed time histories. Figure 27 shows a few of the pertinent details including differences in both response and in the total external tire forces generated on the high- and moderate-friction surfaces. When $\mu_o = 1.05$, the yawing velocity response is reasonably symmetrical, like that obtained when no braking occurs (see Figure 24). Further, the total lateral tire force, F_y, follows the waveform of the input brake torque. For the same tire stiffnesses, but with μ_o reduced from 1.05 to 0.53, the initial peak braking input causes the wheels to spin down, as shown by the time history of longitudinal slip, s_1, for the left front tire. During the short interval in which the longitudinal slip is high, the total lateral force output of the four tires is reduced to a very small value and the yaw rate of the vehicle fails to build up as occurs on the high friction surface. The yaw velocity response and the time history of F_y become asymmetrical, resulting in (1) highly modified lateral displacement trajectories, and (2) variable headings at the completion of the maneuver. The failure of the total longitudinal force, F_x, to follow the trace of the applied brake torque, when $\mu_o = 0.53$, indicates that the tires

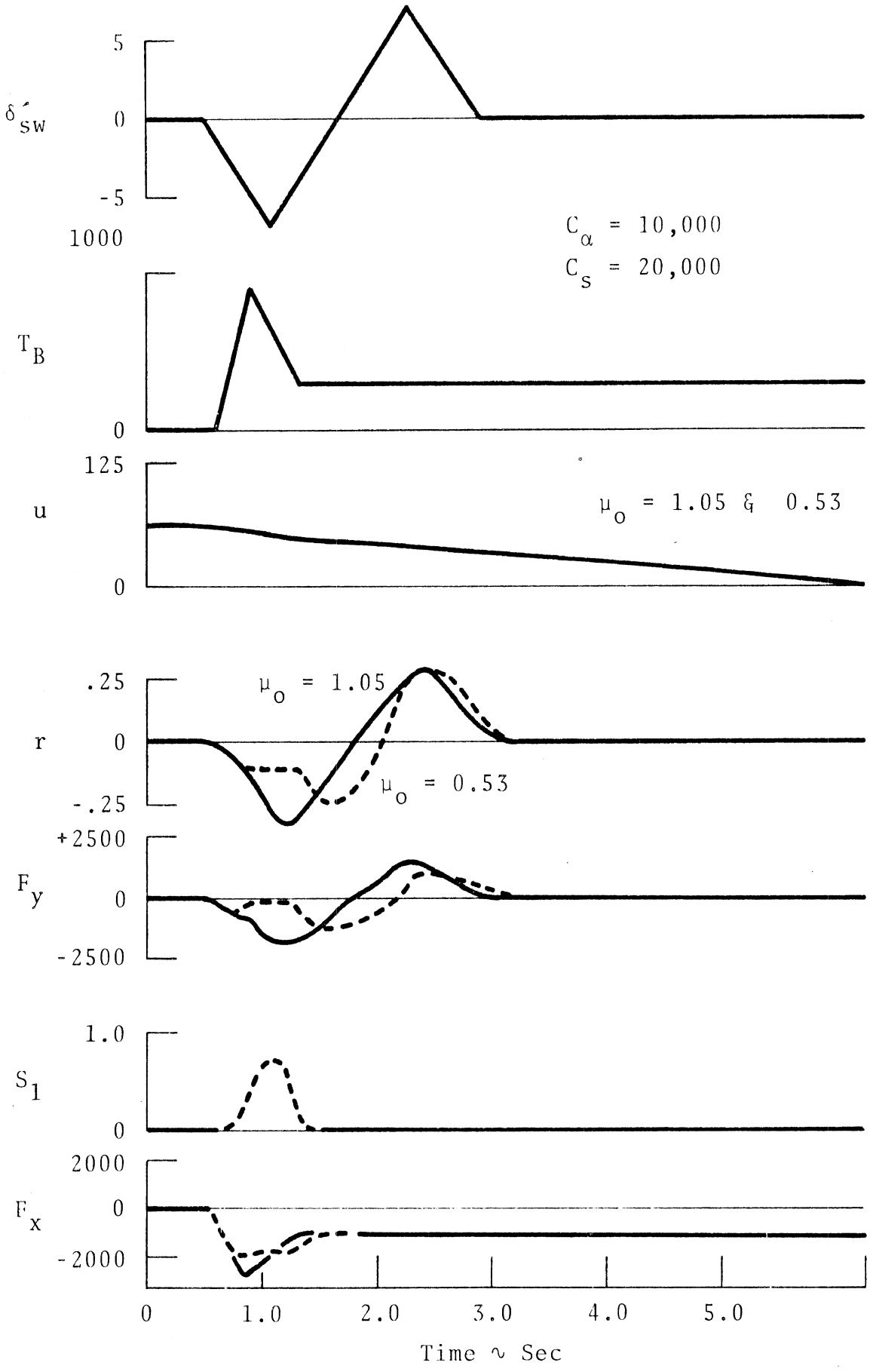

FIGURE 27. TRANSIENT RESPONSE TO STEER AND BRAKE INPUTS

are operating at their friction limit during that period in which peak brake torque occurs. It can be concluded that the open-loop response in a lane-change and stop maneuver is very much dependent on the frictional demands placed on the available surface, and that the motion response is a sensitive function of tire stiffness when the frictional demands are high. For the particular combination of control inputs and friction level used in this study ($\mu_o = 0.53$), increased cornering stiffness and decreased braking stiffness produce an increased lateral displacement in a lane-change and stop maneuver.

5. SUMMARY AND CONCLUSIONS

5.1. SUMMARY OF RESULTS

A theoretical study has been performed to investigate the influence of mechanical characteristics of pneumatic tires on the behavior of an automobile undergoing maneuvers requiring the tires to produce combined longitudinal and lateral forces. The analysis emphasized the characterization of the traction mechanics of the pneumatic tire, rather than the exact representation of the mechanics of the automobile. In spite of this, the model developed to represent the vehicle on an analog computer constitutes a simulation of substantial complexity.

The simulation model was specifically designed to study the dynamic response of a motor vehicle operated at, or near, the "limit" imposed by the frictional couple at the tire-road interface. Given this objective, it was considered necessary that the vehicle mechanics representation take account of the wheels' rotational degrees of freedom. In this respect, the model developed constitutes an extension of the vehicle simulation art. For maneuvers of low and moderate severity (i.e., maneuvers in which no "skidding" occurs), results of both steady-state and dynamic trajectory simulations are in excellent agreement with results obtained from previously developed models. Vehicle testing is required, however, to evaluate the simulation's accuracy in predicting "skidding" behavior when one or more wheels lock.

For the purposes of this study, it was necessary to represent mathematically the dependence of tire-traction components on (1) the kinematic variables associated with the tire's rolling/sliding motion and (2) the mechanical properties of the tire. No existing representation of sufficient generality was available. Further, available experimental data on tire-traction characteristics by no means constituted an adequate base for a strictly empirical determination of the required relationships. Within this context, a

theoretical analysis was undertaken of the shear-force mechanics of a pneumatic tire operating with combined side and longitudinal slip. Expressions for the longitudinal and lateral components of the traction force were derived. The rationale of the analysis was extremely pragmatic, and a number of bold assumptions were made in the interest of reducing mathematical complexity. Nevertheless, the results derived constitute a tire-mechanics model that agrees qualitatively with available experimental data, and represents the complicated phenomena of influence concisely in terms of a limited number of basic parameters.

Because of the lack of established criteria for evaluating the control quality of a tire-vehicle system, the interpretation of vehicle simulation results in terms of the relative merits of alternate system configurations is a very difficult task. The "lack of criteria problem" was more or less sidestepped in this study, by considering a number of open-loop vehicle maneuvers, and merely examining the influence on the vehicle responses of realistic variations in the values of three tire parameters, (1) the lateral stiffness, C_α, (2) the longitudinal stiffness, C_s, and (3) the nominal coefficient of tire-road interface friction, μ_o. It was assumed that the four vehicle tires had identical properties.

The significant findings for each of the open-loop maneuvers considered are summarized in the following sections.

5.1.1. STEADY-STATE TURNING. Nonlinear tire mechanics produce steady turning response characterized by increased understeer with increased thrust, until a thrust level is reached at which the effect reverses. This phenomenon is accentuated by high values of C_α or (to a lesser extent) C_s.

Equilibrium speed in a steady turn established by a given thrust and steer angle is a monotonically increasing function of both C_α and C_s.

For a given thrust and steer angle, steady turning capability (measured in terms of the centripetal acceleration produced) increases with increasing values of C_α . This finding holds for all drive-torque values up to the equilibrium turn limit. Turning capability does not decrease in direct proportion to decreases in the friction coefficient μ_o , i.e., cornering efficiency (peak value of $\frac{V_r}{\mu_o g}$) decreases with increases in μ_o (over the range studied).

5.1.2. BRAKING FROM A STEADY TURN. In this maneuver, high values of two response variables, (1) change of path curvature, and (2) sideslip angle, are considered to reflect poor quality of performance. Based on these criteria, the simulation results indicate that superior performance is achieved with (1) high values of C_α and (2) low values of C_s . The effects of the stiffness variables are accentuated at high values of μ_o . Poor performance in this maneuver is generally associated with wheel slowdown to lockup, or near lockup, conditions.

5.1.3. TRANSIENT STEERING RESPONSE AT HIGH LATERAL ACCELERATION. Because of nonlinear tire characteristics, a vehicle's directional response to a given steer input depends strongly on its initial trim condition. The more severe the initial trim state (i.e., the nearer the tires are to operating at the friction limit), the more pronounced is the difference in response from that associated with variations from straight running conditions.

Response to a short (4°) ramp of steering input from an initial steady turn trim condition (with no change in drive torque) is characterized by (1) a rapid yawing velocity response analogous to the response mode of a constant-speed vehicle, (2) the achievement of a pseudo-steady-state condition (a non-linear function of initial trim), and then (3) a very slow transient stage during which the vehicle slows to a new trim velocity, and the yawing velocity consequently increases because of the vehicle's understeer characteristic.

The initial short period oscillation tends to persist on a lower friction surface and is aggravated by reduction in either C_α or C_s .

5.1.4. COMBINED LANE CHANGING AND BRAKING MANEUVERS. Vehicle response in combined lane changing and braking maneuvers is very much dependent upon the frictional demand placed on the pavement surface. When the frictional demand is high (i.e., when the resultant tire shear forces approach a value equal to the product of the tire-road friction coefficient and the dynamic vertical tire load), the motion response is a sensitive function of tire stiffness properties. At the lower interface-friction level considered here ($\mu_o = 0.53$), lateral displacement per unit steer input (for a given level of braking) increases with increasing values of C_α and decreasing values of C_s .

5.2. CONCLUDING REMARKS

The results summarized above represent only a beginning in the general study of the relationships between tire-traction properties and the pre-crash safety of a motor vehicle. As a starting point for further investigation they raise a number of important, as yet unanswered, questions.

The most compelling of these questions fall within the domain of the experimentalist. The tire-mechanics model presented here agrees qualitatively with the very limited relevant experimental data available. In order to precisely assess the quantitative validity of the model, however, a considerable base of appropriately structured and accurately measured tire shear force data is required.

To evaluate the accuracy of the vehicle simulation model in predicting skidding and near-skidding maneuver responses, it will be necessary to conduct vehicle response tests. Experimental counterparts of the maneuvers performed on the computer in this study would be appropriate for this purpose.

In a more theoretical vein, a great deal of research is certainly needed to formulate basic criteria for assessing vehicle control quality from a safety point of view. Pending the development of such criteria, however, it appears profitable to continue to perform pragmatic simulation studies such as the one just completed. In particular, it would be of interest to investigate the effects associated with the operation of tires with unequal properties, and to study the influence of variations in tire and vehicle parameters other than C_α, C_s, and μ_o .

6. ACKNOWLEDGMENTS

This study was conducted for the Office of Vehicle Systems Research of the National Bureau of Standards as part of their program in support of the standards setting and quality grading activities of the National Highway Safety Bureau. We would like to extend particular thanks to Dr. F. Cecil Brenner, Head of the Tire System Section of that office, for his consistent cooperation throughout the course of the program.

The panel of researchers whose help was enlisted in formulating maneuver conditions for the parametric studies consisted (in addition to the authors) of Mr. P.S. Carroll, Dr. R.L. Hess, Dr. J.W. Melvin, and Dr. R.G. Mortimer, all of this Institute. We wish to thank all of these gentlemen for their time and effort. We also would like to acknowledge the general assistance of Mr. Takesuke Mori, formerly Visiting Engineer at HSRI, who has since returned to his work at the Toyota Motor Co., Ltd., of Japan.

The digital vehicle simulation program employed for comparison purposes was made available to HSRI by the Office of Research and Development of the Bureau of Public Roads. Thanks are due to Messrs Carl F. Izzard and John Eicher of that office, and Mr. R.R. McHenry of Cornell Aeronautical Laboratory, for helping to arrange this.

APPENDIX A

A TIRE MECHANICS MODEL FOR THE CASE OF COMBINED SIDE AND LONGITUDINAL SLIP

The development which follows is directly derivative of the classic analysis of the freely rolling tire due to Fiala [9]. In many respects, however, it is less rigorous; several assumptions made here in the interest of mathematical simplicity represent marked relaxations of the theoretical precision of the earlier work. Each of these simplifications will be carefully pointed out. Refinement of the analysis through elimination of the various simplifications is regarded as manifestly appropriate for subsequent applications wherein greater accuracy may be required.

The derivation is based on an idealization of the tire-road contact region geometry as shown in Figure A-1. The tire is considered to have zero inclination angle; the effects of inclination on the forces produced are accounted for approximately through the introduction of an "equivalent slip angle" which is a function of the inclination angle and the tire's camber stiffness. This approximation, a departure from the Fiala analysis, is discussed in detail at a later point in the development.

Line 0-1-2 (Figure A-1) is the longitudinal centerline of the tire-road contact patch. The ξ-η ground plane coordinate system has its origin at point 0, the tread touchdown point, with the ξ axis passing through point 2, the tread liftoff point. Line 3-4 is the longitudinal centerline of the tire carcass. Each point on the carcass centerline is assumed to be elastically connected to the tread (line 0-1-2)

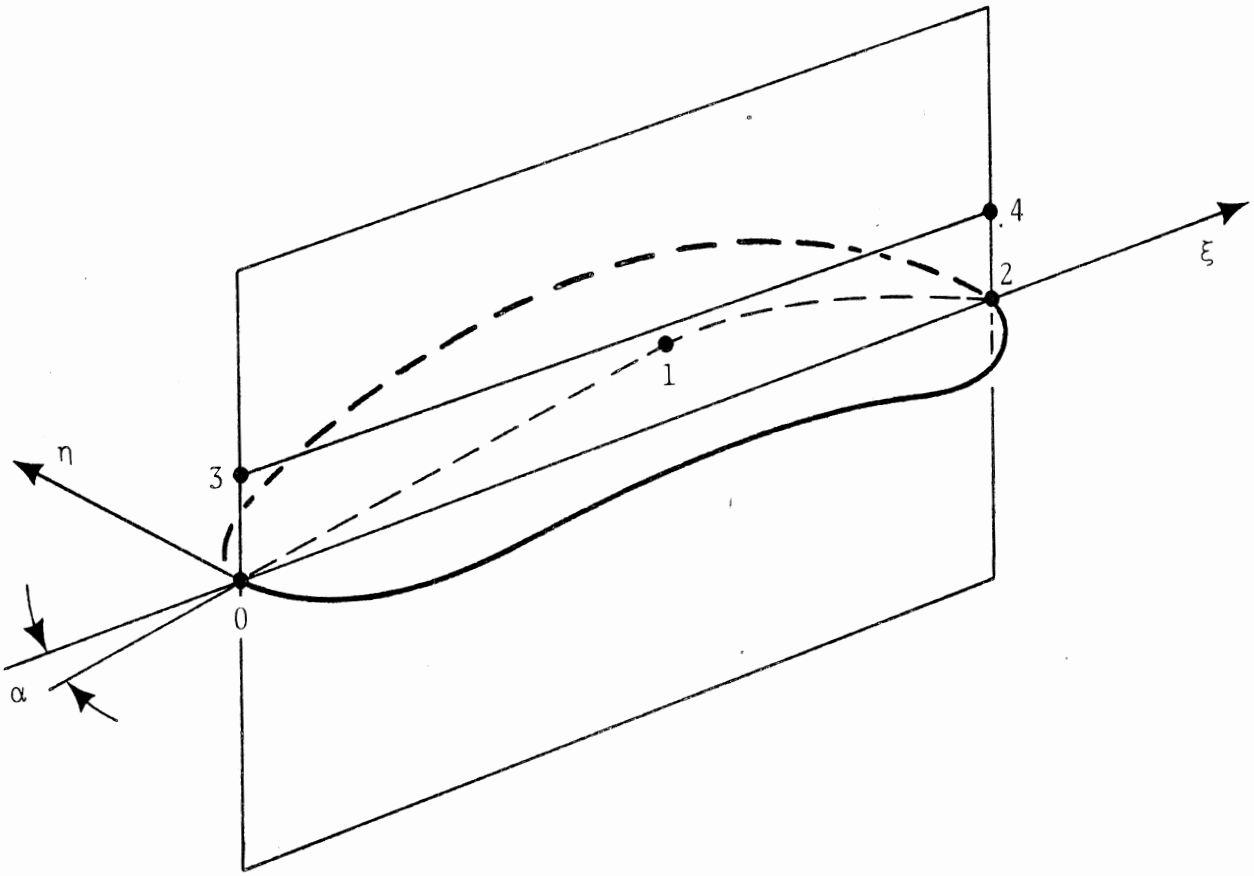

FIGURE A-1. TIRE-ROAD CONTACT REGION GEOMETRY

through orthogonal "springs" producing independent forces in the ξ and η directions. Thus a point on the tread follows the path of the carcass so long as no shear force acts on it; in particular, points 3 and 4 lie on vertical lines passing through points 0 and 2, respectively.

In the original Fiala analysis, the configuration of the carcass centerline, line 3-4, is derived by assuming it to behave as an elastically supported beam subjected to a point (lateral) load at its center. The resulting infinite series is approximated by a parabola. In the present analysis, we make the more arbitrary assumption that the carcass centerline deformation may be approximated by a constant; thus line 3-4 lies in the vertical plane passing through the ξ axis (see Figure A-1). The validity of this rather bold assumption can only be assessed from a practical standpoint on the basis of such comparisons with experiment as in Section 2 of this report.

Point 1 of the tire tread centerline represents the "sliding boundary"; points on the tread forward of point 1 (line segment 0-1) adhere to the ground surface without sliding. At point 1, the elastic stresses due to tread deformation reach a value corresponding to the tire-road shear stress limit and the rubber begins to slide relative to the ground. Accordingly the shear deformation along line segment 1-2 is a function of the local sliding friction potential, dropping off monotonically towards a zero value at the tread liftoff point, point 2.

Figure A-2 is a sketch depicting the hypothesized deformation condition prevailing at a typical point $P(\xi,\eta)$ on the non-sliding segment (0-1) of the patch centerline. The longitudinal coordinate of point P is equal to the product of the tire's longitudinal velocity (u_w) and the time interval, Δt, from the instant when P entered the patch at 0 to the instant pictured, i.e.,

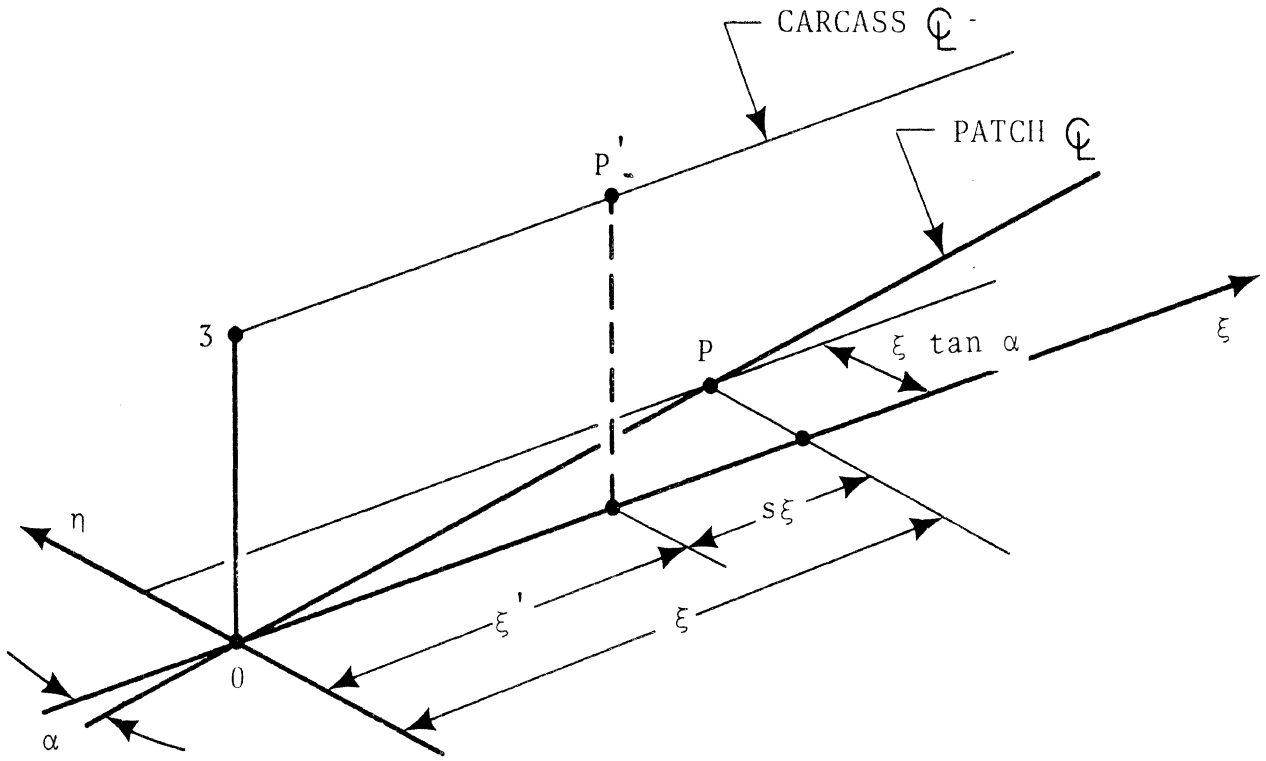

FIGURE A2. STRAIN CONDITION IN NON-SLIDING PORTION OF CONTACT PATCH

$$\xi = u_w \Delta t. \tag{A-1}$$

During the same interval Δt, point P' on the carcass centerline (which coincided with point 3 at the start of the interval) has moved a distance ξ', given by

$$\xi' = \Omega R_e \Delta t \ ^{*} \tag{A-2}$$

Thus the longitudinal deformation of point P relative to point P' is given by

$$\begin{aligned} \xi - \xi' &= u_w \Delta t - \Omega R_e \Delta t \\ &= \left(1 - \frac{\Omega R_e}{u_w}\right) u_w \Delta t \\ &= s\xi, \end{aligned} \tag{A-3}$$

and the longitudinal component of stress at point P is equal to

$$\sigma_\xi = K_x s \xi, \tag{A-4}$$

where K_x is the "longitudinal tire stiffness," in pounds per unit length, per unit width, per unit longitudinal deflection.

The lateral deformation of point P is given by (see Figure A-2):

$$\eta = -\xi \tan \alpha^{**} \tag{A-5}$$

Thus the lateral stress component at P is equal to

$$\sigma_\eta = -K_y (\tan \alpha) \xi, \tag{A-6}$$

where K_y is the "lateral tire stiffness," in pounds per unit length, per unit width, per unit lateral deflection.

---

*In general, symbols defined in the main body of the report are not explicitly redefined in this appendix. All symbols used in either the body of the report or the appendices are defined in the list of symbols appended to the report.

**Note that the sideslip angle α shown in Figure A-2 is a negative angle.

The maximum allowable total shear stress at any point in the contact patch is determined by the tire-road shear stress limit, σ_{max}. The limit, σ_{max}, varies over the contact patch. One of the main factors determining σ_{max} is the normal pressure distribution over the contact patch. For simplicity, we will assume here that the pressure is uniform over the patch, with its value given by

$$p = \frac{|F_z|}{2\ell w} \quad . \tag{A-7}$$

F_z is the normal load on the tire, 2ℓ is the length of the contact patch, and w is the width of the contact patch.

This approximation is fairly realistic except at the edges of the patch. The tire-road shear stress limit accordingly is given by

$$\sigma_{max} = \mu p = \frac{\mu |F_z|}{2\ell w} \tag{A-8}$$

where μ is the coefficient of friction at the interface. (The quantity μ will be discussed later.)

Using equation A-8, we can determine the position of the sliding boundary point (point 1 in Figure A-1), where the resultant elastic deformation stress just equals the tire-road shear stress limit, i.e., where

$$(\sigma_\xi^2 + \sigma_\eta^2)^{1/2} = \sigma_{max} = \frac{\mu |F_z|}{2\ell w} \quad . \tag{A-9}$$

Let ξ_s denote the longitudinal coordinate of the sliding boundary point. Then, substituting into equation A-9 from equations A-4 and A-5, we obtain

$$\xi_s = \frac{\mu |F_z|}{2\ell w} \left[(K_x s)^2 + (K_y \tan \alpha)^2 \right]^{-1/2} \quad . \tag{A-10}$$

Let ξ'_s denote the longitudinal coordinate of the point on the tire carcass associated with point ξ_s, as per Figure A-2. Then, from equation A-3

$$\xi'_s = (1-s)\,\xi_s$$

$$= \frac{\mu|F_z|}{2\ell w}\,(1-s)\,[(K_x s)^2 + (K_y \tan\alpha)^2]^{-1/2} \quad . \qquad \text{(A-11)}$$

In order that we may be able to simply compute the resultant tire shear forces by closed-form integration, we assume that the actual deformation field of the sliding portion of the contact patch may be approximated by a uniform deformation. Although compatible with the assumption of a uniform normal pressure distribution, this approximation is obviously considerably in error at points in the rearmost portion of the contact patch (see Figure A-1). In keeping with the pragmatic philosophy of the analysis, we will not attempt to defend it on any grounds other than it appears to produce answers which are reasonable.

Based on the assumed form of the contact patch deformation field, we may compute the values of the longitudinal and lateral tire shear forces, F_ξ and F_η, respectively, as follows:

$$F_\xi = \int_0^w \left(\int_0^{\xi'_s} \sigma_\xi\,(\xi')d\xi' + \int_{\xi'_s}^{2\ell} \sigma_\xi\,(\xi')d\xi'\right) dw \quad ,$$

where, from equations A-3 and A-4,

$$\sigma_\xi\,(\xi') = \begin{cases} \dfrac{K_x s\,\xi'}{1-s} \quad , & \text{for } \xi' \leq \xi'_s \quad , \\[2ex] \dfrac{K_x s\,\xi'_s}{1-s} \quad , & \text{for } \xi' > \xi'_s \quad , \end{cases}$$

and

$$F_\eta = \int_o^w \left(\int_o^{\xi_s'} \sigma_\eta \ (\xi')d\xi' + \int_{\xi_s'}^{2\ell} \sigma_\eta \ (\xi')d\xi' \right) dw \ ,$$

where, from equations A-3 and A-6,

$$\sigma_\eta \ (\xi') = \begin{cases} -\dfrac{K_y \tan \alpha \ \xi'}{1-s} & , \text{ for } \xi' \leqq \xi_s' \ , \\ -\dfrac{K_y \tan \alpha \ \xi_s'}{1-s} & , \text{ for } \xi' > \xi_s' \ . \end{cases}$$

Note that the stress distribution is assumed to be uniform with respect to the contact patch width. Thus

$$F_\xi = \begin{cases} \dfrac{2\ell^2 w K_x s}{1-s} & , \text{ for } \xi_s' \geqq 2\ell \text{ (no sliding in the patch)}, \\ \dfrac{2\ell w K_x s \xi_s'}{1-s} - \dfrac{w K_x s (\xi_s')^2}{2(1-s)} & , \text{ for } \xi_s' < 2\ell \ , \end{cases} \tag{A-12}$$

$$F_\eta = \begin{cases} \dfrac{-2\ell^2 w \ K_y \tan \alpha}{1-s} & , \text{ for } \xi_s' \geqq 2\ell \text{ (no sliding in the patch)}, \\ \dfrac{-2\ell w \ K_y \tan \alpha \ \xi_s'}{1-s} + \dfrac{w K_y \tan \alpha \ (\xi_s')^2}{2(1-s)} & , \text{ for } \xi_s' < 2\ell \ . \end{cases} \tag{A-13}$$

The derived results can be written more concisely in terms of the following auxiliary variables

$$\bar{\alpha} = \frac{2\ell^2 \ w \ K_y \tan \alpha}{\mu |F_z| \ (1-s)} \ , \tag{A-14}$$

$$\bar{s} = \frac{2\ell\, w\, K_x\, s}{\mu |F_z| (1-s)} \quad , \tag{A-15}$$

$$\bar{s}_R = (\bar{s}^{\,2} + \bar{\alpha}^{\,2})^{1/2} \quad . \tag{A-16}$$

Note that the variable $\bar{s}_R$ may be considered to constitute a "resultant normalized slip vector," whose components are $\bar{\alpha}$ and $\bar{s}$.

Equations A-14, A-15, and A-16 may be used together with equation A-11 to rewrite equations A-12 and A-13 in the form

$$\frac{F_\xi}{\mu |F_z|} = \frac{\bar{s}}{\bar{s}_R} \frac{F_R}{\mu |F_z|} \quad , \tag{A-17}$$

$$\frac{F_\eta}{\mu |F_z|} = - \frac{\bar{\alpha}}{\bar{s}_R} \frac{F_R}{\mu |F_z|} \quad , \tag{A-18}$$

where

$$\frac{F_R}{\mu |F_z|} = \begin{cases} \bar{s}_R \quad , & \text{for } \bar{s}_R < 0.5 \quad , \\ 1 - \dfrac{1}{4\bar{s}_R} \quad , & \text{for } \bar{s}_R \geq 0.5 \quad . \end{cases} \tag{A-19}$$

Note from equations A-16, A-17, and A-18 that the quantity

$$F_R = (F_\xi^2 + F_\eta^2)^{1/2}$$

represents the resultant shear force exerted at the tire-road interface.

By reference to Figures 1 and A-1, equations A-17 and A-18 may be rewritten in terms of the tire coordinate system employed in the main body of the report:

$$\frac{F_{xw}}{\mu\,|F_z|} = -\left(\frac{\bar{s}}{\bar{s}_R}\right)\frac{F_R}{\mu\,|F_z|}\,, \tag{A-20}$$

$$\frac{F_{yw}}{\mu\,|F_z|} = -\left(\frac{\bar{\alpha}}{\bar{s}_R}\right)\frac{F_R}{\mu\,|F_z|}\,. \tag{A-21}$$

Now let us consider for a moment the special case $\alpha=o$. For this case, equations A-14, A-15, A-16, and A-19 may be used together with equation A-20 to obtain

$$\left.\frac{F_{xw}}{\mu\,|F_z|}\right|_{\alpha=o} = -\,\bar{s}\,, \quad \text{for} \quad \bar{s} < 0.5\,,$$

whence, using equation A-15 ,

$$\left.\frac{\partial F_{xw}}{\partial s}\right|_{\alpha=s=o} = -\,2\ell^2\, w\, K_x\,. \tag{A-22}$$

But, by definition (see equation 14 in the main body of the report):

$$\left.\frac{\partial F_{xw}}{\partial s}\right|_{\alpha=s=o} = -C_s \tag{A-23}$$

Equations A-22 and A-23 may be used to rewrite equation A-15 in the form

$$\bar{s} = \frac{C_s s}{\mu\,|F_z|\,(1-s)} \tag{A-24}$$

Similarly, by considering the case $s=o$, we may show that equation A-14 is equivalent to

$$\bar{\alpha} = \frac{C_\alpha \tan \alpha}{\mu \, |F_z| \, (1-s)} \qquad \text{(A-25)}$$

The tire-road friction coefficient, μ , is known to be a function of sliding speed and normal pressure, as well as a host of quantities describing the material and geometric properties of the road surface and any interface contaminants [45]. For the purposes of this study, by far the most important of these effects is that due to speed. On the basis of some very limited experimental data due to Krempel [15], it appears that this effect can be approximated by a simple linear equation of the form

$$\mu = \mu_o (1 - A_s V_s) \ , \qquad \text{(A-26)}$$

where V_s , the "total sliding velocity," is given by

$$V_s = u_w \, [\, s^2 + (\tan \alpha)^2 \,]^{1/2} \ . \qquad \text{(A-27)}$$

The implications of the assumed form of the friction/speed relation are discussed in some detail in the main body of the report.

The influence of tire inclination, i.e., camber angle, remains to be taken into account. This is done on the basis of an "equivalent slip angle" approximation derivative of the work of McHenry, et al. [37]. For the application of reference [37], very large camber angles were studied; for the vehicle maneuvers considered here, the camber angles are small. Thus we have used a much simpler (linear) expression for the equivalent slip angle than employed previously, viz.,

$$\alpha_C = - \frac{C_\gamma}{C_\alpha} \cdot \gamma$$

$$= - C^*_\gamma \gamma \, , \qquad \text{(A-28)}$$

where C^*_γ , the "relative camber stiffness," is an empirically derived property of the tire.

The total slip angle (i.e., the value to be employed for computing the tire forces as per equations A-20 and A-21) is given by

$$\alpha = \alpha_o + \alpha_C$$

$$= \alpha_o - C^*_\gamma \gamma \, , \qquad \text{(A-29)}$$

where α_o is the slip angle as defined by usual convention (c.f., Figure 1 and equation B-30).

APPENDIX B

THE VEHICLE MECHANICS MODEL

This appendix includes a detailed description of all aspects of the vehicle simulation model exclusive of the tire mechanics representation presented in Appendix A.

Vehicle Motion Equations

The motion of the vehicle in the horizontal plane is described in terms of velocity components in a body fixed x-y-z coordinate system with origin at the vehicle center of gravity (see Figure B-1). Application of Newton's second law for forces along the x and y axes and moments about the z-axis, respectively, yields

$$m(\dot{u} - r\,v) = F_x, \tag{B-1}$$

$$m(\dot{v} + r\,u) = F_y, \tag{B-2}$$

$$I\,\dot{r} = T\,. \tag{B-3}$$

m is the mass of the vehicle, I is its yaw moment of inertia, F_x is the total longitudinal force on the vehicle, F_y is the total lateral force on the vehicle, and T is the total torque applied to the vehicle about the vertical (z) axis through its CG.

Applied Forces and Moments in the Horizontal Plane

The external forces considered to act on the vehicle in the horizontal plane are illustrated in Figure B-1. Thus

$$F_x = F_{x1} + F_{x2} + F_{x3} + F_{x4} - F_D \tag{B-4}$$

$$F_y = F_{y1} + F_{y2} + F_{y3} + F_{y4}, \tag{B-5}$$

$$T = t(F_{x1} - F_{x2} - F_{x3} + F_{x4}) + a(F_{y1} + F_{y2}) - b(F_{y3} + F_{t4}). \tag{B-6}$$

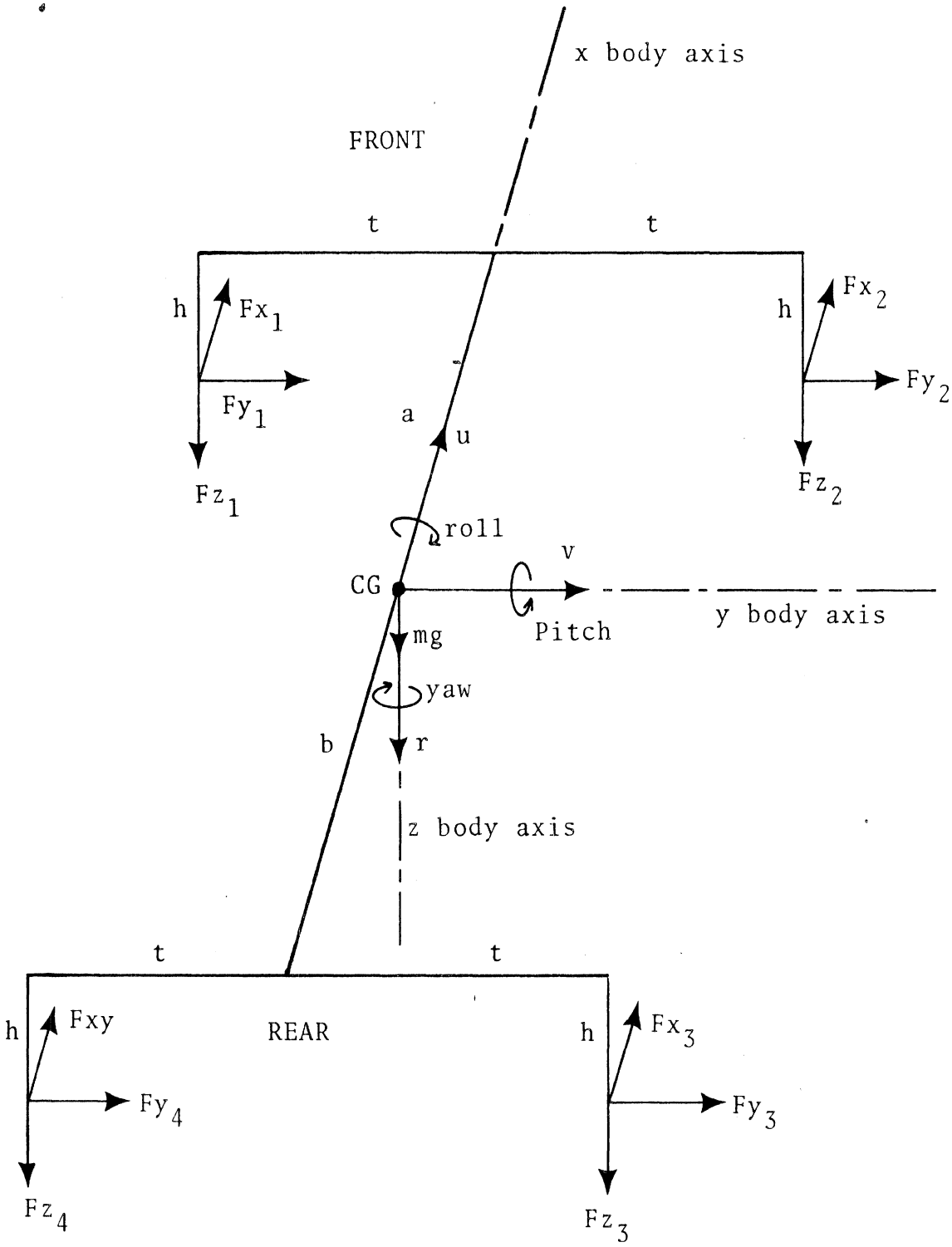

FIGURE B1. VEHICLE GEOMETRY

Note that we have neglected the effects of tire aligning torques in equation B-6. The tire force components along the vehicle axes are computed from the results of the tire mechanics model calculations (equations A-20 and A-21) by application of the following coordinate transformation equations:

$$F_{xi} = F_{xwi} \cos \delta_i - F_{ywi} \sin \delta_i \qquad \text{(B-7)}$$

$$F_{yi} = F_{xwi} \sin \delta_i + F_{ywi} \cos \delta_i \ . \qquad \text{(B-8)}$$

The angle δ_i is the steering angle of the i^{th} wheel. For the front wheels, δ_i is determined by the steering angle δ_{Fw} (see equation B-23). For the rear wheels, δ_i is given by the rear axle roll steer angle δ_{rs} (see equation B-31).

The aerodynamic drag force, F_D , is computed from

$$F_D = 1/2 \ C_D \ \rho \ A_D \ u^2 \ , \qquad \text{(B-9)}$$

where C_D is the vehicle's aerodynamic drag coefficient, ρ is the mass density of the ambient air (taken as .00238 sl/ft^3) and A_D is the cross-sectional (frontal) area of the vehicle.

Tire Normal Loads

The tire normal loads depend upon the static loading of the vehicle and the dynamic load transfer accompanying accelerated vehicle motion. As noted in the main body of the report, the current model makes use of a quasi-static approximation to account for the dynamic load transfer effect. The roll angle of the sprung mass, ϕ , is estimated from

$$\phi = \frac{-hF_y}{K_{r\phi} + K_{f\phi}} \ , \qquad \text{(B-10)}$$

where $K_{r\phi}$ is the rear roll stiffness and $K_{f\phi}$ is the front roll stiffness. Superposing the load transfer components, front and rear, due to this roll angle upon the (quasi-static) load transfer due to pitching [c.f., 44] gives

$$F_{z1} = -\frac{mg}{2}\frac{b}{a+b} + \frac{hF_x}{2(a+b)} - \frac{K_{f\phi}}{K_{f\phi}+K_{r\phi}}\frac{hF_y}{2t}, \qquad \text{(B-11)}$$

$$F_{z2} = -\frac{mg}{2}\frac{b}{a+b} + \frac{hF_x}{2(a+b)} + \frac{K_{f\phi}}{K_{f\phi}+K_{r\phi}}\frac{hF_y}{2t}, \qquad \text{(B-12)}$$

$$F_{z3} = -\frac{mg}{2}\frac{a}{a+b} - \frac{hF_x}{2(a+b)} + \frac{K_{r\phi}}{K_{f\phi}+K_{r\phi}}\frac{hF_y}{2t}, \qquad \text{(B-13)}$$

$$F_{z4} = -\frac{mg}{2}\frac{a}{a+b} - \frac{hF_x}{2(a+b)} - \frac{K_{r\phi}}{K_{f\phi}+K_{r\phi}}\frac{hF_y}{2t}. \qquad \text{(B-14)}$$

Wheel Rotation Dynamics

The coordinate system employed to describe the dynamics of the i^{th} wheel is shown in the sketch below.

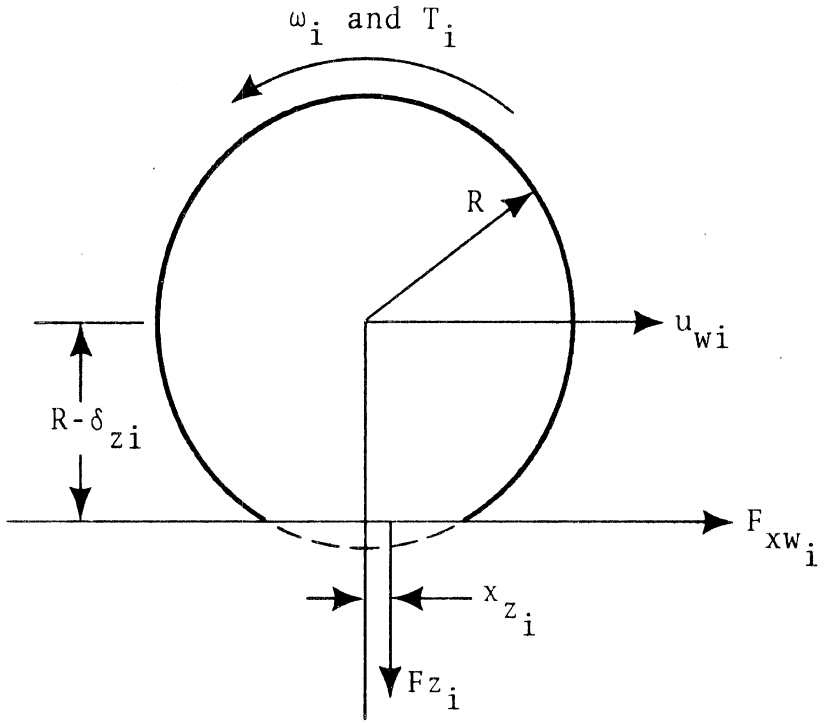

Note that the wheel rotational velocity in this system, ω_i , is the negative of the spin velocity Ω_i defined in the main body of the report (see Figure 1). Application of Newton's second law for moments about the wheel spin axis yields

$$I_{wy}\dot{\omega}_i = T_i + F_{xwi}\,(R-\delta_{zi}) - F_{zi}x_{zi} - C_{wi}\omega_i \qquad \text{(B-15)}$$

I_{wy} is the moment of inertia of the rotating part of the wheel about the spin axis of the wheel, ω_i is the angular velocity of the wheel, T_i is the brake torque applied to the wheel, F_{xwi} is the longitudinal tire force in the wheel plane, R is the undeflected radius of the tire, δ_{zi} is the amount of vertical tire deflection, F_{zi} is the normal load on the tire, x_{zi} is the amount of longitudinal offset of the center of vertical pressure from the wheel center, and C_{wi} is the wheel damping coefficient.

The vertical tire deflection is computed from an empirical equation ,

$$\delta_{zi} = C_{zi}\,(-F_{zi}) + .033\ R\ , \qquad \text{(B-16)}$$

where C_{zi} , the vertical deflection rate of the tire, is an empirically determined property of the tire. The longitudinal offset of the center of vertical pressure is computed from

$$x_{zi} = C_{xi}F_{xwi} + 0.02\ , \qquad \text{(B-17)}$$

where C_{xi} , the "vertical force offset rate," is also determined empirically. The form of equation B-17 was suggested by some very limited experimental data given by Goodenow, et al. [11].

Steering System Dynamics

The representation of the steering system is largely derivative of the model developed in [1]. The input to the system is δ'_{sw}, the steering wheel angle divided by the steering ratio. The degree of freedom associated with the steering wheel inertia is not included. The front wheel steer angles, δ_1 and δ_2, are combined to obtain an effective front wheel angle, δ_{Fw}, where:

$$\delta_{Fw} = \frac{\delta_1 + \delta_2}{2} \tag{B-18}$$

Equation B-18 represents a reasonable way of combining the steer angles to approximate the steering deflections. The moment, M_s, on either of the front wheels due to the steering compliance, K_{ss}, is given by

$$M_s = \frac{K_{ss}}{2} \left(\delta'_{sw} - \delta_{Fw}\right) . \tag{B-19}$$

The equation for rotation of the left front wheel about the kingpin is:

$$I_{Fw} \ddot{\delta}_1 = M_s + C_{F1} + F_{xw_1} K_p + AT_1 . \tag{B-20}$$

I_{Fw} is the wheel moment of inertia about the kingpin, C_{F1} is the coulomb friction in the system, K_p is the kingpin offset, and AT_1 is the aligning torque. The effect of yaw acceleration, $\dot{r}$, has been omitted because it is small. The equation for the right front wheel is

$$I_{Fw} \ddot{\delta}_2 = M_s + C_{F2} - F_{xw_2} K_p + AT_2 . \tag{B-21}$$

For simplification, it is assumed that the effects of coulomb friction can be approximated in terms of an "equivalent viscous damping" coefficient C_F , defined by

$$C_F \dot{\delta}_{Fw} \cong C_{F1} + C_{F2} \tag{B-22}$$

Then, combining equations B-19, 20, and 22, we have

$$2I_{Fw}(\ddot{\delta}_{Fw}) = K_{ss}(\delta'_{sw} - \delta_{Fw}) + C_F\dot{\delta}_{Fw} + K_p(F_{xw_1} - F_{xw_2}) + AT_1 + AT_2 \tag{B-23}$$

The aligning torques are computed using a constant pneumatic trail, x_p . The equations are:

$$AT_1 = -x_p F_{yw_1} \tag{B-24}$$

$$AT_2 = -x_p F_{yw_2} \tag{B-25}$$

Tire Kinematics

The longitudinal and lateral components of the velocities of each wheel are given by (see Figure B-1)

$$\left.\begin{aligned} u_1 &= u + tr , & v_1 &= v + ar , \\ u_2 &= u - tr , & v_2 &= v + ar , \\ u_3 &= u - tr , & v_3 &= v - br , \\ u_4 &= u + tr , & v_4 &= v - br , \end{aligned}\right\} \tag{B-26}$$

The velocity components in the wheel plane u_{wi}, are computed from the above using the following equation:

$$u_{wi} = u_i \cos \delta_i + v_i \sin \delta_i, \qquad \text{(B-27)}$$

where δ_i is the steering angle of the i^{th} wheel (see note after equation B-8).

The longitudinal slip ratio,

$$s_i = 1 + \frac{\omega_i R_{ei}}{u_{wi}} , \qquad \text{(B-28)}$$

is computed using u_{wi} from equation B-27, ω_i from equation B-15, and a value for R_{ei}, the effective rolling radius, estimated from

$$R_{ei} = R - \frac{\delta_{zi}}{3} , \qquad \text{(B-29)}$$

where δ_{zi}, the vertical tire deflection, is given by equation B-16.

The tire sideslip angle, α_i is given by (see sketch):

$$\alpha_i = \tan^{-1} \left(\frac{v_i}{u_i} \right) - \delta_i \qquad \text{(B-30)}$$

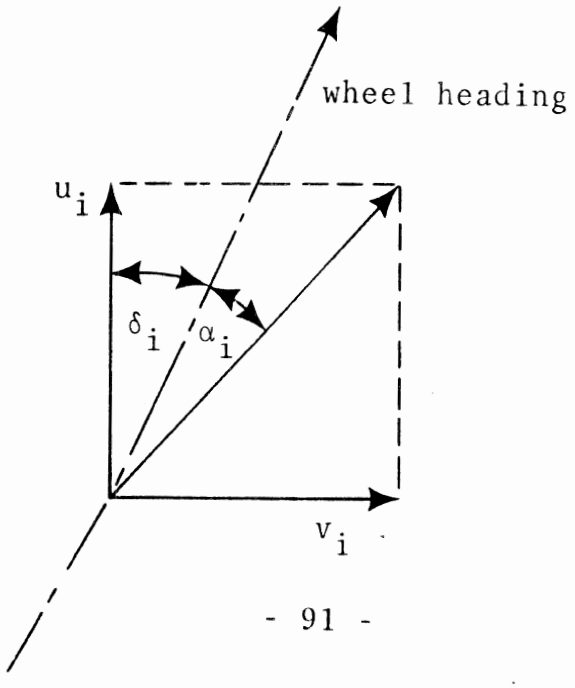

As noted in the main body of the report, quasi-static approximations are employed to account for wheel roll-steer and camber effects. The rear axle roll-steer is given by

$$\delta_{rs} = -C_{sR}\,\phi \ , \qquad \text{(B=31)}$$

where C_{sR} , the roll-steer coefficient, is an empirically derived parameter of the vehicle, and the sprung mass roll angle, ϕ , is given by equation B-10.

The camber angle of the left front wheel γ_1 is a function of the vertical deflection $\bar{z}_1$ of the wheel from the chassis. The deflection of the wheel depends upon both pitch and roll of the sprung mass. The pitch angle θ of the sprung mass is approximated by:

$$\theta = \frac{1}{aK_f}\left(\frac{F_{z1} + F_{z2}}{2} + \frac{mgb}{2(a+b)}\right) \qquad \text{(B-32)}$$

where K_f is the front spring rate. The front suspension deflections are given by:

$$\bar{z}_2 = \frac{1}{2}\left(\frac{mgb}{a+b}\right)\left(\frac{1}{K_f}\right) + \theta a - \phi t \qquad \text{(B-33)}$$

$$\bar{z}_1 = \frac{mgb}{2(a+b)\,(K_f)} + \theta a + \phi t \qquad \text{(B-34)}$$

The front wheel camber angles are functions of $\bar{z}_2$ and $\bar{z}_1$. These functions are implemented in the simulation using diode function generators. The forms of these functions are shown below:

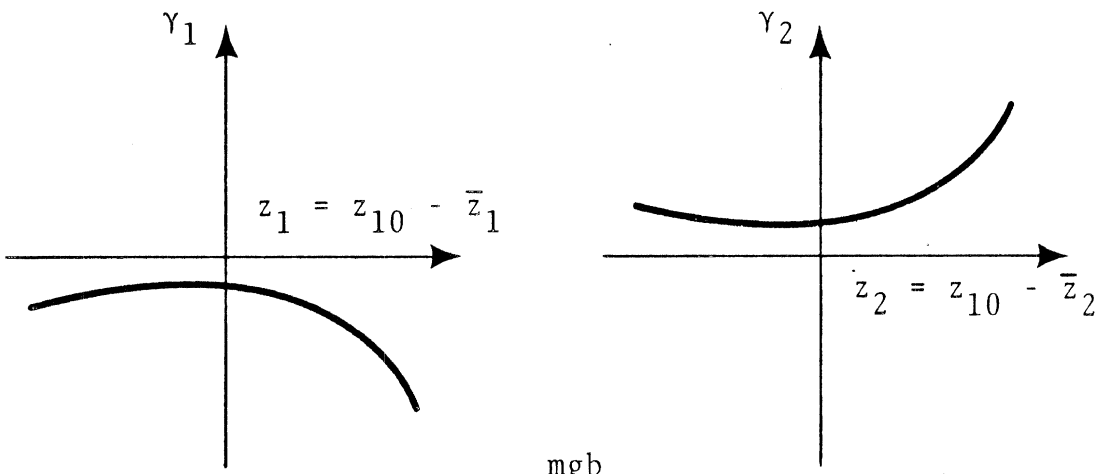

$$z_{10} = \frac{mgb}{2(a+b)\ K_f}$$

The values used for these functions were obtained from the input table for the digital vehicle mechanics model developed by McHenry, et al. [37].

Trajectory Kinematics

The motion equations (B-1), (B-2), and (B-3) are solved by integration, i.e.,

$$u(t) = \int_{t_o}^{t} \dot{u}\ dt + u(t_o)\ , \qquad \text{(B-35)}$$

$$v(t) = \int_{t_o}^{t} \dot{v} \; dt + v(t_o) \; , \tag{B-36}$$

$$r(t) = \int_{t_o}^{t} \dot{r} \; dt + r(t_o) \; . \tag{B-37}$$

The angular orientation of the vehicle body axes with respect to x, y- axes fixed in the earth is illustrated in the sketch below:

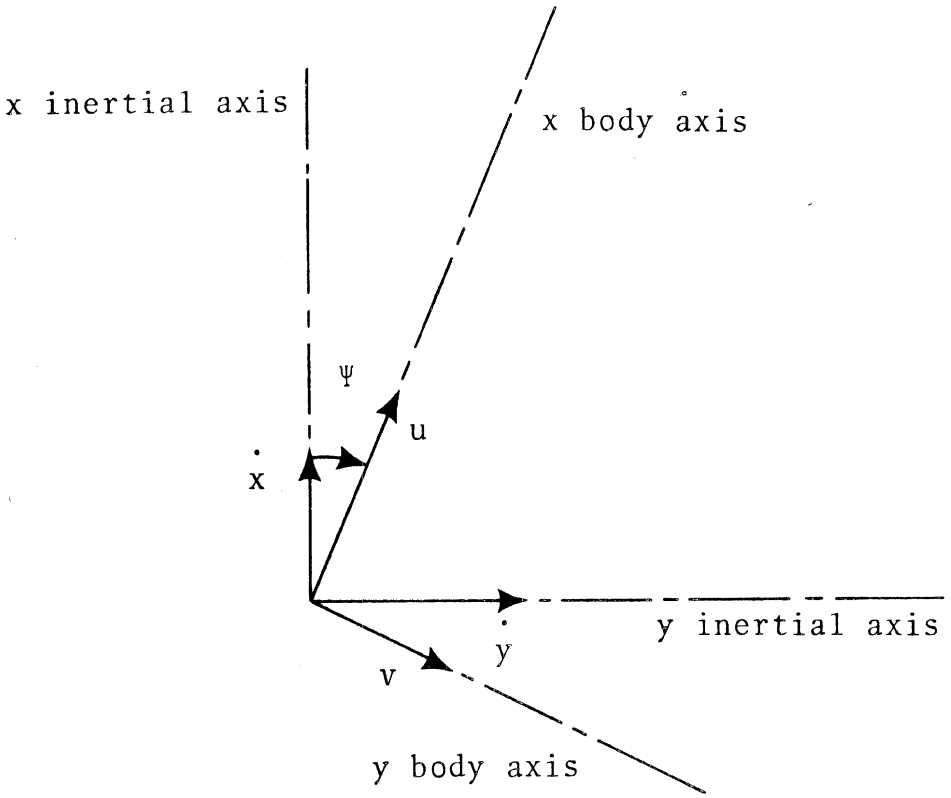

The orientation angle Ψ is the result of the vehicle rotating away from its original orientation angle. Since this rotation takes place with angular velocity r ,

$$\Psi(t) = \int_{t_o}^{t} r(t)dt + \Psi(t_o) \tag{B-38}$$

The components of the vehicle velocity in the body axis system u and v, are resolved into the earth axis system by using the following coordinate conversions:

$$\dot{x} = u \cos \Psi - v \sin \Psi \ , \tag{B-39}$$

$$\dot{y} = u \sin \Psi + v \cos \Psi \ . \tag{B-40}$$

The position of the vehicle is obtained by integrating the velocities. Thus

$$x(t) = \int_{t_o}^{t} \dot{x} \, dt + x(t_o) \tag{B-41}$$

$$y(t) = \int_{t_o}^{t} \dot{y} \, dt + y(t_o) \tag{B-42}$$

APPENDIX C

BRAKING EFFICIENCY SIMULATION

The vehicle simulation was operated at various friction values. At each friction value the brake torque was increased until either a front wheel or a rear wheel locked up. The value of total tire force which would just avoid wheel lock was recorded. The results of the calculations are given in Figure C1. The results for C_s = 20,000 lbs/unit slip compared to those for C_s = 5,000 lbs/unit slip show that decreasing C_s made about a 1% increase in the brake efficiency, $\frac{F_x}{\mu_o mg}$. This is certainly not a significant difference.

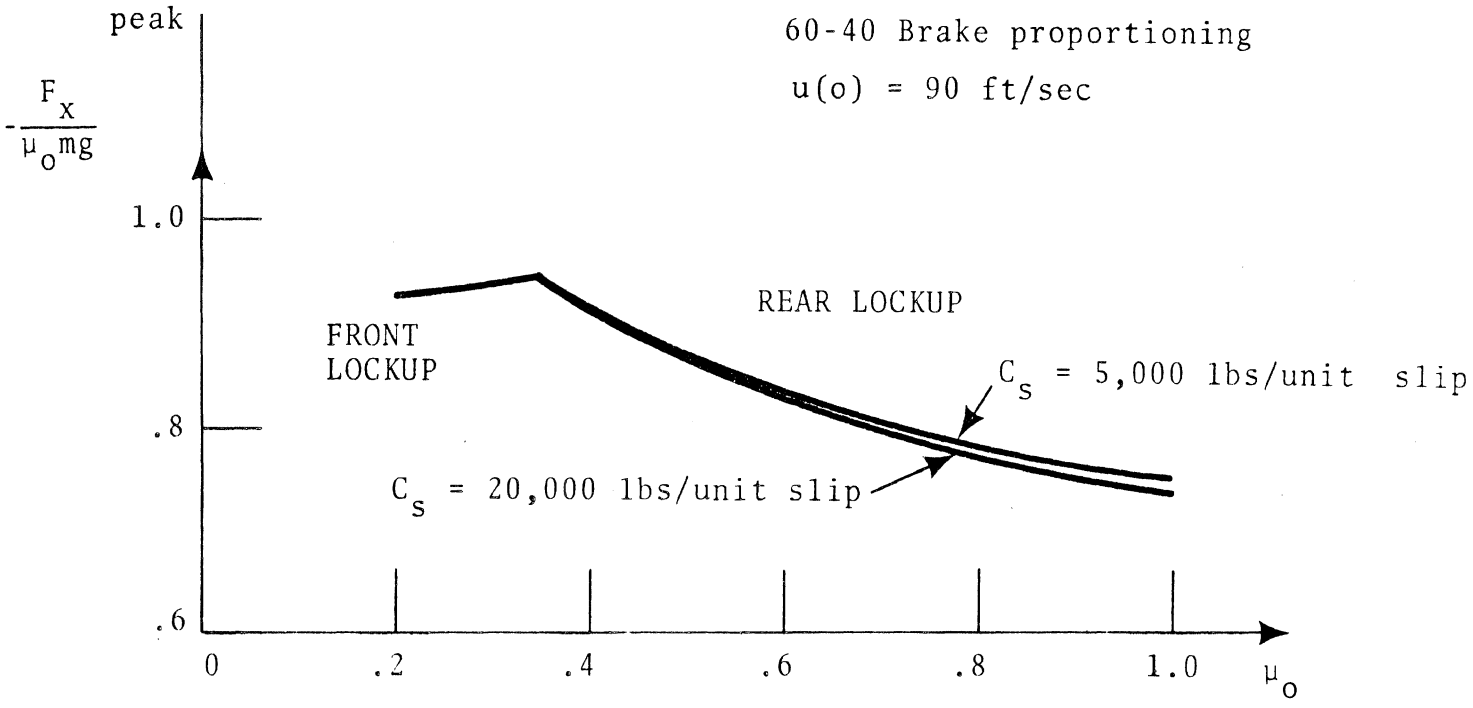

FIGURE C1. BRAKE EFFICIENCY, C_s INFLUENCE

SYMBOLS

A_D	cross-sectional area
A_s	friction reduction factor (see equation 10)
AT_i	tire aligning torque
a	distance, center of gravity to front axle of vehicle
b	distance, center of gravity to rear axle of vehicle
C_D	aerodynamic drag coefficient
C_F	equivalent viscous steering damping coefficient (see equation B-22)
C_{Fi}	steering system coulomb friction associated with i^{th} wheel
C_s	tire traction stiffness (see equation 14)
C_{sr}	rear roll steer coefficient
C_{wi}	wheel damping coefficient
C_{xi}	tire vertical force offset rate
C_{zi}	tire vertical stiffness
C_α	tire cornering stiffness
C_γ	tire camber stiffness
C^*_γ	relative camber stiffness
F_D	aerodynamic drag force
F_R	magnitude of tire shear force vector
F_x	total longitudinal force from tires
F_{xi}	tire force along forward body axis
F_{xwi}	longitudinal tire force in the wheel plane
F_y	total lateral force from tires

F_{yi}	tire force along lateral body axis
F_{ywi}	tire force normal to wheel plane
F_z, F_{zi}	normal load on the tire
g	acceleration of gravity
h	center of gravity height
I	yaw inertia
I_{Fw}	wheel moment of inertia about kingpin
I_{wy}	wheel inertia about wheel spin axis
i	index for tires, 1 means left front, 2 means right front, 3 means right rear, 4 means left rear
K_f	front spring rate
$K_{f\phi}$	front roll stiffness
K_p	kingpin offset
$K_{r\phi}$	rear roll stiffness
K_{ss}	steering stiffness
K_x	tire longitudinal deflection constant
K_y	tire lateral deflection constant
ℓ	contact patch half length
M_s	steering moment
M_z	aligning torque
m	vehicle mass
p	normal pressure in contact patch
R	nominal tire radius
R_e	effective radius
RR	rolling resistance

r	yaw rate
s, s_i	longitudinal slip ratio
$\bar{s}$	normalized slip (see equation A-24)
$\bar{s}_R$	total normalized slip (see equation A-16)
T	yaw moment about vehicle center of gravity
T_{Bi}	brake torque applied to the wheel
T_i	drive torque applied to the wheel
T_{wi}	wheel torque
t	half tread
u	forward velocity of vehicle cg
u_i	wheel center longitudinal velocity
u_{wi}	wheel center velocity component in the wheel plane
V	total velocity
V_s	sliding velocity
v	lateral velocity of vehicle cg
v_i	wheel center lateral velocity
w	tire tread width
x	longitudinal inertial coordinate
$\dot{x}$	x inertial velocity
x_p	tire pneumatic trail
x_{zi}	amount of longitudinal offset of the center of vertical pressure from the wheel center
y	lateral inertial coordinate
$\dot{y}$	y inertial velocity
$\bar{z}_1$, $\bar{z}_2$	suspension deflections
$\bar{z}_{10}$	static suspension deflection

α_o	slip angle
α , α_i	modified slip angle which includes a contribution due to camber angle
$\bar{\alpha}$	normalized slip angle
α_C	equivalent slip angle for camber
β, β_i	$\tan^{-1} \frac{v_i}{u_i}$, sideslip angle
γ_i	camber angle
$\Delta\delta'_{sw}$	increase of steer angle input
δ_{Fw}	front tire steer angle
δ_i	tire steer angle
δ_{rs}	rear axle roll steer angle
δ'_{sw}	steering input
δ_{zi}	amount of vertical tire deflection
η	contact patch lateral coordinate
θ	pitch angle
μ	friction coefficient
μ_o	nominal coefficient of friction at zero velocity
ξ	contact patch longitudinal coordinate
ξ'	carcass longitudinal coordinate
ξ_s	longitudinal coordinate where sliding begins in contact patch
ρ	mass density of air
σ_{max}	tire-road shear stress limit
σ_ξ	tire longitudinal shear stress
σ_η	tire lateral shear stress
ϕ	roll angle

ψ	orientation angle
Ω	wheel spin velocity
Ω_o	spin velocity of freely rolling tire
ω_i	angular velocity of the wheel
F_ξ	tire longitudinal force
F_η	tire lateral force

REFERENCES

1. L. Segel, "On the Stability and Control of the Automobile as Influenced by the Dynamics of the Steering System," Journal of Engineering for Industry (Transaction of the ASME), Vol. 88, Series B, No. 3, August 1966.

2. R. Hadekel, "The Mechanical Characteristics of Pneumatic Tyres," S & T Memo TPA3, Technical Information Bureau, British Ministry of Supply, London, England, October 1952.

3. R. D. Evans, "Properties of Tires Affecting Riding, Steering, and Handling," SAE Journal, February 1935.

4. A. W. Bull, "Tire Behavior in Steering," SAE Journal, August 1939.

5. D. L. Nordeen and A. D. Cortese, "Force and Moment Characteristics of Rolling Tires," SAE Paper 713A, June 1963.

6. G. Freudenstein, "Luftreifen bei Schräg-und Kurvelauf" (Pneumatic Tires Running With Sideslip and on Curves), Deutsche Kraftfahrtforschung und Strassenverkehrstechnik, Vol. 152, 1961.

7. J. L. Ginn and R. L. Marlowe, "Road Contact Forces of Truck Tires as Measured in the Laboratory," SAE Paper 670493, May 1967.

8. J. R. Nothstine and F. N. Beauvais, "Laboratory Determination of Tire Forces," SAE Paper 713B, June 1963.

9. E. Fiala, "Seitenkrafte am rollenden Luftreifen" (Lateral Forces on Rolling Pneumatic Tires), Zeitschrift V.D.I. 96, No. 29, October 1954.

10. T. Saito and I Chuji, "Cornering Characteristics of Automobile Tires (III), " Journal of Mechanical Laboratory of Japan, Vol. 7, No. 1, 1961.

11. G. L. Goodenow, T. R. Kolhoff, and F. D. Smithson, "Tire-Road Friction Measuring System - A Second Generation," SAE Paper 680137, January 1968.

12. G. Kullberg, "Method and Equipment for Continuous Measuring of the Coefficient of Friction at Incipient Skid," HRB Bulletin 348, 1962.

13. C. G. Giles, "Some Recent Developments in Work on Skidding Problems at the Road Research Laboratory," Highway Research Board, No. 46, 1963.

14. G. Förster, "Tests to Determine the Adhesive Power of Passenger-Car Tires," NASA Technical Memorandum 1416, August 1956.

15. G. Krempel, "Untersuchungen an Kraftfahrzeugreifen" (Experiments on Automotive Tires), Parts 1 and 2, Automobiltechnische Zeitschrifte, January and August 1967.

16. T. A. Byrdsong, "Investigation of the Effect of Wheel Braking on Side-Force Capability of a Pneumatic Tire," NASA TN D-4602, February 1968.

17. K. E. Holmes and R. D. Stone, "Tyre Forces as Functions of Cornering and Braking Slip on Wet Road Surfaces," Symposium on Handling of Vehicles Under Emergency Conditions, Instn. Mech. Eng., January 8, 1969.

18. C. G. Giles, F. T. W. Lander, and K. E. Holmes, "A Test Vehicle for Studying the Skid Resisting Properties of Tyre and Road Surfaces Under Controlled Cornering and Braking," Road Research Laboratory Report No. LR 99, 1967.

19. H. S. Radt, Jr. and W. F. Milliken, Jr., "Motions of Skidding Automobiles," SAE Summer Meeting June 5-10, 1960, Chicago, Illinois.

20. J. R. Ellis, "The Dynamics of Vehicles During Braking," Symposium on the Control of Vehicles During Braking and Cornering, Instn. Mech. Eng., June 1963.

21. R. R. McHenry, "An Analysis of the Dynamics of Automobiles During Simultaneous Cornering and Ride Motions," Symposium on Handling of Vehicles Under Emergency Conditions, Instn. Mech. Eng., January 1969.

22. H. Dugoff, General Discussion, Symposium on Handling of Vehicles Under Emergency Conditions, Instn. Mech. Eng., January 1969.

23. L. Segel, "Theoretical Prediction and Experimental Substantiation of the Response of the Automobile to Steering Control," Research in Automobile Stability and Control and in Tyre Performance, The Institute of Mechanical Engineers, Automobile Division, August 1956.

24. Society of Automotive Engineers, "Vehicle Dynamics Terminology," SAE Recommended Practice, SAE J670a, December 1965.

25. D. L. Nordeen, R. E. Rasmussen, J. B. Bidwell, "Tire Properties Affecting Vehicle Ride and Handling," Proceedings General Motors Corporation Automotive Safety Seminar, GM Safety Research & Development Laboratory, July 1968.

26. H. W. Kummer and W. E. Meyer, "Tentative Skid Resistance Requirements for Main Rural Highways," NCHRP Program Report 37, 1967.

27. T. S. Scafer, et al, "Design and Performance Considerations for Passenger Car Anti-Skid Systems," SAE Paper 680458, May 1968.

28. J. L. Harned and L. E. Johnston, "Anti-Lock Brakes," Proceedings General Motors Corporation Automotive Safety Seminar, GM Safety Research & Development Laboratory, July 1968.

29. M. Goland and F. Jindra, "Directional Stability and Control of a Four-Wheeled Vehicle in a Flat Turn," SAE Preprint 211A, August 1960.

30. F. D. Hales, "Automobile Stability, Part III, A Two-Degree-of-Freedom Mathematical Model Compensated for Roll Effects," Davidson Laboratory, Stevens Institute of Technology, Technical Memorandum 152, June 1968.

31. F. N. Beauvais, C. Garelis, and D. H. Iacovoni, "An Improved Analog for Vehicle Stability Analysis," SAE Preprint 295-C January 1961.

32. D. H. Weir, C. P. Shortwell, and W. A. Johnson, "Dynamics of the Automobile Related to Driver Control," Franklin Institute Research Laboratories Report No. 157-1, July 1966.

33. W. Bergman, E. Fox, and E. Saibel, "Dynamics of an Automobile in a Cornering Maneuver On and Off the Highway," paper presented to First International Conference on the Mechanics of Soil-Vehicle Systems, June 1961, Torino, Italy.

34. W. C. Hamman, "Analytical Prediction of Vehicle Handling Behavior," Paper No. 670195 presented at Automotive Engineering Congress, January 1967, Detroit.

35. W. R. B. Morrison, "On the Lateral Dynamics of an Automobile in Accelerated Motions," Mechanical and Chemical Engineering Transactions, The Institution of Engineers, Australia, November 1967.

36. H. S. Radt, H. B. Pacejka, "Analysis of the Steady-State Turning Behavior of an Automobile," Symposium on the Control of Vehicles, Instn. Mech. Engrs., June 1963.

37. R. R. McHenry, D. J. Segal, N. J. Deleys, "Determination of Physical Criteria for Roadside Energy Conversion Systems," Cornell Aeronautical Laboratory, Inc., CAL No. VJ-2251-V-1, Final Report Contract No. CPR-11-3988, July 1967.

38. J. Versace and L. M. Forbes, "Research Requirements for Determining Car Handling Characteristics," Highway Research Record, 247, 1968.

39. W. F. Milliken, Jr. and F. Dell'Amico, "Standards for Safe Handling Characteristics of Automobiles," Joint Symposium on Vehicle and Road Design for Safety, College of Aeronautics, Cranfield, England, July 3-4, 1968.

40. H. Dugoff and J. O'Day, "The Role of Vehicle Dynamic Performance in Highway Accident Causation," 48th Highway Research Board Annual Meeting, January 1969.

41. W. Bergman, "Theoretical Prediction of the Effects of Traction on Cornering Force," Transaction of SAE, 1965.

42. W. H. Metcalf, G. J. Fabian, "Lateral Mechanical Properties of Six Pneumatic Tires," Cornell Aeronautical Laboratory Report No. YD1275-V-1, 1 July 1959.

43. S. A. Batterson, "A Study of the Dynamics of Airplane Braking Systems as Affected by Tire Elasticity and Brake Response," NASA TN -3081, October 1965.

44. T. P. Newcomb and R. T. Spurr, Braking of Road Vehicles, Chapman and Hall, Ltd., London, 1967.

45. L. Segel, K. C. Ludema, and H. Dugoff, "New Areas for Tire Performance Methods," Materials Research and Standards, Vol. 8, No. 6, 1968.